Theory and Modelling of Ultrafast X-ray Imaging of Dynamical Non-equilibrium Systems

Lorenz, Ulf; Henriksen, Niels Engholm; Møller, Klaus Braagaard

Publication date:
2010

Document Version
Publisher's PDF, also known as Version of record

Ulf Lorenz

Theory and Modelling of Ultrafast X-ray Imaging of Dynamical Non-equilibrium Systems

Department of Chemistry
Technical University of Denmark

Abstract in English

Over the next few years, a new generation of x-ray sources is going online. These free-electron lasers will provide extremely bright subpicosecond x-ray pulses. Traditionally, x-ray diffraction has the advantage of directly determining the atomic positions within a sample. With these new machines, it becomes feasible to exploit this concept for ultrafast processes; in effect, we can study chemical reactions as they occur.
This thesis deals with theoretical aspect of ultrafast time-resolved x-ray diffraction (TRXD). We derive general formulas for calculating the diffraction signal that are closely related to those encountered in time-independent diffraction. We also specify the approximations that are required to obtain these formulas, and embed the technique of TRXD in the wider frame of time–domain pump–probe experiments for the study chemical reactions.
Furthermore, we study new opportunities arising in the context of TRXD. We give a detailed treatment of the anisotropies that persist after exciting molecules with an optical pump laser, and specify how to setup an experiment and analyze the diffraction patterns in an optimal way.

Resumé på Dansk

Inden for de næste få år bliver en ny generation af røntgenkilder operationsklare. Disse fri-elektron-lasere vil generere meget intensive røntgenpulse af mindre end et pikosekunds længde. Røntgenspredning har i lang tid været en god metode til at bestemme atomernes position i en prøve. Med disse nye apparater kan vi anvende dette koncept til ultrahurtige processer, hvor vi studerer kemiske reaktioner, mens de finder sted.
Denne afhandling beskæftiger sig med teoretiske problemer omhandlende tidsopløst røntgenspredning (TORS). Vi udleder generelle formler til beregning af spredningsmønstre. Formlerne er næsten de samme, som findes i tidsuafhængig spredning. Vi angiver også approksimationerne, som er nødvendige for udledningen af disse formler, og viser hvilken forbindelse der er mellem TORS og andre tidsopløst pumpe-probe experimenter, som også undersøger kemiske reaktioner.
Desuden undersøger vi nye muligheder, som opstår omkring TORS. Vi giver en detaljeret beskrivelse af anisotropier, som opstår efter man eksiterer molekyler med en optisk pumpe laser, og viser hvordan man opsætter et experiment, og hvordan man analyserer spredningsmønsterne på den mest optimale måde.

Preface and Acknowledgments

This thesis is the result and the summary of the work I have done over the last three years during my PhD studies. The studies were supervised by Niels E. Henriksen and Klaus B. "This I do not understand" Møller, whom I would like to thank for discussions and the sometimes intensive, but helpful suggestions during the preparation of the manuscripts. The two articles on which this work is based, and the thesis itself, have certainly improved a lot in coherence and readability thanks to their input.
When I started my PhD, the overall goal was to do something interesting with time-resolved x-ray diffraction. However, I soon got stuck on the abstract level of theory, namely on the problem whether x-ray diffraction is elastic or not. Almost every article that we found on time-resolved diffraction suggested that x-ray diffraction is somewhat elastic, and used the Born-Oppenheimer approximation in the derivation. This was not an adequate solution, since already a cursory search revealed techniques that employ inelastic x-ray scattering, and a lot of interesting photochemistry involves the violation of the Born-Oppenheimer approximation.
It took some effort to arrange a set of arguments that would avoid these inconsistencies in the form of paper 1 found in the appendix. A notable side effect of this search is our fixation on NaI as one of the simplest model systems whose dynamics are not described by the Born-Oppenheimer approximation.
At some point, I found myself trying to persuade Ivan Vartaniants, a senior scientist at Hasylab, DESY, of our findings. We disagreed on almost every point, but he suggested that I should write up the arguments starting from the very basics. While pondering how to best present the material in the simplest way possible, I realized that the core problem can already be formulated within the time-independent theory. The resulting text formed the nucleus of what eventually became chapters 2 and 3.
Having finished this part, we were then interested in diffraction patterns from aligned diatomic molecules. This came in handy when the application deadline for the first ultrafast time-resolved beam time at the Linear Coherent Light Source arrived, and we were asked to contribute to our collaborator's applications with a paragraph on data processing and colorful images. When we studied various applications, we noticed that several authors were struggling with the, for us at that time, simple concepts of a basis expansion of the density and the diffraction signal. This led to the attempt of giving a detailed, but simple account of how to process the diffraction pattern properly in paper 2 in the appendix.
With this application-centered framework, some more questions arose, for example, how to treat noisy diffraction patterns, and how to parameterize the density, which are treated in chapter 4. I want to thank Kristoffer Haldrup for discussions surrounding his current fitting procedure, and for trying it out in section 4.3. While the test case falls short of what I originally intended, it was still illuminating. I also want to thank Vivien Petzold, who did the very first draft of what would eventually become section 4.4.2,
This thesis does not include the work I have spent on the `WavePacket` code. I spent substantial time implementing several DVR schemes and maintaining the program, and it was very useful for illustrating the abstract procedures. However, the technical details

of wave packet propagation do not really match the overall theme of time-resolved x-ray diffraction, so I omitted them. Those details that have relevance for the calculations on NaI are summarized in appendix B. I want to thank Burkhard Schmidt for getting me started and interested in wave packets, and for his hospitality during my stays in Berlin. In this context, I also thank Johan Schmidt for coming up with interesting applications for wave packets, which eventually led to a joint publication [1], and Michael Fischer for an ongoing collaboration on a certain eternal project [2].
Although it is difficult to put the finger on it, this work as well as well as my understanding has profited from discussions with many people, be it through problems that they encountered, or experiments that were done. I want to highlight here my office mates Jakob Petersen and Thomas Kuhlman, Kestutis Aidas, and all the people at the Center for Molecular Movies.

Contents

List of papers included in the thesis

1. Ulf Lorenz, Klaus B. Møller, Niels E. Henriksen
   Theory of time-resolved inelastic x-ray diffraction
   Phys. Rev. A, *81:023422* (2010)

2. U. Lorenz, K. B. Møller, N. E. Henriksen
   On the interpretation of time-resolved anisotropic diffraction patterns
   New J. Phys., *submitted*

1 Introduction

In 1913, Friedrich, Knippling and Laue published an article [3], in which they described for the first time an x-ray diffraction experiment with a modern interpretation of the diffraction pattern. As Laue explicitly points out, the diffraction patterns are of the same nature as those obtained with optical gratings, such as a double slit. The incoming x-ray wave can be scattered at each atom in the illuminated sample. At the detector plate, the scattered waves from each atom interfere, and produce a diffraction pattern that is highly sensitive to the relative position of the atoms with respect to each other. For the simplest example of a diatomic molecule with fixed geometry, this is demonstrated in Fig. 1.1.
This basic mechanism of x-ray diffraction is still valid nowadays, although one would use

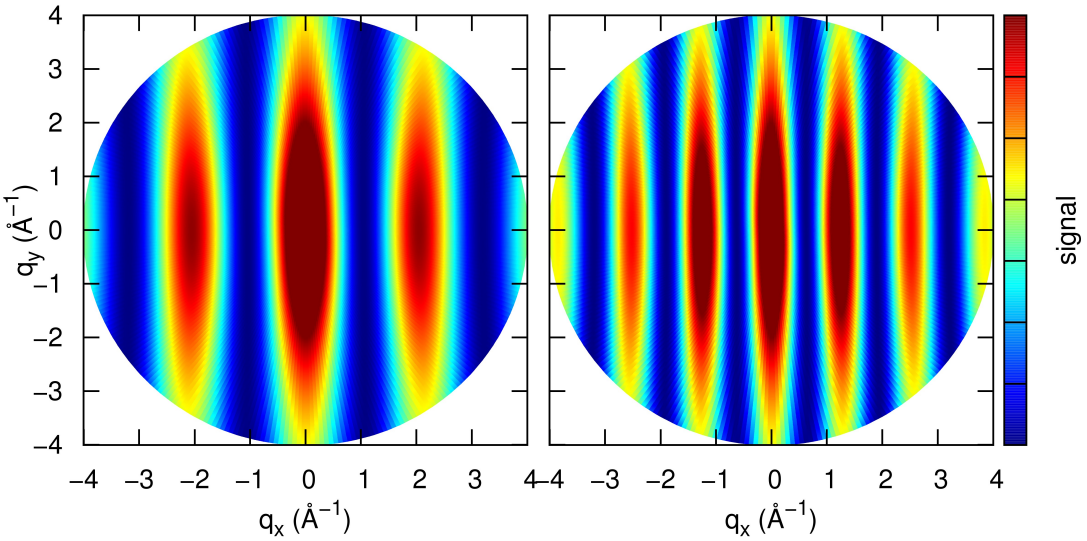

Figure 1.1: Diffraction pattern of a Br_2 molecule with different bond length. Two Bromine atoms were placed along the horizontal direction with an internuclear distance of 3Å (left image) or 5Å (right image). The x-ray beam is unpolarized, and hits the molecule perpendicular to the molecular axis. For each pixel, the corresponding scattering vector $\mathbf{q}$ was constructed, and the squared molecular form factor was evaluated with equation (2.25). Atomic form factors were taken from [4].

a slightly different formal derivation. Using scattering theory, we find that x-rays are dominantly diffracted by the electrons, and the diffraction pattern encodes the electron density distribution of the sample [5]. However, the majority of the electrons assemble in shells of fixed form around the single nuclei, so we can approximate the electron density distribution by that of the respective independent atoms (the so-called independent atom model (IAM)). The diffraction pattern then encodes the position of these atoms in the sample, which is identical to the interpretation of Laue.
This feature of x-ray diffraction sets it apart from many spectroscopy techniques, where one probes molecular properties such as optical resonances, oscillator strengths or electron kinetic energy distributions. These properties depend strongly on the structure of the outer valence electrons, and indirectly on the position of the atomic nuclei as well. Such spectroscopic methods therefore provide an indirect way of determining the atomic arrangement. However, linking the properties of the valence electrons to nuclear geometry requires either a good model, or expensive electronic structure calculations. If we are only interested in the nuclear arrangement, x-ray diffraction seems to be the superior method. However, an invaluable advantage of optical techniques is the widespread availability of femtosecond light sources, which enable the study of not only static equilibrium structures, but also the time-evolution of molecular dynamics (see for example [6–9]).
This situation is expected to change soon. In the near future, next generation x-ray sources, so called x-ray free electron lasers, are becoming operational. The Linear Coherent Light Source (LCLS) [10, 11] has opened for the first experiments this year, the Spring-8 Compact Sase Source (SCSS) [12] is to be commissioned in 2010, and the European XFEL [13] is scheduled for user operation in 2015. These facilities will provide pulses with subpicosecond duration, and a photon flux orders of magnitude above that of current synchrotron facilities. Both parameters make it feasible to use the traditional advantages of x-ray diffraction, the direct determination of the nuclear geometry, for time-resolved studies of ultrafast processes, thereby creating the new field of time-resolved x-ray diffraction (TRXD). The aim of this thesis is to study theoretical aspects within TRXD.
Before we touch the subject of x-ray diffraction itself, it is necessary to introduce some basic theory. Almost all modern theoretical chemistry is built around the Born-Oppenheimer approximation [14] or its extension, the Born-Huang representation [15]. Within this framework, only the atomic nuclei move around, while the electrons are passive spectators that adapt to the nuclear geometry. Knowledge of this geometry enables (almost) complete reconstruction of the whole molecular wave function. Splitting up the molecular degrees of freedom into those of the electrons and nuclei allows us to include the IAM in a natural way into the framework. The formal introduction of these concepts is the content of chapter 2.
With this basic theory in place, we can set out to study x-ray diffraction, especially with respect to time-resolved measurements. A first task will be the derivation of general formulas for TRXD in chapter 3. In traditional time-independent x-ray diffraction theory, it is usually assumed that the scattering is always “elastic”. We will demonstrate that this assumption is in general wrong and not required; dropping it simplifies especially the derivation of the time-dependent signal considerably.

Finally, in chapter 4, we focus on molecular ensembles, and study some new issues that arise in a time-dependent context. A first new phenomenon is molecular alignment. The strength of the interaction between a molecule and a polarized laser field depends on the relative orientation of the molecule with respect to the polarization vector. Consequently, the laser-molecule interaction produces aligned ensembles of molecules, and probing these ensembles with TRXD produces anisotropic diffraction patterns. We will study how to systematically decompose and interpret these patterns. Another new effect that we briefly study are delocalized wave packets after photoexcitation. Typically, in a ground-state molecule, the constituent atoms are strongly bound, and the nuclear wave function is strongly localized around a specific bound-state geometry. When we excite such a molecule, we frequently observe wave–packet dispersion; the initially well-defined bond lengths give rise to a continuous distribution of bond lengths.

Conventions

In the following, I list a few conventions that are used throughout the text.

$x, \mathbf{x}, \mathbf{x}^{(f)}$	Vectors are denoted by bold font, the length of the vector is denoted by the normal italic character. To distinguish normal three-dimensional vectors from general f-dimensional vectors, the latter get the number of dimensions as superscript. This explicit superscript can be dropped if there is no ambiguity.
$\langle f(x)\|\hat{A}\|f(x)\rangle_y$	Partial integration of the expression $f^*(x,y)\hat{A}f(x,y)$ over the coordinate y only.
$\cong$	the left and right hand side of the equation match apart from what I deem uninteresting constant prefactors.
$\tilde{x}, \overline{\tilde{x}}, \sigma^2(\tilde{x})$	Random variables are distinguished from ordinary variables by placing a tilde on top. This notation is exclusively considered in the discussion of noisy data in section 4.4. Expectation values of functions of random variables are denoted by an additional bar on top. Variances are denoted with a σ^2

2 Background concepts

2.1 Born-Oppenheimer approximation and beyond

When we nowadays describe small atom-scale systems, we usually employ quantum mechanics. The molecular wave function $\Psi(\mathbf{R}, \mathbf{r}, t)$ is a function of the set of nuclear coordinates $\mathbf{R}$ and the electronic coordinates $\mathbf{r}$, and its time evolution is described by the time-dependent Schrödinger equation (TDSE)

$$\mathrm{i}\hbar\dot{\Psi} = \hat{H}\Psi \ . \tag{2.1}$$

For the following manipulations, we decompose the Hamiltonian $\hat{H}$ of the unperturbed molecule into the kinetic energy of the nuclei $\hat{T}_{\mathbf{R}}$, the kinetic energy of the electrons $\hat{T}_{\mathbf{r}}$, and all Coulomb potentials between nuclei and electrons $\hat{V}_C$, with the latter two forming the electronic Hamiltonian $\hat{h}$,

$$\hat{H} = \hat{T}_{\mathbf{R}} + \hat{h} = -\frac{\hbar^2}{2}\nabla^2_{\mathbf{R}} + \hat{T}_{\mathbf{r}} + \hat{V}_C \ . \tag{2.2}$$

To simplify the notation, we use scaled nuclear coordinates throughout this section, so that the associated masses become unity. The full Schrödinger equation in the form of (2.1) is only solved for simple molecules, such as H_2^+ or H_2 in intense laser fields (for example [16, 17]). For larger systems, the computational cost explodes, mainly because of the large number of electronic coordinates.
To circumvent this problem, Born and Oppenheimer invented a method of separating the electronic and nuclear wave function [14]. This method is more transparently expressed in the later formulation by Born and Huang [15, 18, 19], which we adopt here.
As basic idea, we use a special decomposition of the total wave function Ψ into products of electronic and nuclear wave functions

$$\Psi(\mathbf{R}, \mathbf{r}, t) = \sum_i \Lambda_i(\mathbf{R}, t)\lambda_i(\mathbf{r}; \mathbf{R}) \ . \tag{2.3}$$

This decomposition is exact if the electronic wave functions λ_i form a complete basis in the electronic subspace. Note that we choose a *different* expansion for each nuclear coordinate $\mathbf{R}$. However, we require the $\lambda_i(\mathbf{r}; \mathbf{R})$ to be orthonormal and twice differentiable with respect to $\mathbf{R}$.
One of the most popular choices for the λ_i are the adiabatic states

$$\hat{h}(\mathbf{r};\mathbf{R})\lambda_i^{\mathrm{adi}}(\mathbf{r};\mathbf{R}) = V_i(\mathbf{R})\lambda_i^{\mathrm{adi}}(\mathbf{r};\mathbf{R}) \ . \tag{2.4}$$

Inserting the expansion (2.3) with the adiabatic states (2.4) into the TDSE (2.1), multiplying with $\lambda_j^{\mathrm{adi}*}$, and integrating over all electronic coordinates gives a set of coupled equations for the nuclear wave functions Λ_j

$$\begin{aligned} i\hbar\dot{\Lambda}_j(\mathbf{R},t) = &\left(\hat{T}_{\mathbf{R}} + V_j(\mathbf{R})\right)\Lambda_j(\mathbf{R},t) \\ &- \sum_i \left(2F_{ji}(\mathbf{R})\Big[\nabla_{\mathbf{R}}\Lambda_i(\mathbf{R},t)\Big] + G_{ji}(\mathbf{R})\Lambda_i(\mathbf{R},t)\right) , \end{aligned} \tag{2.5}$$

where the non-adiabatic couplings are defined as

$$F_{ji}(\mathbf{R}) = \frac{\hbar^2}{2}\langle\lambda_j^{\mathrm{adi}}(\mathbf{R})|\nabla_{\mathbf{R}}|\lambda_i^{\mathrm{adi}}(\mathbf{R})\rangle_{\mathbf{r}} \tag{2.6}$$

$$G_{ji}(\mathbf{R}) = \frac{\hbar^2}{2}\langle\lambda_j^{\mathrm{adi}}(\mathbf{R})|\nabla_{\mathbf{R}}^2|\lambda_i^{\mathrm{adi}}(\mathbf{R})\rangle_{\mathbf{r}} \ . \tag{2.7}$$

These equations suggest a simple and intuitive way of describing the molecular dynamics. If we only consider the first line of (2.5), we have a set of Schrödinger equations, each of which describes the nuclei moving on a potential energy surface V_j. This surface is "spanned" by the electrons, and depends on the electronic quantum number j.
The second line in (2.5) produces some energy shifts, and describes the non-adiabatic couplings, which connect the nuclear wave functions of different electronic states. In many cases of interest, they can either be neglected (the Born-Oppenheimer approximation), or they are restricted to certain ranges of nuclear structures $\mathbf{R}$, and few states only. In consequence, the simple picture of uncoupled nuclear wave functions holds most of the time; we also need to consider only a handful of electronic states (typically between one and three) instead of all the electronic coordinates in (2.1).
We should point out that the nuclear wave functions carry all the information that is necessary to reconstruct the molecular wave function. The adiabatic electronic states can be calculated via (2.4) (other choices of λ_i have similar defining equations), and the total wave function can then be assembled from (2.3).
As a side note, we can also solve the time-independent Schrödinger equation to obtain the eigenstates of the Hamiltonian,

$$\hat{H}\Psi_x = E_x\Psi_x \ . \tag{2.8}$$

If we are determined to use the Born-Oppenheimer approximation and neglect the non-adiabatic couplings between different electronic states, we can drop the general decomposition of the form (2.3) in favor of a special choice,

$$\Psi_{ij}(\mathbf{R},\mathbf{r}) = \Lambda_i(\mathbf{R})\lambda_j(\mathbf{r};\mathbf{R}) \ , \tag{2.9}$$

so that each eigenstate is determined by a nuclear quantum number i and an electronic quantum number j. The Λ_i and the eigenenergies E_{ij} are then determined by

$$\Big(\hat{T}_{\mathbf{R}} + V_j(\mathbf{R})\Big)\Lambda_i(\mathbf{R}) = E_{ij}\ \Lambda_i(\mathbf{R}) \ . \tag{2.10}$$

To get a complete description for molecules excited by an electric field, we can add an interaction Hamiltonian $\hat{H}_{\text{int}}$ with an electric field to (2.2). Within the semi-classical electric dipole approximation, we use

$$\hat{H}_{\text{int}} = \boldsymbol{\varepsilon}(t)\cdot\hat{\boldsymbol{\mu}} = \boldsymbol{\varepsilon}(t)\cdot\sum_{i=1}^{\#\text{particles}} q_i\ \hat{\mathbf{r}}_i \ , \tag{2.11}$$

where $\mathbf{r}_i$ is the position vector of the i-th particle, q_i its charge, and $\boldsymbol{\varepsilon}(t)$ is the time-dependent electric field. If we repeat the derivations, we end up with a set of equations similar to (2.5), but where the right hand side gets an additional term

$$\sum_i \boldsymbol{\varepsilon}(t)\mathbf{D}_{ji}(\mathbf{R})\Lambda_i(\mathbf{R},t) \tag{2.12}$$

with the dipole coupling

$$\mathbf{D}_{ji}(\mathbf{R}) = \langle\lambda_j^{\text{adi}}(\mathbf{R})|\hat{\boldsymbol{\mu}}|\lambda_i^{\text{adi}}(\mathbf{R})\rangle_{\mathbf{r}} \ . \tag{2.13}$$

An electric field can thus couple different nuclear wave functions Λ_i, which suggests using laser pulses for populating excited electronic states.
This completes the basics of the modern picture of molecular dynamics. To demonstrate this powerful and intuitive description, we can study a one-dimensional model of NaI (i.e., neglecting rotation) excited by a short laser pulse. NaI is one of the simplest molecules that exhibits dynamics that go beyond the Born-Oppenheimer approximation [7,20,21]. The wave–packet dynamics were calculated with the `WavePacket` code [22], and the calculated wave function at different times is displayed in figure 2.1. [1] Some details of the calculation method can be found in appendix B.
Initially, the molecule is in the electronic and vibrational ground state, which is strongly localized around the minimum of the ground state potential energy surface at 3Å. When we turn on the laser, the electronic ground and first excited state are coupled by the

[1] It should be noted that I simulated the laser pulse by manually transfering the wave function to the excited state. This corresponds to the limit of an infinitely short pulse within a perturbation approach, which was chosen mainly for aesthetic reasons, a more realistic laser pulse would either excite only a small part of the wave function or significantly broaden the wave packet.

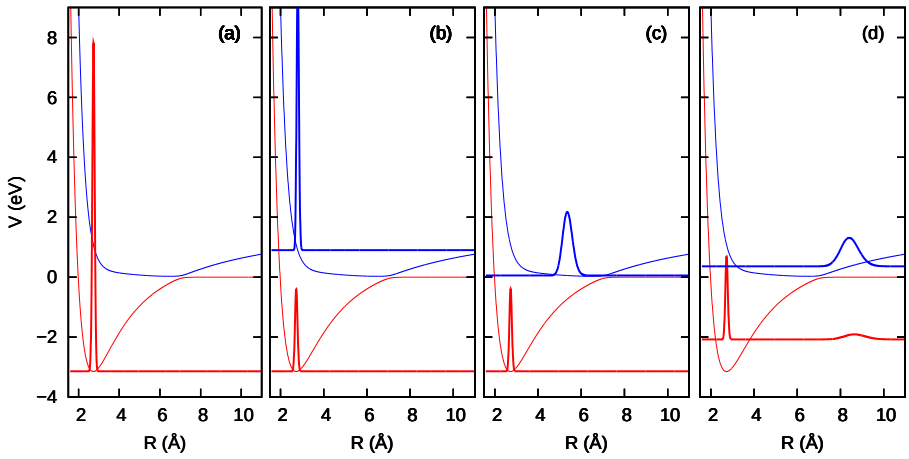

Figure 2.1: Sketch of the potential energy surface and the nuclear dynamics of NaI excited by a short laser pulse at $t = 0$. Thin lines are the potential energy surfaces V_i, the thick lines are the respective nuclear densities $|\Lambda_i|^2$ with the expectation value of the potential energy V_i as baseline. (a) Nuclear wave function before the laser pulse ($t = 0$), (b) shortly after the laser pulse ($t = 10$fs), (c) subsequent dynamics ($t = 100$fs) (d), after passing the avoided crossing around 7Å ($t = 200$fs).

electric field, and part of the wave function is transfered to the electronically excited state. The ground state wave function basically stays where it is, but the excited state wave function starts to move on the corresponding excited state surface, which we can describe as a vibration of the Na-I bond. Within the Born-Oppenheimer approximation, the time evolution of the ground and excited state nuclear wave function are uncoupled. In the case of NaI, this approximation is violated, and there is a strong non-adiabatic coupling at $R \approx 7$ Å. Consequently, when the excited state wave function passes this region, part of it is transfered back to the ground state.

It is not difficult to extrapolate the dynamics to longer time scales. The excited state wave function will continue to oscillate between approximately 3 and 10 Å, and whenever it passes the avoided crossing, some part is transfered to the electronic ground state. This continues until the excited state is completely depleted.

After we have excited a molecule with a (pump) laser pulse, we can try to measure the subsequent dynamics. This can be done by measuring how the system changes a suitably chosen probe, such as another laser pulse or an x-ray pulse, at a well-defined delay time after the excitation. Such setups are called pump–probe experiments. As mentioned earlier, once we have settled for an electronic basis set, we obtain all information about the molecular wave function if we can retrieve the set of nuclear wave functions.

For simplicity, let us choose the adiabatic states, and assume that our probe measurement gives the expectation value of a purely electronic operator $\hat{a}$ at a specific point in time. While this model is too crude, and not applicable to practical situations, it can serve

as a didactive introduction to simple time-resolved measurements such as TRXD. Using the expansion (2.3), we obtain

$$\langle \hat{a} \rangle(t) = \int \mathrm{d}\mathbf{R} \sum_{i,j} \Lambda_i^*(\mathbf{R},t)\Lambda_j(\mathbf{R},t)\ \langle \lambda_i^{\mathrm{adi}}(\mathbf{R})|\hat{a}|\lambda_j^{\mathrm{adi}}(\mathbf{R})\rangle_{\mathbf{r}}\ . \tag{2.14}$$

There is often no significant overlap $\Lambda_i^*\Lambda_j$ between nuclear wave functions on different electronic states (see figure 2.1). For this reason, and to further simplify the discussion, we drop these cross terms. The remaining expression is

$$\langle \hat{a} \rangle(t) = \int \mathrm{d}\mathbf{R} \sum_{i} |\Lambda_i(\mathbf{R},t)|^2\ \langle \lambda_i^{\mathrm{adi}}(\mathbf{R})|\hat{a}|\lambda_i^{\mathrm{adi}}(\mathbf{R})\rangle_{\mathbf{r}}\ . \tag{2.15}$$

This simplified measurement now reveals only the squared amplitudes $|\Lambda_i|^2$, which can be interpreted as the probability density of finding a certain nuclear geometry with a given electronic quantum number, while all the phase information was contained in the cross terms that we have dropped.
Equation (2.15) contains the basic problem we need to solve. Given one or more sets of experimental data $\langle \hat{a} \rangle(t)$, and being able to calculate in principle the electronic matrix elements $a_{ii}(\mathbf{R}) = \langle \lambda_i^{\mathrm{adi}}(\mathbf{R})|\hat{a}|\lambda_i^{\mathrm{adi}}(\mathbf{R})\rangle_{\mathbf{r}}$, we need to invert (2.15) to obtain information about the nuclear wave functions.
It is clear that the matrix elements $a_{ii}(\mathbf{R})$ should ideally fulfill two requirements:

Uniqueness

: Different nuclear geometries $\mathbf{R}$ should yield different values a_{ii}. Otherwise, the measurement might not be sensitive to the actual nuclear motion, and it can be difficult or impossible to extract the amplitudes from the experiment.

Fast evaluation

: At the end of the day, we have to search for geometries $\mathbf{R}$ where the nuclear densities $|\Lambda_i|^2$ are substantial. For larger molecules, this search can take place in a high-dimensional space, and the matrix elements need to be evaluated for many different nuclear geometries. For this reason, we prefer operators whose matrix elements can either be evaluated analytically, or which do not require a high-quality electronic wave function.

As an example for a time-resolved spectroscopic method, we can study femtosecond transition-state spectroscopy (FTS) [6, 7]. Simply put, one probes the molecule by exciting it to a reference electronic state $\lambda_{\mathrm{ref}}^{\mathrm{adi}}$ with a short laser pulse, and measures the absorption of the pulse, which corresponds to the number of excited molecules. This process is only efficient for resonant conditions. In an idealized model, we can approximate the matrix elements as δ-functions,

$$a_{ii}^{\mathrm{FTS}}(\mathbf{R}) \approx \delta\Big\{\hbar\omega - \Big[V_{\mathrm{ref}}(\mathbf{R}) - V_i(\mathbf{R})\Big]\Big\} \,, \tag{2.16}$$

with ω being the frequency of the probing pulse.
In the experiment by Rose, Rosker, and Zewail [7], this method was applied to NaI, and two different probe wavelengths were chosen. One frequency corresponded to a resonant transition of a free Na atom. The idea behind this choice was that the electronic ground state $\lambda_{\mathrm{GS}}^{\mathrm{adi}}$ corresponds for large internuclear distances $R \geq R_0$ to a free Na, and a free I atom, so we can approximate

$$a_{ii}^{\mathrm{FTS,Na}}(R) \approx \delta_{i,\mathrm{GS}}\ \Theta(R - R_0) \tag{2.17}$$

with the Heaviside step function Θ. The signal (II in figure 2.2) shows a stepping form, that we can understand from the dynamics in figure 2.1. Whenever the excited state passed the avoided crossing, some part of the wave packet makes a transition to the ground state, and moves towards $R \to \infty$. So the photodissociation proceeds in steps, which we can observe in the experimental signal.
The other wavelength was detuned from the Na resonance, with the understanding that now the excitation to a resonant state is only efficient for a "perturbed" Na atom, which

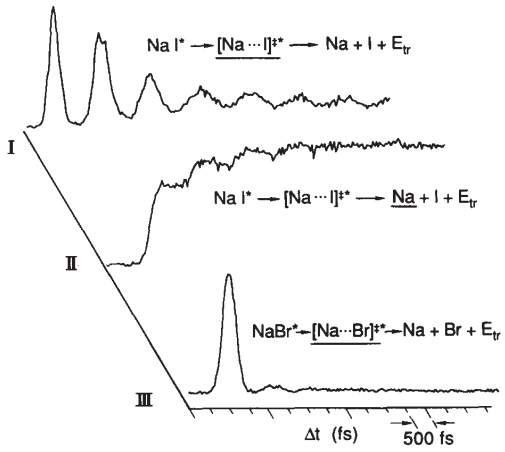

Figure 2.2: FTS signal for NaI and different choices of ω, i.e., the probed electronic state and internuclear distance. I: the excited state at $R_{\mathrm{exc}}(\omega) > 7$Å, II: the ground state at large distance, III: FTS signal for NaBr (not discussed in the text). Reprinted with permission from [7]. Copyright 1988, American Institute of Physics

is roughly the situation of the excited state for internuclear distances smaller than the avoided crossing at 7 Å. That is, one can "assume" [20] that

$$a_{ii}^{\text{FTS, NaI}^*}(R) \approx \delta_{i,\text{exc}}\ \Theta(7\text{Å} - R)\ . \tag{2.18}$$

In the excited state, the wave packet bounces back and forth, and is depleted over time, so the experimental signal (I in figure 2.2) shows a damped oscillation.
This simple example serves to demonstrate a common problem in optical spectroscopy: the indirect link between the measured signal and the underlying nuclear geometry. While the matrix elements are certainly somewhat unique, already the simple hand-waving argument for the definition of the $a_{ii}(R)$ requires a lot of detailed knowledge about the electronic structure and the dynamics of the system. For more quantitative data processing, we would need high-quality expressions for the potential energy surfaces that are used in (2.16) (of course, it would also be appropriate to use a more realistic model of the experiment in this case). However, the calculation of good potential energy surfaces is rather expensive, and might not be feasible for larger molecules.
In the next section, we contrast this with the electronic matrix elements that typically occur in x-ray diffraction. Within the independent atom model, we obtain an analytic approximation of these matrix elements.

2.2 Independent atom model

As we will see in the next chapter, x-ray diffraction measurements always involve the electronic scattering operator

$$\hat{L} = \sum_{i=1}^{\#\text{electrons}} \mathrm{e}^{\mathrm{i}\mathbf{q}\hat{\mathbf{r}}_i}\ , \tag{2.19}$$

where $\mathbf{r}_i$ is the position of the i-th electron, and $\mathbf{q}$ is the scattering vector. This operator is more conveniently rewritten in terms of the electronic density. We first write $\hat{L}$ in a basis of one-electron orbitals $\phi_P(\mathbf{r})$, using the appropriate creation and annihilation operators $\hat{a}_P^\dagger, \hat{a}_P$ as [23]

$$\hat{L} = \sum_{P,Q} L_{PQ}\ \hat{a}_P^\dagger \hat{a}_Q \tag{2.20}$$

with

$$L_{PQ} = \int \mathrm{d}^3x\ \phi_P^*(\mathbf{x})\ \mathrm{e}^{\mathrm{i}\mathbf{q}\mathbf{x}}\ \phi_Q(\mathbf{x})\ . \tag{2.21}$$

From the action on an arbitrary state, we can identify

$$\hat{\varrho}(\mathbf{x}) = \sum_{P,Q} \phi_P^*(\mathbf{x})\phi_Q(\mathbf{x})\ \hat{a}_P^\dagger \hat{a}_Q \tag{2.22}$$

as the density operator, whose expectation value gives the electronic density at position $\mathbf{x}$. [2] This allows us to rewrite

$$\begin{aligned} F_i(\mathbf{q}) &\equiv \langle \lambda_i^{\mathrm{adi}}(\mathbf{R}^{(3N)})|\ \hat{L}|\lambda_i^{\mathrm{adi}}(\mathbf{R}^{(3N)})\rangle_{\mathbf{r}} \\ &= \int \mathrm{d}^3x\ \langle \lambda_i^{\mathrm{adi}}(\mathbf{R}^{(3N)})|\ \hat{\varrho}(\mathbf{x})\ \mathrm{e}^{\mathbf{iqx}}|\lambda_i^{\mathrm{adi}}(\mathbf{R}^{(3N)})\rangle_{\mathbf{r}} \\ &= \int \mathrm{d}^3x\ \varrho_i(\mathbf{x};\mathbf{R}^{(3N)})\ \mathrm{e}^{\mathbf{iqx}}\ . \end{aligned} \tag{2.23}$$

$\varrho_i(\mathbf{x};\mathbf{R}^{(3N)})$ is the electronic density of the state λ_i^{adi}, and N is the number of atoms in the sample. The quantity F_i is called the molecular form factor; as we argue below, it is only weakly dependent on the electronic state, so that we can drop the subscript.
X-ray scattering is sensitive to all electrons in a sample, not just the valence electrons; this can be seen in (2.23), where the total electronic density contributes. Most of the electrons usually stick to their parent atom, and move around with it, the exception being a handful of valence electrons that pair to form valence bonds or get transferred directly to neighboring atoms to make ionic bonds. This gives rise to the crude, but successful independent atom model (IAM) (e.g., [24]).
Within the IAM, we assume that all atomic nuclei have the same electron cloud that an isolated atom of this species has. If we denote the electron density of an isolated atom A as ϱ^A, and the position of the nucleus within the system with $\mathbf{R}_A$, the approximation can be formally written as

$$\varrho_i(\mathbf{x};\mathbf{R}^{(3N)}) = \sum_{A=1}^{N} \varrho^A(\mathbf{x}-\mathbf{R}_A)\ . \tag{2.24}$$

Inserting this into (2.23) yields

$$F_i(\mathbf{q}) = \sum_{A=1}^{N} f_A(\mathbf{q})\ \mathrm{e}^{\mathbf{iqR}_A} \tag{2.25}$$

[2] $\hat{\varrho}(\mathbf{x})$ must be a one-electron operator, since it makes sense to apply it to states with a single electron. In second quantization, it therefore has the form [23] $\hat{\varrho}(\mathbf{x}) = \sum_{PQ} \varrho_{PQ}\hat{a}_P^\dagger\hat{a}_Q$, where ϱ_{PQ} is a linear functional of ϕ_P^* and ϕ_Q.

To determine the ϱ_{PQ}, we calculate the density of a single-electron state $\psi(\mathbf{r}) = \phi_1(\mathbf{r}) + \phi_2(\mathbf{r})$, and compare the results from forming the absolute square $|\psi(\mathbf{x})|^2$, and from applying $\hat{\varrho}(\mathbf{x})$.

with the atomic form factor

$$f_A(\mathbf{q}) = \int \mathrm{d}^3x \; \varrho^A(\mathbf{x}) \; \mathrm{e}^{\mathrm{i}\mathbf{q}\mathbf{x}} \; . \tag{2.26}$$

Analytical approximations for the atomic form factors f_A can be found in standard tabulations [4]. Within the IAM, the electronic matrix elements (2.25) can be calculated analytically, and are basically Fourier transforms of the atomic positions. If the electronic density distributions (and thus the form factors) are sufficiently different from each other, we can expect that these matrix elements are also sensitive to the nuclear geometry of a molecule.
While it is relatively easy to introduce the IAM, it is rather difficult to give general estimates of the errors of this model. Qualitatively, we have ignored all effects from chemical binding, by introducing three approximations:

1. Polarization effects have been neglected, i.e., changes of the electronic density around an atom due to the electric field from the other atoms. The most obvious polarization effect is that a free atom has a spherically symmetric density distribution due to rotational degeneracies, while this is usually not the case for bound atoms; especially valence p- or d-orbitals should show a strong directional preference.

2. Correlations between the electronic shells of different atoms have been neglected. Due to the Pauli principle, a significant distortion of the electron wave function should occur when occupied orbitals of different atoms overlap. Thus, we have indirectly assumed that the overlap of the electronic shells of different atoms is negligible.

3. We assumed that the electronic density distribution is the same for each electronic state. For chemically relevant processes, the electronic states only differ by the rearrangement of few valence electrons. Since the IAM already assumes that the behavior of the valence electrons is not important, this approximation seems a natural extension.

I want to conclude this section with some general remarks. As can be seen from (2.25), the matrix elements are in general complex quantities. When we insert this into (2.15) introduced in the last section, we get a complex measured value, which seems odd. It signals that the idea of describing a time-resolved measurement as the expectation value of an electronic operator, while appealing and able to capture many essential points, is ultimately wrong. In the next chapter, we will employ formal scattering theory and show that the absolute square of the matrix elements is measured.
Furthermore, it is instructive to study the value of the atomic form factor at $q = 0$. We obtain

$$f_A(q = 0) = \int \mathrm{d}^3x \; \varrho^A(\mathbf{x}) \; , \tag{2.27}$$

which is just the number of electrons of the atom. We can infer that for small enough q, the signal is dominated by the heavy atoms in a sample. That is, x-ray scattering is especially suited for molecules consisting of heavy atoms (Pt, Ir, I) in a light-atom framework (C, O, H). In a first approximation, we can ignore the light atoms, and only "see" the motion of the heavy atoms.
As a convenient side effect, the approximations are easier fulfilled for heavy atoms. The (core) electrons are tighter bound and less susceptible to polarization effects, and there are relatively less valence electrons that are poorly described by the IAM.
Finally, electronic structure calculations are more expensive and less reliable for heavy atoms, due to the need for larger basis sets, relativistic corrections etc. Thus, spectroscopic measurements, which typically require some knowledge of the electronic structure, can be especially difficult to interpret for molecules containing heavy atoms, whereas x-ray diffraction is especially well-suited for such samples.

3 Theory of TRXD

In this chapter, we will derive general formulas for TRXD, that is, we will investigate the scattering of x-ray pulses from a system that is just described by an abstract wave function, and interpret the results in the context of the Born-Huang representation.

The chapter can be understood as a supplement to paper 1, which itself draws on a previous article by my supervisors [25]. These two articles already introduce a self-contained description of TRXD, so I will mostly focus on what I consider the most important aspects of the formal theory. I will also adopt a number of simplifications that limit the range of validity of the derivation, but hopefully make the equations easier to read.

A proper derivation should generally use a density–operator formalism. With this formalism, we can describe the dynamics of complex quantum system and write them down with equally complex formulas. However, in an effort to make formulas simple, I drop this formalism in favor of a wave function formalism throughout this chapter. Also, it is difficult to measure for example decoherence effects, which would require a density–operator description, because of the properties of standard x-ray free electron lasers (coherence time of about 1 fs), so if we represent the system with a density operator, we can just sum up the signals of its eigenstates. When the wave function is factorized into a nuclear and electronic wave function, I will usually employ the Born–Oppenheimer approximation. Finally, I stick to the Schrödinger picture throughout the text.

We start with a formal introduction into time-independent x-ray diffraction in section 3.1, and continue with a discussion of elastic and inelastic scattering in section 3.2, which is identical in the time-dependent and time-independent context. This discussion forms the core content of paper 1. The chapter concludes with a brief derivation of the time-resolved diffraction signal in 3.3.

3.1 Introduction to time-independent x-ray diffraction

In a time-independent context, x-ray diffraction is usually derived from standard perturbation theory [5, 26]. The key idea is to rephrase the question "How many photons hit a given detector pixel?" in a more formal way. This is done by first defining a rate Γ for a transition from an initial state I to one or more final states F due to a perturbation (i.e., interaction Hamiltonian $\hat{H}_{\mathrm{int}}$), then choosing the states and the perturbation to reflect the diffraction of x-rays.

With some calculation, standard perturbation theory yields Fermi's Golden Rule, which in lowest order perturbation reads [26, 27]

$$\Gamma = \frac{2\pi}{\hbar} \sum_F |\langle F|\hat{H}_{\text{int}}|I\rangle|^2 \; \delta(E_F - E_I) \; . \tag{3.1}$$

Higher order perturbations can be included. However, they are usually only important for special diffraction schemes (see for example anomalous scattering further below), or they correspond to nonlinear scattering events that contribute only in the case of extreme photon fluxes or highly efficient scattering, both of which we will not discuss here.
As initial state, we choose a product of the studied system in some eigenstate ψ_i with energy ϵ_i, and an incoming photon with wave vector $\mathbf{k}_0$ and polarization ν_0,

$$|I\rangle = |\psi_i\rangle_{\text{S}}|\mathbf{k}_0, \nu_0\rangle_{\text{P}} \; . \tag{3.2}$$

The subscripts S, P denote the system and photon degrees of freedom, respectively.
In a similar way, each final state consists of the electronic system in some eigenstate ψ_f, and an outgoing photon that hits the detector pixel. That is, the photon has a wave vector $\mathbf{k}'_s$ with a certain direction and polarization ν_s

$$|F\rangle = |\psi_f\rangle_{\text{S}}|\mathbf{k}'_s, \nu_s\rangle_{\text{P}} \; . \tag{3.3}$$

The energies are then given by

$$E_F - E_I = \epsilon_f - \epsilon_i + \hbar(\omega'_s - \omega_0) \tag{3.4}$$

with $\omega'_s = k'_s c$. Inserting (3.2), (3.3) and (3.4) into (3.1), we obtain

$$\Gamma = \frac{2\pi}{\hbar} \sum_{f,\mathbf{k}'_s,\nu_s} \Big|\langle \mathbf{k}'_s, \nu_s|\langle\psi_f| \; \hat{H}_{\text{int}} \; |\psi_i\rangle_{\text{S}}|\mathbf{k}_0, \nu_0\rangle_{\text{P}}\Big|^2 \; \delta\Big[\epsilon_f - \epsilon_i + \hbar(\omega'_s - \omega_0)\Big] \; , \tag{3.5}$$

which is rather difficult to handle because of the awkward $\mathbf{k}'_s$-summation. To get rid of this, imagine that the detector pixel covers a solid angle $\Delta\Omega_{\text{pixel}}$ that is so small that the matrix elements do not vary noticeably. In this case, we could replace $\mathbf{k}'_s$ by a representative wave vector $\mathbf{k}_s$ in the direction Ω_{pixel} of the pixel, and the sum over $\mathbf{k}'_s$ by the number of outgoing photon modes that would hit the detector. More formally, we introduce a differential transition rate $\mathrm{d}\Gamma/\mathrm{d}\Omega$, and integrate it over the solid angle of the detector pixel

$$\Gamma = \int_{\text{pixel}} \frac{\mathrm{d}\Gamma}{\mathrm{d}\Omega}(\Omega) \; \mathrm{d}\Omega \approx \frac{\mathrm{d}\Gamma}{\mathrm{d}\Omega}(\Omega_{\text{pixel}}) \; \Delta\Omega_{\text{pixel}} \; . \tag{3.6}$$

Note further that in (3.4), the energy of the outgoing photon ω_s', and of the final state are coupled, so the outgoing photons can also have different energies. Repeating the same procedure, we can introduce a double-differential transition rate

$$\frac{\mathrm{d}\Gamma}{\mathrm{d}\Omega}(\Omega) = \int_{\omega_{\min}}^{\omega_{\max}} \frac{\mathrm{d}^2\Gamma}{\mathrm{d}\Omega \mathrm{d}\omega_s}(\Omega, \omega_s)\ \mathrm{d}\omega_s\ . \tag{3.7}$$

Here, $[\omega_{\min}, \omega_{\max}]$ is the range of angular frequencies that is accepted by the detector. The double-differential transition rate is then

$$\begin{aligned}\frac{\mathrm{d}^2\Gamma}{\mathrm{d}\Omega \mathrm{d}\omega_s}(\Omega, \omega_s) = \frac{2\pi}{\hbar}\rho(\Omega, \omega_s) \sum_{f,\nu_s} \Big| \langle \mathbf{k}_s, \nu_s | \langle \psi_f |\ \hat{H}_{\mathrm{int}}\ | \psi_i \rangle_{\mathrm{S}} | \mathbf{k}_0, \nu_0 \rangle_{\mathrm{P}} \Big|^2 \\ \times\, \delta\Big[\epsilon_f - \epsilon_i + \hbar(\omega_s - \omega_0)\Big]\ ,\end{aligned} \tag{3.8}$$

where $\mathbf{k}_s$ is the "representative" wave vector whose direction is given by the solid angle Ω, and whose length is determined by ω_s, and

$$\rho(\Omega, \omega_s)\mathrm{d}\Omega\mathrm{d}\omega_s = \frac{V}{(2\pi)^3 c^3}\omega_s^2 \mathrm{d}\Omega\mathrm{d}\omega_s \tag{3.9}$$

is the number of photon modes whose angular frequency and direction is in an infinitesimal region $\mathrm{d}\Omega\mathrm{d}\omega_s$. V is the quantization volume, and c the speed of light. In the following, I will always suppress the arguments of differential quantities. Also, since the transition rate for a given detector pixel is trivially related to the differential transition rate (3.6), we will continue studying only the latter.
The final ingredient for the calculation of the rates is the interaction Hamiltonian that tells about how the system proceeds from the initial to the final state. This requires a small detour before we assemble the final equations.

3.1.1 Matter-photon interaction

When treating the combined matter-photon system in non-relativistic theory, we can impose Coulomb gauge $\nabla_{\mathbf{x}} \hat{A}(\mathbf{x}) = 0$ on the electric field and obtain as starting point the minimal coupling Hamiltonian of the form [27]

$$\hat{H} = \sum_{\alpha=1}^{A} \frac{1}{2m_\alpha}\Big(\hat{\mathbf{p}}_\alpha - q_\alpha \hat{\mathbf{A}}(\hat{\mathbf{r}}_\alpha)\Big)^2 + V(\hat{\mathbf{r}}_1, \ldots, \hat{\mathbf{r}}_A) + \sum_{\mathbf{k},\nu} \hbar\omega_{\mathbf{k}}\ \hat{a}^\dagger_{\mathbf{k},\nu}\hat{a}_{\mathbf{k},\nu}\ . \tag{3.10}$$

In writing down the Hamiltonian, we have neglected the coupling between particle spins and photons. The first sum runs over all A charged particles with mass m_α and charge q_α, whose canonical momentum and coordinate operators are given as $\hat{\mathbf{p}}_\alpha$ and $\hat{\mathbf{r}}_\alpha$. The operators $\hat{a}^\dagger_{\mathbf{k},\nu}$ (/$\hat{a}_{\mathbf{k},\nu}$) are the creation (/annihilation) operators of a photon with polarization ν, wave vector $\mathbf{k}$ and corresponding angular frequency $\omega_{\mathbf{k}}$. The function V

contains all static Coulomb interactions between the charges, and $\hat{A}$ is the vector potential given by

$$\hat{\mathbf{A}}(\mathbf{x}) = \sum_{\mathbf{k},\nu} \mathbf{e}_{\mathbf{k},\nu} \sqrt{\frac{\hbar}{2\epsilon_0 V \omega_{\mathbf{k}}}} \left(\hat{a}_{\mathbf{k},\nu} \, \mathrm{e}^{\mathrm{i}\mathbf{k}\mathbf{x}} + \hat{a}^{\dagger}_{\mathbf{k},\nu} \mathrm{e}^{-\mathrm{i}\mathbf{k}\mathbf{x}} \right) . \tag{3.11}$$

$\mathbf{e}_{\mathbf{k},\nu}$ describes a unit vector in the polarization direction, and V is the cavity volume. If we expand the square, we can rewrite the Hamiltonian as

$$\hat{H} = \hat{H}_0 + \hat{H}_{\mathrm{int}} \ , \tag{3.12}$$

where

$$\hat{H}_0 = \sum_{\alpha=1}^{A} \frac{\hat{\mathbf{p}}_{\alpha}^2}{2m_{\alpha}} + V(\hat{\mathbf{r}}_1, \ldots, \hat{\mathbf{r}}_A) + \sum_{\mathbf{k},\nu} \hbar\omega_{\mathbf{k}} \, \hat{a}^{\dagger}_{\mathbf{k},\nu} \hat{a}_{\mathbf{k},\nu} \tag{3.13}$$

does not couple the photon and system degrees of freedom (i.e., forms the unperturbed Hamiltonian), and the interaction Hamiltonian reads

$$\hat{H}_{\mathrm{int}} = \sum_{\alpha=1}^{A} \left\{ \frac{q_{\alpha}^2}{2m_{\alpha}} \hat{\mathbf{A}}^2(\hat{\mathbf{r}}_{\alpha}) - \frac{q_{\alpha}}{m_{\alpha}} \hat{\mathbf{p}}_{\alpha} \hat{\mathbf{A}}(\hat{\mathbf{r}}_{\alpha}) \right\} . \tag{3.14}$$

Here, we used the Coulomb gauge to commute $\hat{\mathbf{p}}_{\alpha}$ and $\hat{A}(\hat{\mathbf{r}}_{\alpha})$. As first step in condensing the interaction Hamiltonian, we note that the prefactors of q/m and q^2/m are much larger for electrons than nuclei, so we can restrict the sum over the electrons only.
Let us consider the first term in (3.14). From (3.1) with the appropriately defined initial and final states, we can see that the interaction Hamiltonian has to remove the incoming and create the scattered photon to give a nonzero contribution to the transition rate. If we combine the $\mathbf{A}^2$-term with the definition (3.11), we can see that only those contributions survive that include one photon creation and one annihilation operator, so that we obtain for the first term

$$\begin{aligned} \hat{\mathbf{A}}^2(\hat{\mathbf{r}}_{\alpha}) &\longrightarrow \frac{\hbar}{2\epsilon_0 V} \sum_{\substack{\mathbf{k_1},\nu_1 \\ \mathbf{k_2},\nu_2}} \sqrt{\frac{1}{\omega_1 \omega_2}} \, \mathbf{e}_{\mathbf{k}_1,\nu_1} \mathbf{e}_{\mathbf{k}_2,\nu_2} \left(\hat{a}^{\dagger}_{\mathbf{k}_2,\nu_2} \hat{a}_{\mathbf{k}_1,\nu_1} + \hat{a}_{\mathbf{k}_1,\nu_1} \hat{a}^{\dagger}_{\mathbf{k}_2,\nu_2} \right) \mathrm{e}^{\mathrm{i}(\mathbf{k}_1 - \mathbf{k}_2)\hat{\mathbf{r}}_{\alpha}} \\ &= \frac{\hbar}{\epsilon_0 V} \sum_{\substack{\mathbf{k_1},\nu_1 \\ \mathbf{k_2},\nu_2}} \sqrt{\frac{1}{\omega_1 \omega_2}} \, \mathbf{e}_{\mathbf{k}_1,\nu_1} \mathbf{e}_{\mathbf{k}_2,\nu_2} \, \hat{a}^{\dagger}_{\mathbf{k}_2,\nu_2} \hat{a}_{\mathbf{k}_1,\nu_1} \mathrm{e}^{\mathrm{i}(\mathbf{k}_1 - \mathbf{k}_2)\hat{\mathbf{r}}_{\alpha}} + \sum_{\mathbf{k},\nu} \frac{\hbar}{2\epsilon_0 V \omega_{\mathbf{k}}} [\hat{a}_{\mathbf{k},\nu}, \hat{a}^{\dagger}_{\mathbf{k},\nu}] \ . \end{aligned} \tag{3.15}$$

The first sum represents a scattering event, where a photon with wave vector $\mathbf{k}_1$ and polarization ν_1 is transformed into a photon with wave vector $\mathbf{k}_2$ and polarization ν_2.

The second sum with the commutator adds an infinite contribution to all calculations. Since this contribution is an infinite, but constant number, independent of the exact photon or system state, we just discard it.
If we insert (3.11) into the second expression of (3.14), we get

$$\hat{\mathbf{p}}_\alpha \hat{\mathbf{A}}(\hat{\mathbf{r}}_\alpha) = \sum_{\mathbf{k},\nu} \sqrt{\frac{\hbar}{2\epsilon_0 V \omega_{\mathbf{k}}}}\, \hat{\mathbf{p}}_\alpha \mathbf{e}_{\mathbf{k},\nu} \left(\hat{a}_{\mathbf{k},\nu}\, \mathrm{e}^{\mathrm{i}\mathbf{k}\hat{\mathbf{r}}_\alpha} + \hat{a}^\dagger_{\mathbf{k},\nu}\, \mathrm{e}^{-\mathrm{i}\mathbf{k}\hat{\mathbf{r}}_\alpha} \right) . \tag{3.16}$$

The action of this operator on a given state (electron + electric field) can be described as follows: A photon is either created or destroyed ($\hat{a}^\dagger_{\mathbf{k},\nu}, \hat{a}_{\mathbf{k},\nu}$), the recoil is transferred to the electron ($\exp(\pm\mathrm{i}\mathbf{k}\hat{\mathbf{r}})$), and this process takes place preferably if the electron ends up with a large momentum along the photon's polarization vector ($\hat{\mathbf{p}}\mathbf{e}_{\mathbf{k},\nu}$).
This interaction has obvious importance for photoelectron spectroscopy. However, in a second-order perturbation, this process also contributes to scattering by first absorbing a photon, and later emitting a photon with a different wave vector, and is well-known under the term "anomalous scattering" (see, e.g., [28,29]). For small-angle scattering and within the independent atom model, it is formally included by augmenting the atomic form factor $f(\mathbf{q})$ from (2.26) with dispersion corrections f', f'' [26, 28, 29]

$$\tilde{f}(\mathbf{q}, \omega_0) = f(\mathbf{q}) + f'(\omega_0) + \mathrm{i} f''(\omega_0) , \tag{3.17}$$

which, for incident energies of typically about 10 keV and elements with $Z > 18$, modify the atomic form factors by a few percent. This is the same order of magnitude we would intuitively expect from the incorrect description of the electronic density of the valence electrons by the IAM, so we will also discard these terms.

3.1.2 Putting it all together

We can now insert the only remaining contribution of the interaction Hamiltonian from (3.15) into (3.8). Integrating over the photon coordinates gives $\mathbf{k}_1 = \mathbf{k}_0$, $\nu_1 = \nu_0$, $\mathbf{k}_2 = \mathbf{k}_s$ and $\nu_2 = \nu_s$. If we also clean up the prefactors, we obtain

$$\frac{\mathrm{d}^2\Gamma}{\mathrm{d}\Omega \mathrm{d}\omega_s} = \sigma_T\, \frac{\hbar c}{V}\, \frac{\omega_s}{\omega_0} \sum_f \left| \langle \psi_f |\, \hat{L}\, | \psi_i \rangle_S \right|^2 \delta\Big[\epsilon_f - \epsilon_i + \hbar(\omega_s - \omega_0) \Big] , \tag{3.18}$$

where σ_T is the Thomson cross section

$$\sigma_T = \left(\frac{e^2}{4\pi c^2 m_e \epsilon_0} \right)^2 \sum_{\nu_s} (\mathbf{e}_{\mathbf{k}_s,\nu_s} \mathbf{e}_{\mathbf{k}_0,\nu_0})^2 , \tag{3.19}$$

and the scattering operator

$$\hat{L} = \sum_\alpha \mathrm{e}^{\mathrm{i}\mathbf{q}\hat{\mathbf{r}}_\alpha} = \sum_\alpha \mathrm{e}^{\mathrm{i}\mathbf{q}\hat{\mathbf{r}}_\alpha} \tag{3.20}$$

has the form used in equation (2.19).

3.2 Elastic and inelastic scattering

In the literature that is concerned with theory of TRXD, one regularly finds as a critical point that x-ray diffraction can be elastic or inelastic [24,25,30,31]. This can be deduced from (3.18). In the case of elastic scattering, we have $\psi_f = \psi_i$, and consequently, through the delta-function $\omega_s = \omega_0$. However, there are no principal obstacles for having a different final state of the system (inelastic scattering), which leads to scattered x-ray photons with a different frequency than that of the incoming photons.
The same basic problem of whether x-ray diffraction is elastic or inelastic also occurs in the time-independent context, where we can treat the core problem without various complications arising from the time-dependent structure of the x-ray pulses from free electron lasers.
Technically, we start with (3.18), choose the ground state $\psi_i = \psi_0$ as initial state (i.e., neglect temperature for simplicity), and restrict the choice of final states to some subsets of all allowed states to arrive at scattering that leaves all quantum numbers intact (fully elastic scattering), does not change the electronic quantum number (electronically elastic scattering), or has no restrictions whatsoever (inelastic scattering).
I want to point out that this line of argument, going from elastic to inelastic scattering, is partly motivated by an article by Liu and Lin [32], which deals with the equivalent problem in ultrafast electron diffraction.

3.2.1 Purely elastic scattering

As a first step, let us assume that the scattering process does not change a single quantum number. In this case, the summation in (3.18) reduces to the case $f = i$. If we assume infinite boundaries for all practical purposes, the energy integration in (3.7) can be performed immediately, and we obtain apart from various constant prefactors

$$\frac{\mathrm{d}\Gamma_{\text{elastic}}}{\mathrm{d}\Omega} \cong \left| \langle \psi_0 |\ \hat{L}\ | \psi_0 \rangle_S \right|^2 . \tag{3.21}$$

To evaluate the bracket, we employ the Born-Oppenheimer approximation, and write the ground state of N nuclei and N_e electrons as

$$\psi_0(\mathbf{R}^{(3N)}, \mathbf{r}^{(3N_e)}) = \Lambda_0(\mathbf{R}^{(3N)}) \lambda_0(\mathbf{r}^{(3N_e)}; \mathbf{R}^{(3N)}) . \tag{3.22}$$

The integration over the electronic coordinates can be evaluated with the independent atom model (see section 2.2), and produces the molecular form factor F of (2.23). We write out the integration over the nuclear coordinates to obtain

$$\begin{aligned} \frac{\mathrm{d}\Gamma_{\text{elastic}}}{\mathrm{d}\Omega} &\cong \left| \int \mathrm{d}^{3N} R\ |\Lambda_0(\mathbf{R}^{(3N)})|^2 F(\mathbf{q}; \mathbf{R}^{(3N)}) \right|^2 \\ &= \int \mathrm{d}^{3N} R_1 \int \mathrm{d}^{3N} R_2\ |\Lambda_0(\mathbf{R}_1^{(3N)})|^2\ |\Lambda_0(\mathbf{R}_2^{(3N)})|^2 F^*(\mathbf{q}; \mathbf{R}_1^{(3N)}) F(\mathbf{q}; \mathbf{R}_2^{(3N)}) . \end{aligned} \tag{3.23}$$

We can immediately see that this equation is too complex for practical use. Instead of obtaining information about $|\Lambda_0|^2$ (i.e., the probability density of finding certain nuclear arrangements), we get an expression resembling some correlation function that is much harder to invert. We conclude that purely elastic scattering is not what we are looking for.

3.2.2 Electronically elastic scattering

As a next step, we can assume that the electronic quantum number is not changed by the scattering event, but all the other (vibrational, rotational, etc.) quantum numbers associated with the nuclear wave function may change freely, that is, we allow all final states of the type

$$\psi_f(\mathbf{R}^{(3N)}, \mathbf{r}^{(3N_e)}) = \Lambda_f(\mathbf{R}^{(3N)})\lambda_0(\mathbf{r}^{(3N_e)}; \mathbf{R}^{(3N)}) \tag{3.24}$$

in the summation (3.18), where Λ_f is a solution of the time-independent Schrödinger equation using the electronic ground state surface. Combining this with the integration in (3.7), and dropping uninteresting prefactors gives us for the differential transition rate

$$\frac{\mathrm{d}\Gamma}{\mathrm{d}\Omega} \cong \int_{\omega_{\min}}^{\omega_{\max}} \mathrm{d}\omega_s \; \frac{\omega_s}{\omega_0} \sum_f \Big| \langle \psi_f | \hat{L} | \psi_0 \rangle_S \Big|^2 \; \delta\Big[\epsilon_f - \epsilon_i + \hbar(\omega_s - \omega_0)\Big] \; . \tag{3.25}$$

Let us further assume that we collect all photons. Formally, we can set $\omega_{\min} \to -\infty$, $\omega_{\max} \to \infty$, and the integration effectively fixes the value of ω_s to some value $\omega_s(f)$ depending on the final state through the delta-function. If we then write out the integration over the nuclear coordinates, we obtain

$$\begin{aligned} \frac{\mathrm{d}\Gamma_{\text{el. elastic}}}{\mathrm{d}\Omega} \cong \int \mathrm{d}^{3N}R_1 \int \mathrm{d}^{3N}R_2 \; \Lambda_0^*(\mathbf{R}_1^{(3N)}) \sum_f \Lambda_f(\mathbf{R}_1^{(3N)}) \Lambda_f^*(\mathbf{R}_2^{(3N)}) \Lambda_0(\mathbf{R}_2^{(3N)}) \\ \times \frac{\omega_s(f)}{\omega_0} \; F^*(\mathbf{q}; \mathbf{R}_1^{(3N)}) F(\mathbf{q}; \mathbf{R}_2^{(3N)}) \end{aligned} \tag{3.26}$$

Note that the scattering vector $\mathbf{q}$ depends in principle on the final state ψ_f through the value of $\omega_s(f)$. However, for highly excited final states, the overlap $\Lambda_0^*\Lambda_f$ becomes negligible. Thus, the dominant contribution to the transition rate comes from states with low excitation energies, which for nuclear excitation means that $\epsilon_f - \epsilon_i$ is of the order 1 eV or less, and much smaller than the photon energy $\hbar\omega_0 \approx 10$ keV. We can ignore these problems, and set $\omega_s(f) \approx \omega_0$ for all purposes to obtain

$$\frac{\mathrm{d}\Gamma_{\text{el. elastic}}}{\mathrm{d}\Omega} \cong \int \mathrm{d}^{3N}R \; |\Lambda_0(\mathbf{R}^{(3N)})|^2 \; |F(\mathbf{q}; \mathbf{R}^{(3N)})|^2 \; . \tag{3.27}$$

The states Λ_f form a complete basis in the space of the functions of the nuclear coordinates, so the summation produces a delta-function that simplifies the result.
Equation (3.27) has a form similar to (2.15), and allows us in principle to reconstruct the nuclear density $|\Lambda_0|^2$ from the diffraction pattern. However, while the theoretical interpretation is simple, it is rather difficult to do electronically elastic scattering in practice.
One problem is that if we impose a separation of the electronic and vibrational energy scales, we exclude systems with close-lying potential energy surfaces, NaI being a simple example, especially when we later go on to time-resolved diffraction. Furthermore, once we assume that inelastic x-ray scattering is possible, there is no physical basis for assuming that the electronic quantum number must be preserved, as we have done in (3.24). In fact, tabulations for single atoms show that electronically inelastic components can dominate for large scattering angles [33].
So the electronic elasticity must be ensured by the experimental setup. If we now assume that there is an energy gap between vibrational, rotational etc. excitation on one side ($\Delta\epsilon \ll 1$ eV), and electronic excitation on the other side ($\Delta\epsilon > 1$ eV), we can choose to collect only photons from electronically elastic scattering events.
For this, we first monochromatize the incoming beam, so that the energy spread of the incoming photons is well below the electronic excitation energy. After the scattering region, we monochromatize again, and cherry-pick all photons whose energy deviates from that of the incoming beam by less than 1 eV. Through the delta function of (3.18), we are then guaranteed that we collected only data from electronically elastic scattering. The main drawback of this method, though, is a huge loss of photon flux.
To monochromatize an x-ray beam, it is usually scattered from a crystal [5]. For each photon energy, there exist certain outgoing wave vectors where the Bragg condition is fulfilled, and photons with this energy are scattered with a large cross section. We can then put our sample or detector at the corresponding position. There are two loss mechanisms here. First, we loose a lot of photons that are scattered in the "wrong" directions. Second, if we monochromatize the photons after they hit the target, we can only tune the monochromator to photons scattered in a certain direction; this setup is incompatible with a pixelated area detector. Both mechanism lead to a loss of flux of several orders of magnitude, which is why this setup is hardly used in practice. [1]
To fix this inconsistency requires us to allow for electronically inelastic scattering events as well, which is what we do next.

3.2.3 Inelastic scattering

For the most general treatment, we allow *all* possible final states in the summation of (3.18). Inserting again (3.18) into (3.7), we obtain (3.25), only with the summation running over all states.

[1] Such a setup is, however, used in the context of non-resonant inelastic x-ray scattering, see for example [34, 35]. Although interesting in itself, it requires a different approach in theory and experiment, so we will not discuss this technique further.

We first assume again that we accept all scattered photons irrespective of their frequency, that is, we set $\omega_{\min} \to -\infty$ and $\omega_{\max} \to \infty$. At this point, we note again that the vectors $\mathbf{k}_s$ point into the same direction Ω, and their lengths depend on the exact excitation in question through the delta function. As a consequence, the vector $\mathbf{q}$ hidden in the scattering operator $\hat{L}$ also depends on the final state f.
However, we can assume that all important inelastic scattering events have excitation energies that are small compared to $\hbar\omega_0$, and set for all practical purposes $\omega_s \approx \omega_0$. This is the widely-used "static approximation" [36]; as with the independent atom model, it is rather difficult to quantify the approximation properly. The problem is that the range of accessible final states and the relation $\mathbf{q}(\omega_s)$ depend on the scattering angle in a non-trivial manner. A not too conclusive attempt is done in appendix B of paper 1.
If we adopt this approximation, (3.25) condenses to

$$\begin{aligned}\frac{\mathrm{d}\Gamma_{\text{inelastic}}}{\mathrm{d}\Omega} &\cong \sum_f |\langle\psi_f|\,\hat{L}\,|\psi_0\rangle_S|^2 = \langle\psi_0|\,\hat{L}^\dagger\hat{L}\,|\psi_0\rangle_S \\ &= \int \mathrm{d}^{3N}R\;|\Lambda_0(\mathbf{R}^{(3N)})|^2\;\langle\lambda_0(\mathbf{R}^{(3N)}|\,\hat{L}^\dagger\hat{L}\,|\lambda_0(\mathbf{R}^{(3N)}\rangle_{\mathbf{r}}\;, \end{aligned} \tag{3.28}$$

where we first exploited the completeness of the set of states ψ_f, and then used the Born-Oppenheimer approximation. Formally, this is similar to the result from electronically elastic scattering, but with a difficult to handle two-electron operator.
However, as is shown in greater detail in appendix B of paper 1, within the independent atom model, these matrix elements reduce to the ordinary squared form factor $\langle\lambda_0|\,\hat{L}^\dagger\hat{L}|\lambda_0\rangle_{\mathbf{r}} \approx |\langle\lambda_0|\,\hat{L}|\lambda_0\rangle_{\mathbf{r}}|^2$ apart from two correction terms. The first correction is independent of the position of the atoms, and can be removed by difference diffraction techniques, while the magnitude of the second term depends on the overlap between occupied atomic orbitals around different atoms; since we assumed this overlap to be small when introducing the IAM, it is only consistent to neglect this term as well.
In consequence, we arrive at the same expression as the one we obtained for electronically elastic scattering, but without the problems with the experimental design. However, while this whole derivation might seem like a purely academic exercise, we have to keep in mind that the two formulations are only equal within the IAM! As soon as we go beyond this model, for example, when imaging atomic orbitals with x-rays [37], we either have to impose electronically elastic scattering conditions, or we need to treat the explicit two-particle operator.

3.3 Time-dependent theory

Here, I will briefly write down the derivation of the time-resolved diffraction signal. Although, as mentioned before, reference [25] and paper 1 have essentially the same content, I redo the derivation here for several reasons:

1. With the time-independent treatment already laid out, it is possible to derive an

expression for the signal in a more compact way than what is scattered over the two articles.

2. Both articles use a slightly different notation. For example, the definition of the intensity in [25] deviates from that used in paper 1.

3. There are some minor improvements one can do over the references. For example, it is possible to extend the treatment to more general photon states. Also, some of the approximations (for example, that of evaluating the field only at the position of the sample) can be introduced in a more thorough way.

3.3.1 Introduction

Before we start with the derivation in terms of formulas, it might be helpful to first specify which type of experiments we have in mind; after all, the choice of the experimental setup strongly determines which approximations we will use.
The basic pump–probe setup is shown in figure 3.1. In addition to the experimental layout, we will assume that the sample consists of many identical quantum systems, such as one can find in solutions or molecular beams.
The general idea is the same as before: We want to calculate how many photons hit a given detector pixel. By analogy to the time-independent case, we can introduce a double-differential signal as the number of photons scattered into a certain solid angle with a given angular frequency, which reads

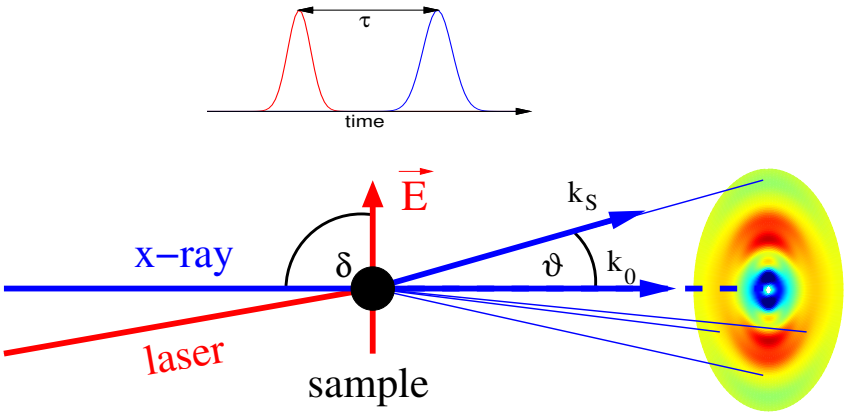

Figure 3.1: Scheme of the experimental setup. An optical pump laser brings the sample into an excited state. After a tunable delay time τ, an x-ray pulse is scattered from the sample, and produces a diffraction pattern. Also included are several angles mainly used in section 4.4.

$$\frac{\mathrm{d}^2 S}{\mathrm{d}\Omega \mathrm{d}\omega_s} = \rho(\omega_s) \lim_{\substack{t\to\infty \\ t_0\to-\infty}} \langle \Xi(t_0)|\hat{U}^\dagger(t,t_0) \sum_{\nu_s} \hat{a}^\dagger_{\mathbf{k}_s,\nu_s} \hat{a}_{\mathbf{k}_s,\nu_s} \hat{U}(t,t_0)|\Xi(t_0)\rangle \ . \tag{3.29}$$

The formula reads as follows: At some time t_0 prior to the scattering, we have an initial state Ξ that consists of our sample, and the x-ray pulse moving towards the sample. We let this state evolve in time, denoted by the time evolution operator $\hat{U}$, and after what is for all practical purposes an infinite time, we measure how many scattered photons with wave vector $\mathbf{k}_s$ and polarization ν_s have been created. Here, we do not care about the polarization of the scattered photons. Finally, we multiply this by the density of photon modes ρ from (3.9) to get the signal per solid angle and final frequency.
To convert (3.29) into something more instructive, we next introduce the initial state and the time evolution operator in some more detail, then we will integrate over the photon degrees of freedom, which leaves us with some simple functions that describe the x-ray pulse. Some further algebraic manipulations lead us to the final result.

3.3.2 The initial state

The initial state is a product of the sample in some state state ψ, and an x-ray pulse η on its way to the target,

$$|\Xi(t_0)\rangle = |\psi(t_0)\rangle_S |\eta(t_0)\rangle_P \ . \tag{3.30}$$

At this point, we can assume a rather general x-ray pulse that is only characterized by a few properties.
First, we assume that η has a definite polarization ν_0. This is purely for convenience; the polarization will eventually be hidden in the Thomson cross section, which allows an easy extension to unpolarized pulses. Second, the pulse does not contain the scattered photon mode, that is $\hat{a}_{\mathbf{k}_s,\nu_s}|\eta(t)\rangle = 0$. Finally, we assume that the pulse is approximately a monochromatic plane wave. The European XFEL, for example, has a small divergence on the order of 1μrad, and a spectral bandwidth of the order of 10^{-4} [13]. Consequently, for photon modes $\mathbf{k}$ contributing appreciably to η, we will occasionally do the replacements

$$\mathbf{e}_{\mathbf{k},\nu_\mathbf{0}} \approx \mathbf{e}_{\mathbf{k}_0,\nu_0} \qquad \omega_\mathbf{k} \approx \omega_0 \qquad \mathbf{k} \approx \mathbf{k}_0 \ , \tag{3.31}$$

where $\mathbf{k}_0$ is the central wave vector, and $\omega_0 = ck_0$ the corresponding angular frequency.

3.3.3 The propagator

Following standard perturbation theory [18, 38], we separate the Hamiltonian $\hat{H}$ into a noninteracting part $\hat{H}_0$ and an interacting part $\hat{H}_{\mathrm{int}}$, and write the time evolution operator as an expansion in powers of $\hat{H}_{\mathrm{int}}$

$$\hat{U}(t,t_0) \approx \hat{U}_0(t-t_0) - \frac{\mathrm{i}}{\hbar}\int_{t_0}^{t} \mathrm{d}t'\ \hat{U}_0(t-t')\hat{H}_{\mathrm{int}}(t')\hat{U}_0(t'-t_0)$$
$$- \frac{1}{\hbar^2}\int_{t_1}^{t}\mathrm{d}t_2\int_{t_0}^{t}\mathrm{d}t_1\ \hat{U}_0(t-t_2)\hat{H}_{\mathrm{int}}(t_2)\hat{U}_0(t_2-t_1)\hat{H}_{\mathrm{int}}(t_1)\hat{U}_0(t_1-t_0)+\cdots\ , \quad (3.32)$$

where $\hat{U}_0(t_2,t_1)$ is the propagator that propagates the noninteracting system from t_1 to t_2, and can be further decomposed into the propagator of the system and the photon state

$$\hat{U}_0(t,t_0) = \hat{U}_P(t,t_0)\hat{U}_S(t,t_0) = \mathrm{e}^{-\mathrm{i}\hat{H}_P(t-t_0)/\hbar}\,\mathcal{T}\mathrm{e}^{-\mathrm{i}\int_{t_0}^{t}\hat{H}_S(t')\mathrm{d}t'/\hbar}\ . \quad (3.33)$$

$\mathcal{T}$ denotes the time-ordering operator, and the operators have been mostly introduced in section 3.1.1 as

$$\hat{H}_S(t) = \sum_{\alpha=1}^{A}\frac{\hat{\mathbf{p}}_\alpha^2}{2m_\alpha} + V(\hat{\mathbf{r}}_1,\ldots,\hat{\mathbf{r}}_A) + \hat{W}(\hat{\mathbf{r}}_1,\ldots,\hat{\mathbf{r}}_A,t) \quad (3.34)$$

$$\hat{H}_P = \sum_{\mathbf{k},\nu}\hbar\omega_{\mathbf{k}}\ \hat{a}^\dagger_{\mathbf{k},\nu}\hat{a}_{\mathbf{k},\nu} \quad (3.35)$$

$$\hat{H}_{\mathrm{int}} = \frac{\hbar}{\epsilon_0 V}\sum_{\substack{\mathbf{k_1},\nu_1\\ \mathbf{k_2},\nu_2}}\sqrt{\frac{1}{\omega_1\omega_2}}\ \mathbf{e}_{\mathbf{k}_1,\nu_1}\mathbf{e}_{\mathbf{k}_2,\nu_2}\ \hat{a}^\dagger_{\mathbf{k}_2,\nu_2}\hat{a}_{\mathbf{k}_1,\nu_1}\mathrm{e}^{\mathrm{i}(\mathbf{k}_1-\mathbf{k}_2)\hat{\mathbf{r}}_\alpha}\ . \quad (3.36)$$

The new operator $\hat{W}$ describes the action of the pump pulse on the sample. It is necessary to explicitly include this term since, in contrast to [25], we place our start time t_0 now at $-\infty$.
Furthermore, if we measure the scattered x-ray photons away from the beam direction, we need to convert the incoming photons at some point into scattered photons. Since the non-interacting contribution $\hat{U}(t,t_0)$ does not do this, it gives no contribution to the cross section, and we can drop it.
Making use of these simplifications, and keeping only the first order of the interaction in (3.32), we can finally replace the propagator in (3.29)

$$\hat{U}(t,t_0) \longrightarrow -\frac{\mathrm{i}}{\hbar}\int_{t_0}^{t}\mathrm{d}t'\ \hat{U}_P(t,t')\hat{U}_S(t,t')\,\hat{H}_{\mathrm{int}}\,\hat{U}_P(t',t_0)\hat{U}_S(t',t_0)\ . \quad (3.37)$$

Note that the interaction Hamiltonian removes a single photon from one of the modes of the incoming beam, and creates one new photon in some other mode. That is, if we apply the propagator (3.37) on the initial state (3.30), we get a final state at time t that contains at most one scattered x-ray photon.

This forms the underlying approximation, that the quantum system creates on average less than one scattered photon. The equations we will derive are therefore only valid in the limit of sufficiently low intensity. If we want more scattered photons, we can add more quantum systems (gas phase or solute molecules); for sufficiently low densities, they do not interfere with each other, and we can just add the signal from the single molecules. We can always check that this approximation is fulfilled by requiring

$$\int \mathrm{d}\Omega \int \mathrm{d}\omega_s \, \frac{\mathrm{d}^2 S}{\mathrm{d}\Omega \mathrm{d}\omega_s} < 1 \; . \tag{3.38}$$

3.3.4 Removing the photon brackets

If we insert (3.9), (3.30), (3.37) into (3.29), we obtain after some manipulations

$$\frac{\mathrm{d}^2 S}{\mathrm{d}\Omega \mathrm{d}\omega_s} = \sigma_T \, \frac{c}{2\pi V} \, \frac{\omega_s}{\omega_0} \int_{-\infty}^{\infty} \mathrm{d}T \int_{-\infty}^{\infty} \mathrm{d}\delta \; \mathrm{e}^{-\mathrm{i}\omega_s \delta} \; g_{\mathbf{R}}(T,\delta) \\ \times \langle \psi(T+\frac{\delta}{2})| \; \hat{L}^\dagger \, \hat{U}(T+\frac{\delta}{2}, T-\frac{\delta}{2}) \, \hat{L} \; |\psi(T-\frac{\delta}{2})\rangle_S \; . \tag{3.39}$$

σ_T is the Thomson cross section of (3.19), and $\mathbf{R}$ is the position of the sample. Furthermore, we used the shorthand notation $|\psi(t)\rangle = \hat{U}_S(t,t_0)|\psi(t_0)\rangle$, and

$$g_{\mathbf{R}}(T,\delta) = \langle \eta(T)| \sum_{\mathbf{k}_1} \hat{a}^\dagger_{\mathbf{k}_1,\nu_0} \mathrm{e}^{-\mathrm{i}\mathbf{k}_1\mathbf{R}} \sum_{\mathbf{k}_2} \hat{a}_{\mathbf{k}_2,\nu_0} \mathrm{e}^{\mathrm{i}\mathbf{k}_2\mathbf{R}} \; \mathrm{e}^{\mathrm{i}\frac{\omega_1+\omega_2}{2}\delta} |\eta(T)\rangle_P \tag{3.40}$$

with a similar definition for $\eta(t)$.
In deriving this result so far, we used a couple of approximations. First, for each mode $\mathbf{k}$ that contributes to η, we replaced $\sqrt{1/\omega_{\mathbf{k}}} \approx \sqrt{1/\omega_0}$, and $\mathbf{e}_{\mathbf{k},\nu_0} \approx \mathbf{e}_{\mathbf{k}_0,\nu_0}$. Then, for each such mode, we assumed

$$\mathrm{e}^{\mathrm{i}(\mathbf{k}-\mathbf{k}_0)\hat{\mathbf{r}}_\alpha} |\psi(t)\rangle_S = \mathrm{e}^{\mathrm{i}(\mathbf{k}-\mathbf{k}_0)\hat{\mathbf{R}}_s} \mathrm{e}^{\mathrm{i}(\mathbf{k}-\mathbf{k}_0)(\hat{\mathbf{r}}_\alpha - \hat{\mathbf{R}}_s)} |\psi(t)\rangle_S \\ \approx \mathrm{e}^{\mathrm{i}(\mathbf{k}-\mathbf{k}_0)\hat{\mathbf{R}}_s} |\psi(t)\rangle_S \approx |\psi(t)\rangle_S \mathrm{e}^{\mathrm{i}(\mathbf{k}-\mathbf{k}_0)\mathbf{R}} \; . \tag{3.41}$$

$\hat{\mathbf{R}}_s$ denotes some degree of freedom that describes the location of the system (e.g., the nuclear center of mass of a molecule), and commutes with the electronic operator $\hat{\mathbf{r}}_\alpha$.
The physical content of this approximation is the assumption that the typical spatial variation of the x-ray pulse, approximately given by $2\pi/\max(|\mathbf{k}-\mathbf{k}_0|)$, is much larger than the extension of the system, which is roughly what we get from applying the operator $\hat{\mathbf{r}}_\alpha - \hat{\mathbf{R}}_s$ to the state ψ. If we further assume that the system is confined to some small region around $\mathbf{R}$, we can replace the operator by this vector (it is also possible to integrate out the coordinate $\mathbf{R}_s$ explicitly, but we do not do this here for simplicity).

To arrive at the formulation (3.40), we used

$$\mathrm{e}^{\mathrm{i}\hat{H}_P t/\hbar}\ \hat{a}_{\mathbf{k},\nu}\ \mathrm{e}^{-\mathrm{i}\hat{H}_P t/\hbar} = \hat{a}_{\mathbf{k},\nu}\mathrm{e}^{-\mathrm{i}\omega_{\mathbf{k}} t}\ , \tag{3.42}$$

and a similar equation for $\hat{a}^\dagger_{\mathbf{k},\nu}$. This equation can be easily verified by applying the left and right hand side of (3.42) to an arbitrary photon number state.
Finally, if t_1, t_2 are the time integration variables when inserting (3.37) into (3.29), we made a transformation

$$T = \frac{t_1 + t_2}{2} \qquad\qquad \delta = t_1 - t_2\ . \tag{3.43}$$

It should be pointed out that up to normalization issues, $g_{\mathbf{R}}$ is related to the first-order coherence function of the x-ray pulse [39]. However, we mostly do not need to dwell explicitly on this relation, and will discuss the important properties in the next section. After that, we go back to (3.39). It would seem as if the details of the function $g_{\mathbf{R}}$, especially its dependence on δ have a major impact on the way the signal looks like. However, for all but a few exotic cases, we can show that using the inelastic limit of x-ray diffraction washes out all details.

3.3.5 Properties of the photon state

Now let us have a deeper look at the function $g_{\mathbf{R}}(T, \delta)$. The intensity of the approximately plane wave η at position $\mathbf{R}$ and time t is given by [39]

$$I'(\mathbf{R}, t) = \frac{c}{V}\langle\eta(t)|\ \sum_{\mathbf{k}_1}\sqrt{\hbar\omega_{\mathbf{k}_1}}\hat{a}^\dagger_{\mathbf{k}_1,\nu_0}\mathrm{e}^{-\mathrm{i}\mathbf{k}_1\mathbf{R}}\sum_{\mathbf{k}_2}\sqrt{\hbar\omega_{\mathbf{k}_2}}\hat{a}_{\mathbf{k}_2,\nu_0}\mathrm{e}^{\mathrm{i}\mathbf{k}_2\mathbf{R}}\ |\eta(t)\rangle_P\ . \tag{3.44}$$

If we approximate again $\omega_{\mathbf{k}_1} \approx \omega_{\mathbf{k}_2} \approx \omega_0$, and compare (3.44) with (3.40), we find for the photon number intensity

$$I(\mathbf{R}, t) \approx \frac{I'(\mathbf{R}, t)}{\hbar\omega_0} = \frac{c}{V}\ g_{\mathbf{R}}(t, 0)\ . \tag{3.45}$$

For the further manipulations, it will be more convenient to write

$$g_{\mathbf{R}}(T, \delta) = \frac{V}{c}\ I(\mathbf{R}, T)C(T, \delta)\ , \tag{3.46}$$

where $C(T, 0) = 1$. Correspondingly, the Fourier-transform

$$C_{\mathrm{F}}(T, \omega) = \frac{1}{2\pi}\int_{-\infty}^{\infty}\mathrm{d}\delta C(T, \delta)\ \mathrm{e}^{-\mathrm{i}\omega\delta} \tag{3.47}$$

is a normalized function $\int \mathrm{d}\omega C_\mathrm{F}(T,\omega) = 1$, and from (3.40) and the properties of η, we can determine that it is strongly localized at $\omega = \omega_0$.
A last point that we will not prove is that $C(T,\delta)$ typically decays within some coherence time δ_c. This is in line with other derivations [24,25,30], which also assume that $C(T,\delta)$ is a coherence function independent of T.

3.3.6 Final result

To cast (3.39) into a different form, we now assume that the system's time evolution for the typical durations δ can be approximated by that of a time-independent system,

$$\hat{U}_S(T+\frac{\delta}{2}, T-\frac{\delta}{2}) \approx \mathrm{e}^{-\mathrm{i}\hat{H}_\mathrm{eff}(T)\delta/\hbar} \ . \tag{3.48}$$

with an "effective Hamiltonian" $\hat{H}_\mathrm{eff}$. This holds obviously if the preparation of the system and the scattering of the x-rays are well separated in time. Otherwise, we need to assume adiabatic conditions, possibly combined with, e.g., Floquet theory (see appendix A of paper 1). We can then expand the wave function in eigenstates of $\hat{H}_\mathrm{eff}$

$$|\psi(T+\delta)\rangle = \sum_i c_i(T)\ |\psi_i(T)\rangle\ \mathrm{e}^{-\mathrm{i}E_i(T)\delta/\hbar} \ , \tag{3.49}$$

$$\text{where} \qquad \hat{H}_\mathrm{eff}(T)|\psi_i(T)\rangle = E_i(T)\,|\psi_i(T)\rangle \ . \tag{3.50}$$

If we insert this into (3.39), and integrate over ω_s to get the differential signal strength, some algebra gives us

$$\begin{aligned}\frac{\mathrm{d}S}{\mathrm{d}\Omega} = \sigma_T \int_{-\infty}^{\infty} \mathrm{d}T\ I(\mathbf{R},T) \sum_{i,j,k} c_i^*(T)c_j(T) \int_{\omega_\mathrm{min}}^{\omega_\mathrm{max}} \mathrm{d}\omega_s\ \frac{\omega_s}{\omega_0} \\ \times \langle\psi_i(T)|\,\hat{L}^\dagger\,|\psi_k(T)\rangle_S \langle\psi_k(T)|\,\hat{L}\,|\psi_j(T)\rangle_S\ C_\mathrm{F}\Big(T, \frac{1}{\hbar}\Big[E_k - \frac{E_i+E_j}{2}\Big] + \omega_s\Big) \ .\end{aligned} \tag{3.51}$$

Note that the whole integration over ω_s is similar to (3.25). Instead of a delta-function, we have a function C_F that is only relevant for frequency arguments close to ω_0; instead of eigenstates of the unperturbed Hamiltonian we have introduced parametric eigenstates, and we can have contribution from coherence terms $i \neq j$.
Since $C_\mathrm{F}(T,\omega)$ is strongly localized around $\omega = \omega_0$, the integrand is only different from zero for $1/\hbar[E_k - (E_i+E_j)/2] + \omega_s = \omega_0$. If we further apply the static approximation from section 3.2.3 that the brackets are negligible unless $E_k - (E_i+E_j)/2 \ll \hbar\omega_0$, the ω_s-integration only gives a contribution for $\omega_s \approx \omega_0$.
Consequently, we can set $\omega_s/\omega_0 \approx 1$, assume that $\mathbf{q}$, and thus $\hat{L}$, is independent of ω_s, and move the brackets out of the integration to get

$$\frac{\mathrm{d}S}{\mathrm{d}\Omega} = \sigma_T \int_{-\infty}^{\infty} \mathrm{d}T\ I(\mathbf{R},T) \sum_{i,j,k} c_i^*(T) c_j(T) \langle\psi_i(T)|\, \hat{L}^\dagger\, |\psi_k(T)\rangle_S \langle\psi_k(T)|\, \hat{L}\, |\psi_j(T)\rangle_S \times \int_{\omega_{\min}}^{\omega_{\max}} \mathrm{d}\omega_s\ C_{\mathrm{F}}\left(T, \frac{1}{\hbar}\Big[E_k - \frac{E_i+E_j}{2}\Big] + \omega_s\right) . \quad (3.52)$$

If the range $[\omega_{\min}, \omega_{\max}]$ is large enough to contain the dominant part of C_{F} for all contributing i, j, k, we can approximate

$$\int_{\omega_{\min}}^{\omega_{\max}} C_{\mathrm{F}}\left(T, \frac{1}{\hbar}\Big[E_k - \frac{E_i+E_j}{2}\Big] + \omega_s\right) \approx \int_{-\infty}^{\infty} \mathrm{d}\omega_s\ C_{\mathrm{F}}(T,\omega_s) = 1 \quad (3.53)$$

independent of the value of i, j, k. After this, we can piece the system's wave function together again, and remove the summation over k, which just gives a 1, to obtain

$$\frac{\mathrm{d}S}{\mathrm{d}\Omega} = \sigma_T \int_{-\infty}^{\infty} \mathrm{d}T\ I(\mathbf{R},T) \langle\psi(T)|\, \hat{L}^\dagger \hat{L} |\psi(T)\rangle_S\ . \quad (3.54)$$

By introducing the Born-Huang representation (2.3), and integrating explicitly over the nuclear coordinates, we get

$$\frac{\mathrm{d}S}{\mathrm{d}\Omega} = \sigma_T \int_{-\infty}^{\infty} \mathrm{d}T\ I(\mathbf{R},T) \times \sum_{i,j} \int \mathrm{d}^{3N}R\ \Lambda_i^*(\mathbf{R}^{(3N)},T) \Lambda_j(\mathbf{R}^{(3N)},T) \langle\lambda_i(\mathbf{R}^{(3N)})|\, \hat{L}^\dagger \hat{L} |\lambda_j(\mathbf{R}^{(3N)}\rangle_{\mathbf{r}}\ . \quad (3.55)$$

The electronic matrix elements with $i = j$ can be converted into the squared molecular form factor as detailed in section 3.2.3. The non-diagonal elements $i \neq j$ can be neglected; in a Hartree-Fock world and a second quantization description, at least one of the two creation/annihilation pairs that make up the operator $\hat{L}^\dagger \hat{L}$ has to transfer an electron from one fixed orbital to another one (see also appendix B in paper 1), which gives less terms and thus negligible weight in the summation.
As a final step, we can reorganize the terms, and normalize the signal to obtain the differential cross-section

$$\frac{\mathrm{d}\sigma}{\mathrm{d}\Omega} = \frac{1}{I_0}\ \frac{\mathrm{d}S}{\mathrm{d}\Omega} = \sigma_T \int \mathrm{d}^{3N}R\ \bar{\varrho}(\mathbf{R}^{(3N)}) \Big| F(\mathbf{q};\mathbf{R}^{(3N)}) \Big|^2\ , \quad (3.56)$$

where the time-averaged nuclear density is

$$\bar{\varrho}(\mathbf{R}^{(3N)}) = \int \mathrm{d}T\ \frac{I(\mathbf{R},T)}{I_0} \sum_i \Big| \Lambda_i(\mathbf{R}^{(3N)},T) \Big|^2 \quad (3.57)$$

has the exact interpretation of the probability density of finding a system described by the coordinates $\mathbf{R}^{(3N)}$, averaged over the x-ray pulse, and $I_0 = \int \mathrm{d}T\ I(\mathbf{R}, T)$ is the number of photons that hit the sample.
Note, however, that (3.56) only holds up to terms independent of the nuclear geometry. To get rid of these terms, we illuminate two samples with an identical x-ray pulse, one with a pump laser turned on, giving an averaged density $\bar{\varrho}^{(\mathrm{on})}$, and one without a pump laser, giving $\bar{\varrho}^{(\mathrm{off})}$. By subtracting the resulting diffraction patterns, all these additional terms cancel, and we get for the difference cross section

$$\Delta\frac{\mathrm{d}\sigma}{\mathrm{d}\Omega} = \frac{\mathrm{d}\sigma^{(\mathrm{on})}}{\mathrm{d}\Omega} - \frac{\mathrm{d}\sigma^{(\mathrm{off})}}{\mathrm{d}\Omega} = \sigma_T \int \mathrm{d}^{3N}R\ \Delta\bar{\varrho}(\mathbf{R}^{(3N)}, \tau)\left|F(\mathbf{q}; \mathbf{R}^{(3N)})\right|^2 , \tag{3.58}$$

where we introduce the averaged difference density $\Delta\bar{\varrho} = \bar{\varrho}^{(\mathrm{on})} - \varrho^{(\mathrm{off})}$ of finding a certain nuclear geometry $\mathbf{R}^{(3N)}$. In practice, we repeat the diffraction with multiple delay times τ between the pump pulse and the x-ray probe, which can be trivially incorporated by making the density dependent on this pump-probe delay time.
Note finally that the squared molecular form factor is invariant under space inversion, $|F(\mathbf{q}; -\mathbf{R}^{(3N)})|^2 = |F(\mathbf{q}, \mathbf{R}^{(3N)})|^2$, so that only the even contribution of the difference density contribute to the diffraction pattern. We will exploit this relation in the next chapter.

4 Applications - Diffraction from special quantum systems

In this chapter, we will consider slightly more application-oriented aspects of TRXD. One new effect that we need to take into account when we go to subpicosecond time resolution is diffraction from aligned ensembles. This has been treated before [40, 41] and is discussed extensively in paper 2, so again, I will not repeat the article, but present supplementary information. However, in contrast to chapter 3, the presented material is not self-contained, but relies heavily on concepts introduced in the paper.
Section 4.1 presents an alternative introduction into the concept of aligned molecules and the principal idea of how to approach diffraction from such ensembles. The link between the aligned ensemble and the resulting diffraction pattern is presented in 4.2, which mainly presents the previous derivations with the formalism used in this thesis. These two sections can be understood as an introduction into paper 2.
The other two sections provide supplementary information on the article. Section 4.3 discusses the problem of how to parameterize the difference density, and presents preliminary results on the performance of what we call the "stick model". Finally, in section 4.4, we study in detail how the difference diffraction pattern should be analyzed, and what geometry is best for experiments if the diffraction pattern is distorted by random noise.

4.1 Aligning molecules

Imagine you are asked to calculate the dynamics of a molecular system within the Born-Huang expansion. Typically, as a first step, you would probably remove the angular and center-of-mass (CM) degrees of freedom. That is, if we consider a sample with N atoms, we divide the $3N$ degrees of freedom into the CM vector $\mathbf{R}_\mathrm{s}$, three Euler angles (α, θ, γ) that specify the orientation of the system, and $3N-6$ "internal" coordinates ($3N-5$ for a strictly linear system, but this case will be thoroughly excluded from all the following considerations; see, however, appendix B for diatomics).
$\mathbf{R}_\mathrm{s}$ simply describes a movement of the whole system, and does not influence the other degrees of freedom except for high velocities, where it contributes to the non-adiabatic coupling between electronic states. We will always silently drop these coordinates in this chapter. The same argument holds for the rotational degrees of freedom. Substantial rotation can modify the internal dynamics of the system, with the classical centrifugal force being an obvious example, however, we can entirely neglect these effects for most problems.

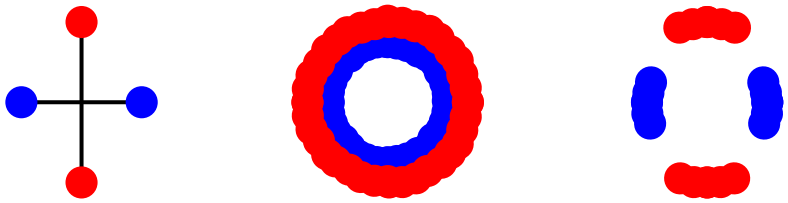

Figure 4.1: Sketch of a two-dimensional molecule consisting of two different atom types ("blue" and "red") with and without alignment. Left: The molecule in the molecule-fixed frame with a well-defined geometry. Middle: The isotropic distribution of molecules in the laboratory frame. Right: The rotational distribution of the molecule in the laboratory frame when it is partially aligned. Note that because of the restriction to two dimensions, all axes are aligned at once; in a three dimensional world, only one axis is aligned by a linearly polarized laser pulse.

This leaves us with the internal coordinates, for example bond lengths or bond angles, which are sufficient to calculate and express the fundamental dynamics of the system, such as the formation or cleavage of bonds within a molecule. All quantities we extract from a calculation are thus expressed with such internal coordinates.
However, if we want to compare the results of our calculations with experiments, we need to take the orientation of the molecules into account. In thermal equilibrium, the corresponding distribution is completely isotropic. For a two-dimensional world, this is depicted in a simplistic way in figure 4.1.
Obviously, an experiment performed in the laboratory frame (i.e., after including rotational degrees of freedom) gives less detailed information than we can calculate in the molecule-fixed frame (i.e., when fixing the rotational coordinates).
A solution is to restrict the rotation by aligning the molecule. As sketched in figure 4.1, this enables us to recover more detailed information from the molecule-fixed frame. There are two different forms of alignment.
We can align molecules with a non-resonant laser pulse (*dynamic alignment*) [42, 43]. Here, the laser–molecule interaction is treated perturbatively, and creates an effective potential that depends on the angle between the laser polarization axis and the most polarizable axis of the molecule, leading to molecular alignment, ideally without vibrational or electronic excitation.
Since the molecule is not excited, we can then try to obtain the ground–state structure of the molecule [44]. We can also excite the molecule afterwards in an attempt to follow the nuclear dynamics directly in the molecule-fixed frame. However, imaging ground state structures without prior information seems to be a formidable challenge, and the method we will develop in the next section is not easily applied to strongly-aligned systems with multiple structures because a large number of unknown rotational coefficients enter the equations. So while all the following results and derivations apply in principle to the case of dynamic alignment, they might not be useful in practice.

Besides dynamic alignment, molecules are always aligned as a side effect of the excitation, which leads to *geometric alignment*. If, for example, we excite molecules with a linearly polarized laser pulse, then, in a classical view, the excitation probability depends on the angle between the polarization axis and an appropriate transition dipole vector defined in the molecule-fixed frame. So if we prepare a sample of excited molecules from an isotropic distribution of ground–state molecules, this sample always has a preferred orientation with respect to the laser polarization axis.

If we use the long (100 ps) x-ray pulses currently produced by synchrotrons, all geometric alignment is usually lost through dephasing. The ensemble is on average isotropic, and one can use the well-known Debye formula for isotropic distributions [45]. While we lose all explicit angular information, we still obtain information on the atom-atom distances, which can be enough for following molecular dynamics (see, e.g., [46]).

However, as we go to subpicosecond dynamics, we need to take geometric alignment into account. In the closely-related field of electron diffraction, attempts have been made to treat the resulting anisotropic diffraction pattern with models based on the Debye formula [41, 47], mostly with poor results. For example, in a simple photodissociation of I_2, substantial bond breakage at around 1 Å is predicted (the equilibrium distance of the iodine atoms is approximately 2.5 Å) [47]. Similarly, for the dissociation of CF_3I into CF_3 + I, some extracted curves predict the breakage of bonds at odd distances [41]. Consequently, it is necessary to go beyond the Debye formula and study in a systematic way the link between alignment and the diffraction pattern. The essential results have been derived before [40, 41], and we will mostly interpret, refine and build on them.

The principal idea, however, can be expressed in a very simple and general way. We take the difference density of (3.58) as a function of the coordinates $\mathbf{R}^{(3N)}$ in the laboratory frame, and expand it in Wigner rotation matrices D^J_{MK}, which form a complete basis for the Euler angles

$$\Delta\bar{\varrho}(\mathbf{R}^{(3N)},\tau) = \sum_{J,M,K} \Delta\bar{\varrho}_{JMK}(\mathbf{r}^{(3N-6)},\tau)\; D^J_{MK}(\alpha,\theta,\gamma)\;. \tag{4.1}$$

This expansion is actually not terribly useful, unless we have the difference density given from start (see the calculation of diffraction patterns for NaI in appendix B), since it is difficult to relate the $\Delta\bar{\varrho}_{JMK}$ to the underlying dynamics of the system.

However, if we assume that the vibration of the molecule (described by the coordinates $\mathbf{r}^{(3N-6)}$) and the rotation (given by the Euler angles α,θ,γ) are approximately uncoupled, the difference density can be written as a product of a "rotational" part that describes the rotation of the whole molecule, and a "vibrational" density that includes all structural changes within the molecule

$$\Delta\bar{\varrho}(\mathbf{R}^{(3N)},\tau) = \Delta\bar{\varrho}_{\mathrm{rot}}(\alpha,\theta,\gamma,\tau)\;\Delta\bar{\varrho}_{\mathrm{vib}}(\mathbf{r}^{(3N-6)},\tau)\;. \tag{4.2}$$

If we then expand in the basis D^J_{MK}, we get

$$\Delta\bar{\varrho}(\mathbf{R}^{(3N)},\tau) = \sum_{J,M,K} c_{JMK}(\tau)\Delta\bar{\varrho}_{\mathrm{vib}}(\mathbf{r}^{(3N-6)},\tau)D^J_{MK}(\alpha,\theta,\gamma)\ , \tag{4.3}$$

which is equivalent to

$$\Delta\bar{\varrho}_{JMK}(\mathbf{r}^{(3N-6)},\tau) = c_{JMK}(\tau)\Delta\bar{\varrho}_{\mathrm{vib}}(\mathbf{r}^{(3N-6)},\tau)\ , \tag{4.4}$$

that is, all the $\Delta\bar{\varrho}_{JMK}$ describe the same "fundamental" time evolution $\Delta\bar{\varrho}_{\mathrm{vib}}$, and differ only in a real-valued rotational coefficient c_{JMK}. Our goal is then to express the differential cross section as a function of the coefficients and the vibrational difference density.
In what follows, we will focus exclusively on symmetric top molecules excited by a linearly polarized laser with a transition dipole moment along the figure axis. In this case, the difference density depends only on the angle θ between the laser polarization axis and the transition dipole moment, and (4.1), (4.3) become the much simpler expression

$$\Delta\bar{\varrho}(\mathbf{R}^{(3N)},\tau) = \sum_n \Delta\bar{\varrho}_n(\mathbf{r}^{(3N-6)},\tau)P_n(\cos\theta) \tag{4.5}$$

$$= \sum_n c_n(\tau)\Delta\bar{\varrho}_{\mathrm{vib}}(\mathbf{r}^{(3N-6)},\tau)P_n(\cos\theta) \tag{4.6}$$

with P_n the n-th order Legendre polynomial. In principle, we only need the sum to run over all even n; the density components with odd n are antisymmetric under space inversion, and drop out when calculating the differential cross section.
As we will show in the next section, the differential cross section can be expanded into products of Legendre polynomials and diffraction curves $S_n(q)$ such, that the n-th curve is linked to the n-th rotational coefficient. As a special case, we recover the Debye formula for isotropic ensembles, which connects the "isotropic" part of the diffraction pattern to the vibrational difference density.

4.2 Anisotropic signals

Let us start with a few technicalities surrounding rotating molecules. If we consider a fixed orientation of the molecule, we can introduce three coordinate systems:

1. A laboratory system $\mathcal{J}$, whose z-axis is defined by the laser polarization axis.
2. Another laboratory system $\mathcal{J}'$ that takes the direction of the scattering vector as z-axis. This is used purely for convenience when evaluating integrals.
3. A molecule-fixed system $\mathcal{J}_M$, whose z-axis is defined by the symmetry axis of the symmetric top.

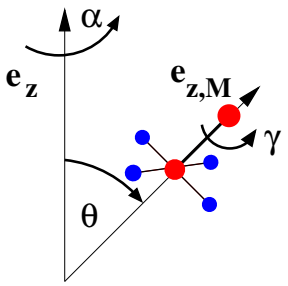

Figure 4.2: Sketch of the three Euler angles. To transform from the laboratory frame to the molecule-fixed frame, we first rotate the coordinate axes around $\mathbf{e}_z$ by an angle α. In a second step, a rotation around the new y-axis by an angle θ transforms $\mathbf{e}_z$ into the z-axis of $\mathcal{J}_M$, $\mathbf{e}_{z,M}$. A third rotation around $\mathbf{e}_{z,M}$ by an angle γ concludes the process.

The x and y-axes can be defined freely, the end result does not depend on a particular choice. The transformation from the laboratory frame $\mathcal{J}$ into the molecule-fixed frame $\mathcal{J}_M$ is defined by three Euler angles α, θ, γ. We will use the convention of [48] (active-sense, right-screw, z-y-z convention) for the Euler angles, see figure 4.2 for an illustration. Obviously, each set of the Euler angles corresponds to a certain orientation of the molecule.
In addition, we specify the rotation that transforms $\mathcal{J}'$ into $\mathcal{J}_M$ by the Euler angles $\alpha', \theta', \gamma'$, and the rotation transforming $\mathcal{J}$ into $\mathcal{J}'$ by $\alpha_q, \theta_q, \gamma_q$. Now let us insert (2.25) and (4.5) into (3.58), and obtain

$$\begin{aligned}\Delta\frac{\mathrm{d}\sigma}{\mathrm{d}\Omega} &= \sigma_T \sum_{a,b} f_a^*(q) f_b(q) \int \mathrm{d}^{3N-3}R \sum_n \Delta\bar{\varrho}_n(\mathbf{r}^{(3N-6)},\tau) P_n(\cos\theta)\ \mathrm{e}^{\mathrm{i}\mathbf{q}\mathbf{R}_{ab}} \\ &= \sigma_T \sum_{a,b} f_a^*(q) f_b(q) \int \mathrm{d}^{3N-6}r \sum_n \Delta\bar{\varrho}_n(\mathbf{r}^{(3N-6)},\tau)\ F_{abn}(\mathbf{q})\ , \end{aligned} \tag{4.7}$$

where

$$F_{abn}(\mathbf{q}) = \int_0^{2\pi} \mathrm{d}\alpha' \int_0^{\pi} \mathrm{d}\theta' \sin\theta' \int_0^{2\pi} \mathrm{d}\gamma'\ P_n(\cos\theta)\ \mathrm{e}^{\mathrm{i}\mathbf{q}\mathbf{R}_{ab}}\ . \tag{4.8}$$

$\mathbf{R}_{ab} = \mathbf{R}_b - \mathbf{R}_a$ is the vector pointing from atom a to atom b, and F_{abn} collects all terms that depend on the rotation of the molecule.
What we have done is to represent a given molecular geometry not by the position of all of its atoms, but by the orientation $(\alpha', \theta', \gamma')$ of the molecule, and some internal coordinates $\mathbf{r}^{(3N-6)}$ (bond lengths etc.) whose value does not change if we rotate the whole molecule. We have split off the integration over all possible orientations of the molecule together with all terms that depend on the Euler angles. Obviously, this

includes the rotational distribution, or the Legendre polynomials as expansion basis. Also, the vector $\mathbf{R}_{ab}$ is defined in the molecule-fixed frame $\mathcal{J}_M$, and thus dependent on the Euler angles; when we rotate the molecule, we also rotate the atoms a, b, thus changing the value of $\mathbf{R}_{ab}$.
Now let us extract the explicit dependence on the integration variables. First, we can use the addition theorem for Legendre polynomials. With $\mathbf{e}$ being the unit vector in the direction of the laser polarization, and $\mathbf{d}$ being the unit vector along the symmetry axis of the molecule, we get

$$P_n(\cos\theta) = P_n(\mathbf{e}\cdot\mathbf{d}) = \frac{4\pi}{2n+1}\sum_{m=-n}^{n} Y^*_{nm}(-\theta_q,-\alpha_q)Y_{nm}(\theta',\alpha') \ . \tag{4.9}$$

Similar, with some algebra, we transform $\mathbf{q}$ into the coordinate system $\mathcal{J}_M$ to evaluate the scalar product

$$\mathbf{q}\mathbf{R}_{ab} = q(-\sin\theta'\cos\gamma' x_{ab} - \sin\theta'\sin\gamma' y_{ab} + \cos\theta' z_{ab}) \ , \tag{4.10}$$

where x_{ab}, y_{ab}, z_{ab} are the components of the vector $\mathbf{R}_{ab}$ in $\mathcal{J}_M$. Inserting (4.9), (4.10) into (4.8), we get

$$F_{abn}(\mathbf{q}) = \int_0^\pi \mathrm{d}\theta' \ \sin\theta' \ \mathrm{e}^{\mathrm{i}qz_{ab}\cos\theta'} \int_0^{2\pi}\mathrm{d}\alpha' \ \frac{4\pi}{2n+1}\sum_{m=-n}^{n} Y^*_{nm}(-\theta_q,-\alpha_q)Y_{nm}(\theta',\alpha') \times \int_0^{2\pi}\mathrm{d}\gamma' \ \mathrm{e}^{\mathrm{i}q(-\sin\theta'\cos\gamma' x_{ab} - \sin\theta'\sin\gamma' y_{ab})} \ . \tag{4.11}$$

The integrations can now be solved one at a time. For the integration over α', we use that

$$\int_0^{2\pi}\mathrm{d}\alpha' \ Y_{nm}(\theta',\alpha') = 2\pi Y_{nm}(\theta',0)\delta_{m0} \ , \tag{4.12}$$

which also collapses the sum over m. The integration over γ' is solved by using the identity [40, 41]

$$\int_0^{2\pi}\mathrm{d}\gamma' \ \mathrm{e}^{\mathrm{i}A\cos\gamma' + \mathrm{i}B\sin\gamma'} = 2\pi J_0(\sqrt{A^2+B^2}) \ , \tag{4.13}$$

where J_0 is the zeroth Bessel function. Applying these integrations converts (4.11) into

$$F_{abn}(\mathbf{q}) = (2\pi)^2 P_n(\cos\theta_q)\int_0^\pi \mathrm{d}\theta' \sin\theta' P_n(\cos\theta') \ \mathrm{e}^{\mathrm{i}qz_{ab}\cos\theta'} J_0(\sqrt{x_{ab}^2+y_{ab}^2}\, q\sin\theta') \ . \tag{4.14}$$

For even n, we note that the integral gives a real number, so we can add the complex conjugate to the integrand, which effectively replaces the complex exponential by a cosine. Furthermore, we can rewrite the components of the ab-vector as $z_{ab} = r_{ab}\cos\vartheta_{ab}$, $\sqrt{x_{ab}^2 + y_{ab}^2} = r_{ab}\sin\vartheta_{ab}$, where r_{ab} is the length of the vector $\mathbf{R}_{ab}$, and ϑ_{ab} its enclosing angle with the symmetry axis.
The thus modified integral can be found in standard integral tables [41, 49], and we obtain

$$F_{abn}(q,\theta_q) = 2(2\pi)^2 P_n(\cos\theta_q)(-1)^{n/2} P_n(\cos\vartheta_{ab}) j_n(qr_{ab}) \ . \tag{4.15}$$

We exploited the fact that the Gegenbauer polynomial in our case is just a Legendre polynomial, $C_n^{1/2} = P_n$, and applied the definition of the spherical Bessel functions $j_n(x) = \sqrt{\pi/2x} J_{n+1/2}(x)$.
Combining (4.15) with (4.7) gives us the set of final equations

$$\Delta\frac{\mathrm{d}\sigma}{\mathrm{d}\Omega} = 2(2\pi)^2\sigma_T \sum_{n \text{ even}} (-1)^{n/2} P_n(\cos\theta_q) S_n(q) \tag{4.16}$$

$$S_n(q) = \sum_{a,b} f_a^*(q) f_b(q) \int \mathrm{d}^{3N-6} r \ \Delta\bar{\varrho}_n(\mathbf{r}^{(3N-6)},\tau) P_n(\cos\vartheta_{ab}) j_n(qr_{ab}) \ . \tag{4.17}$$

Equation (4.16) tells us that the difference diffraction pattern is a function of q and θ_q only. The dependence on the angle is through some Legendre-polynomials, and we can resolve it to obtain a set of diffraction curves S_n. As can be seen from equation (4.17), these curves only depend on q, and carry all the physical information about the system.
It should be pointed out that we did not formally require a symmetric top. We only required a difference density distribution in the form of (4.5), which is independent of α and γ, and has no stray terms of $\sin\theta$; this is fulfilled by symmetric tops, see the appendix of paper 2 and appendix A. So if, for example, a molecule that is initially a symmetric top is excited to some state that renders the molecule asymmetric, the results (4.16), (4.17) are still valid as long as the rotational distribution can be expanded in the form of (4.5).
If we can further assume that the rotation and vibration are uncoupled, equations (4.2), (4.6), we can bring (4.17) into the form

$$S_n(q) = c_n(\tau) \sum_{a,b} f_a^*(q) f_b(q) \int \mathrm{d}^{3N-6} r \ \Delta\bar{\varrho}_{\mathrm{vib}}(\mathbf{r}^{(3N-6)},\tau) P_n(\cos\vartheta_{ab}) j_n(qr_{ab}) \ , \tag{4.18}$$

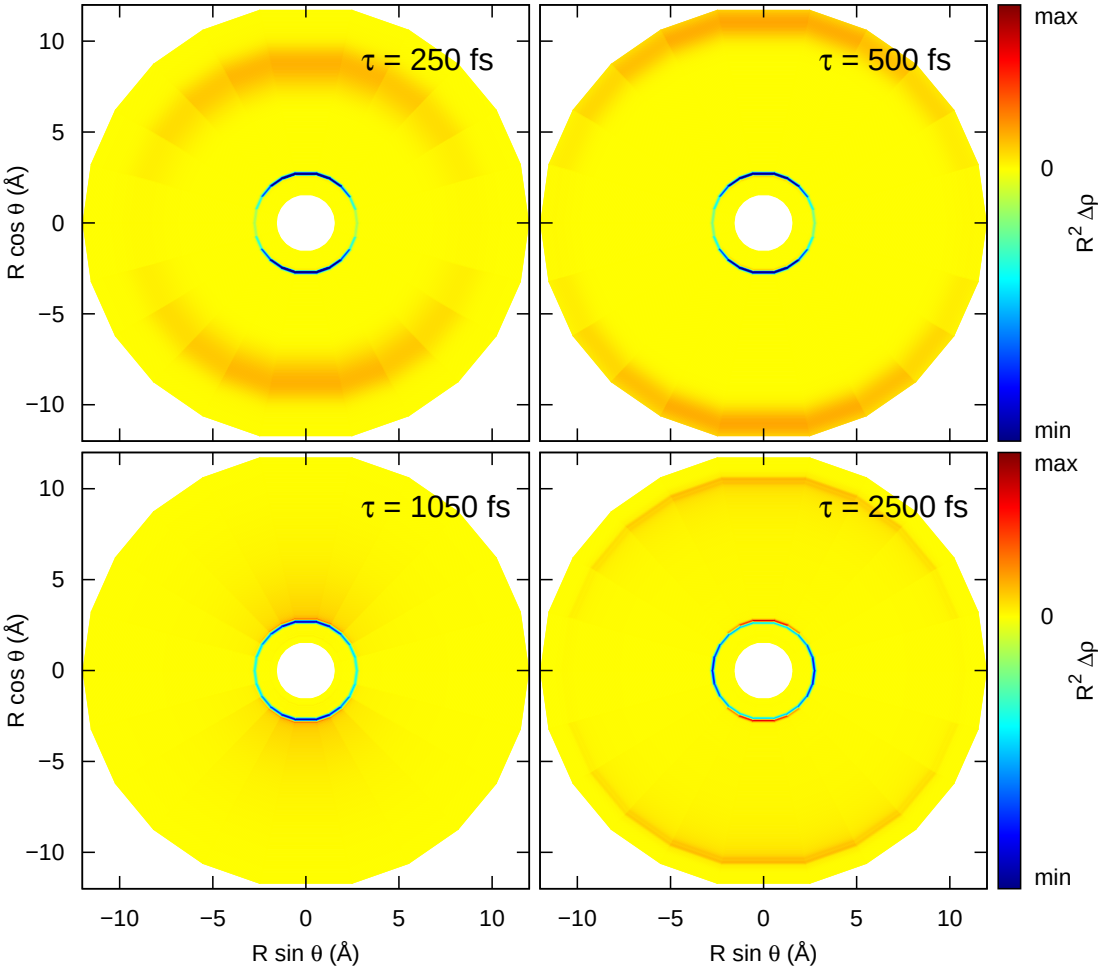

Figure 4.3: Angle-resolved densities of NaI, $R^2\Delta\bar{\varrho}(R,\theta,\tau)$, at different delay times between the laser pump and x-ray probe. The same calculation as in paper 2 has been used, and the resulting density has been convoluted with a $\sin^2$ x-ray pulse of 100 fs FWHM. See appendix B for computational details. The laser polarization axis is along the vertical direction. Note the rotation of the hole term at long delay times, which is extensively discussed in paper 2. The difference density in this figure is related to the components $\Delta\bar{\varrho}_n$ in figure 3 of paper 2 by $\Delta\bar{\varrho}(R,\theta,\tau) = \Delta\bar{\varrho}_0(R,\tau) + P_2(\cos\theta)\Delta\bar{\varrho}_2(R,\tau)$

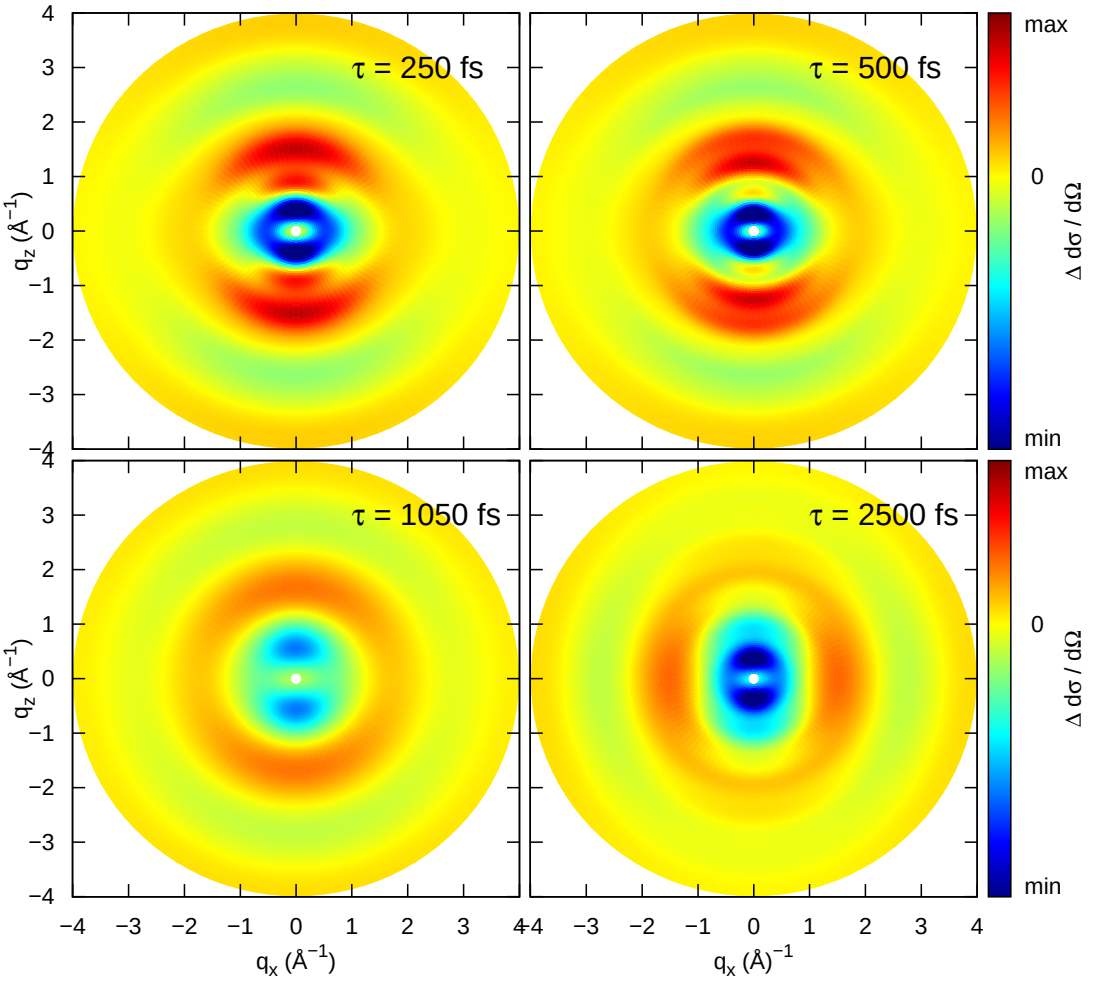

Figure 4.4: Diffraction patterns for the densities in figure 4.3. See appendix B for computational details. A perpendicular setup (i.e., incoming x-ray beam perpendicular to laser polarization axis) has been used. The projection of the laser polarization axis is vertical in the images.

that is, the single diffraction curves differ in information content only by the rotational coefficient c_n. In general, (4.2) does not hold, though. In figure 4.3, for example, we can see that the excited-state wave packet always remains aligned with the laser polarization axis, while the depleted ground state changes its orientation. This complication can be formally overcome by separating the difference density into summands, each describing a "species", and requiring (4.2) to hold for each such species. This is spelled out in detail in paper 2 found in the appendix.
The article also deals with the more technical details of how to express (4.16), (4.18) using atom-atom pair distribution functions, presents direct inversion schemes to extract the components $\Delta\bar{\varrho}_n$ from (4.18). It also demonstrates how to decompose the diffraction pattern into the single curves, which I will continue in section (4.4). Finally, the article shows with the example of NaI that one should be careful with a-priori assumptions about the rotational coefficients.

4.3 Stick models and wave functions

Up to now, we have represented the physical content of the diffraction pattern in the form of a vibrational difference density $\Delta\bar{\varrho}_{\mathrm{vib}}$, or by an expansion into $\Delta\bar{\varrho}_n$. For calculations of NaI, we can extract the $\Delta\bar{\varrho}_n$ from the full quantum calculations. Also, for diatomic molecules, we can directly invert the diffraction curves (see paper 2). However, for practical applications that involve more complex molecules, we have to use some parameterized model for the difference density, and fit for the parameters within this model.
In the simplest model, we assume that all atoms have a well-defined position in the molecule-fixed frame. Since this is similar to the ball-and-stick models than are commonly used to illustrate molecular structures, we will refer to this approximation as the "stick model".
On a more explicit level, the model is probably best introduced using difference pair distribution functions, see equations (15), (16) in paper 2. We approximate

$$\Delta g^S_{ab}(r,\vartheta,\tau) = \frac{f_S(\tau)}{r^2}\delta\Big[r - r^S_{ab}(\tau)\Big]\ \delta\Big[\cos\vartheta - \cos\vartheta^S_{ab}(\tau)\Big]\ . \tag{4.19}$$

f_S is a real-valued prefactor whose sign determines if the given species was populated (positive sign) or depleted (negative sign), and whose absolute value gives the magnitude of the population/depletion. $r^S_{ab}(\tau)$, $\vartheta^S_{ab}(\tau)$ give the length of the ab-vector and its enclosed angle with the symmetry axis. Inserting this into equation (15) of paper 2 gives the relation

$$S_n(q,\tau) = \sum_S c^S_n(\tau) f_S(\tau) \sum_{a,b} f^*_a(q) f_b(q)\ P_n\Big(\cos\vartheta^S_{ab}(\tau)\Big) j_n\Big(q r^S_{ab}(\tau)\Big)\ . \tag{4.20}$$

For molecules in the ground state or in long-lived excited states, the nuclear densities are often strongly localized around the minimum of the corresponding potential energy

surfaces, see figure 4.5 for an example. In this case, the stick model provides a simple approximation of the molecular structure.
However, when we use ultrashort x-ray pulses to follow the molecular wave–packet dynamics, and take into account the finite duration of the x-ray pulse, which further smears out the dynamics, we would intuitively expect the difference pair distributions Δg_{ab}^S to be poorly represented by a delta function. To check if this was indeed the case, we tested the performance of the stick model for a NaI wave–packet calculation.
We used the NaI calculation described in paper 2. With the techniques described in appendix B, I calculated the isotropic difference density $\int_{-1}^{1} \mathrm{d}(\cos\theta) R^2 \Delta\bar{\varrho}(R, \cos\theta, \tau)$ and the corresponding isotropic difference diffraction curve S_0 for five different delay times τ. The chosen difference densities are plotted in figure 4.6.
The isotropic difference diffraction curves were sampled on a grid from $q = 0.1$ Å^{-1} to 10 Å^{-1} with a step size of 0.05 Å^{-1}, and were then processed by Kristoffer Haldrup with a fitting procedure [50–52] that uses a maximum likelihood estimation with a stick model (4.19). In detail, it was assumed that the NaI ground state was depleted at $R = 2.6$Å, and another structure was populated at some R_0, that is, the (isotropic) difference pair distribution function was assumed to be

$$g_{\mathrm{NaI}}(R, \tau) = f(\tau)\delta(R - R_0(\tau)) - f(\tau)\delta(R - 2.6\text{Å}) \ , \tag{4.21}$$

where f is the excitation probability. For each of the five difference diffraction curves, a likelihood function of f, R_0 was calculated. The results are shown in figures 4.7 and 4.8.

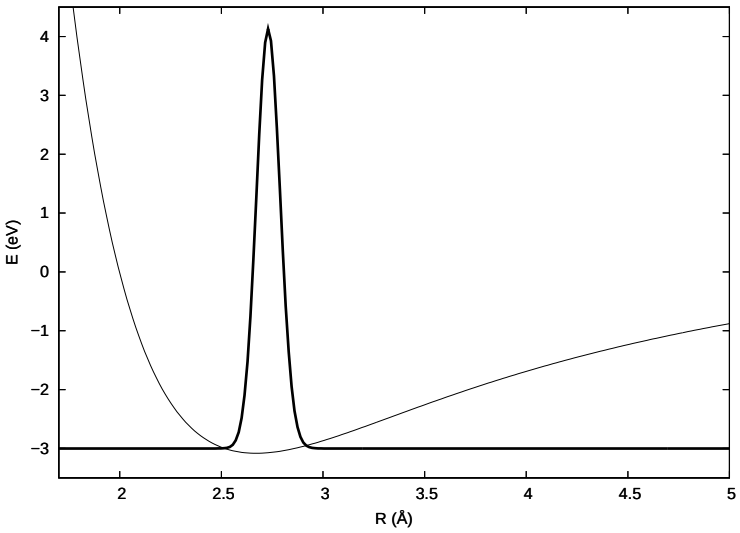

Figure 4.5: Nuclear density of the vibrational ground state of NaI as a function of the Na-I distance R. The thin line is the adiabatic electronic ground state potential energy.

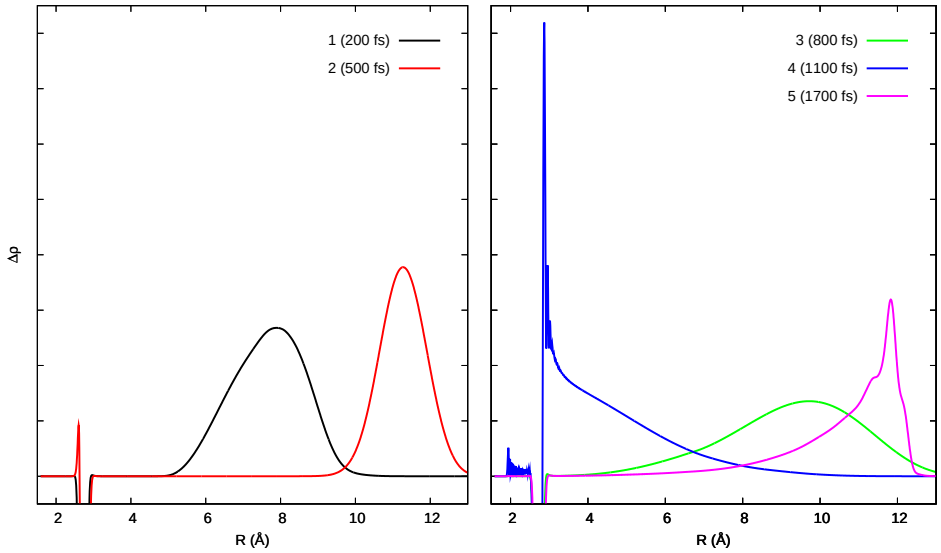

Figure 4.6: Isotropic difference densities for five different pump–probe delay times. Each difference density has a negative contribution similar of the form of the ground state density in figure (4.5).

Our main conclusions from this preliminary study are:

- The likelihood functions can significantly deviate from the actual difference densities, and should not be used as an approximation to the latter.

- However, the stick model is able to estimate the overall position of the wave packet correctly (see figure 4.7). The width of the wavepacket is only estimated qualitatively correctly in most cases. Relatively large error bars for the parameters are to be expected, and should be reported.

Finally, we want to stress that this was just a simple, preliminary study using calculations and tools we already had available. It should be repeated using a more complex molecule, and with more realistic parameters; it is rather unusual that atoms with an internuclear distance of about 10 Å contribute significantly to the diffraction pattern, or that the difference pair distribution function (i.e., difference density for diatomics) is spread out over a distance of as much as 4 Å.
However, given the shortcomings of this model system, the stick model performed better than we initially expected, which gives some confidence that it will be possible to follow real wave–packet dynamics with it.

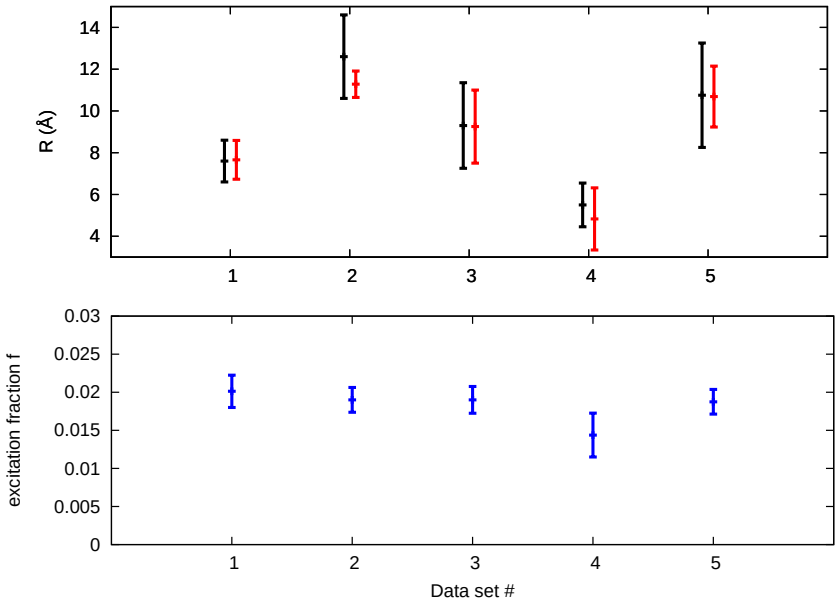

Figure 4.7: Upper image: peak position and width of the likelihood function when varying R_0 (black), and mean radial distance and standard deviation of the calculated excited wave packet (red). Lower image: Peak position and width of the likelihood function when varying f in (4.21). Data for each of the difference densities in figure 4.6. Note that the drop in the population of sample 4 comes from the fact that the positive difference density of the excited state and the negative difference density of the depleted ground state partly overlap and cancel. Courtesy of Kristoffer Haldrup.

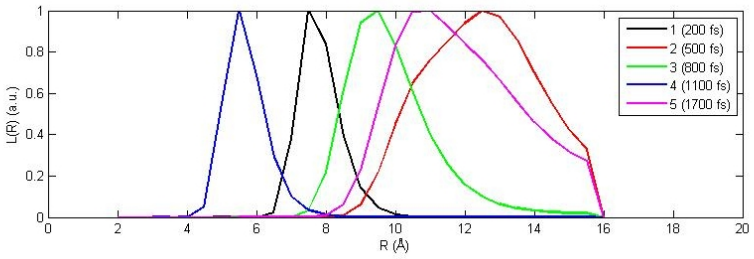

Figure 4.8: Likelihood as a function of the parameter R_0 for each of the difference diffraction curves calculated from the difference densities in figure 4.6. Courtesy of Kristoffer Haldrup.

4.4 Data evaluation and optimal experiments

We will now change focus and discuss how to do experiments and process the data optimally. We will narrow our scope to experiments that involve excitation by single photon absorption. In this case, the difference density is a second order polynomial of $\cos\theta$, and only the terms $n = 0, 2$ contribute to (4.16), (4.18), see appendix A for a proof. Apart from being accessible to an analytic treatment, this should also be the most interesting process in practice because one-photon excitations often have the largest excitation probabilities.

The basic idea put forward extensively in paper 2, and encoded in equations (4.16), (4.18) is that of a two-step process. First, we separate the difference diffraction pattern $\cong \Delta \mathrm{d}\sigma/\mathrm{d}\Omega$ into a set of diffraction curves S_n. In a second step, we fit a given guess for the rotational coefficients c_n and the structure $\Delta\bar{\varrho}_{\mathrm{vib}}$ to all the diffraction curves at once.

When we consider the separation of the difference diffraction pattern, the basic idea is obvious. The diffraction curves only depend on the length of the scattering vector q, and they are mixed together depending on the value of the angle θ_q. The way to go is then to take all points on the detector with a fixed value of q (corresponding to a circle on the detector), assigning each of the thus selected points its value of θ_q, and then use some fitting method to extract $S_0(q)$, $S_2(q)$. This is shown in figure 4 of paper 2, and works equally well for (almost) any setup.

However, in practice, we will have significant random noise in the diffraction pattern. In this case, we would expect that such a fit gives better results, i.e., smaller error bars

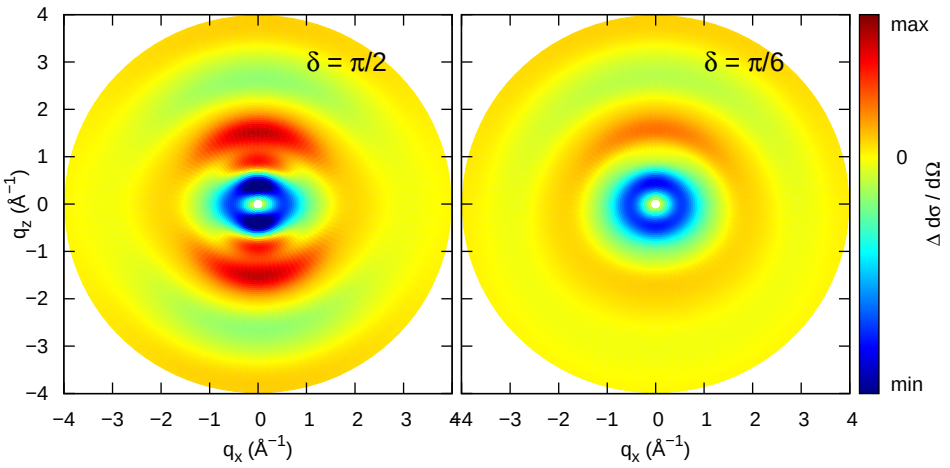

Figure 4.9: Difference diffraction patterns for laser-excited NaI for different angles δ of $\pi/2$ (left image) and $\pi/6$ (right image). The same parameters as in paper 2 were used, the time delay τ is 250 fs.

on the fitted curves, if we span a large range of different angles θ_q. This range is linked to the experimental setup via the angle δ between the wave vector $\mathbf{k}_0$ of the incoming x-ray beam and the laser polarization vector $\mathbf{E}$ (see figure 3.1). If ϑ is the scattering angle defined by

$$\sin\frac{\vartheta}{2} = \frac{q}{2k_0} \ , \tag{4.22}$$

if we assume that the detector plane is orthogonal to $\mathbf{k}_0$, and if we introduce ϕ as the angle between the projections of $\mathbf{q}$ and $\mathbf{E}$ on the detector plane, we can obtain from geometrical considerations

$$\cos\theta_q = \sin\frac{\vartheta}{2}\cos\delta + \cos\frac{\vartheta}{2}\cos\phi\sin\delta \ . \tag{4.23}$$

We see that the decomposition is impossible for $\delta = 0$ (the "parallel" setup), and the range becomes larger as δ goes to $\pi/2$. As an illustration, figure 4.9 shows difference diffraction patterns for two different values of δ.
However, it would be nice if we could express more quantitatively how the angle δ influences the "error bars" of the extracted scattering curves for difference diffraction patterns with random noise. As a side effect and second goal, we will introduce a recipe of how to obtain a best fit of the structure $\Delta\bar{\varrho}_{\mathrm{vib}}$ and the coefficient c_2, and the corresponding uncertainties from such a noisy pattern.
After introducing some basic concepts about probability theory in section 4.4.1, we will discuss how to guess the isotropic and anisotropic diffraction curves S_0, S_2 in section 4.4.2. This yields the requested quantitative relationship between the experimental geometry δ and the uncertainty of the extracted curves. In section 4.4.3, we finally demonstrate that the extracted curves have an actual meaning for the fitting process. For this, we construct a statistical problem around these diffraction curves, and show that this yields the same likelihood function as a fitting procedure that takes the full diffraction pattern as input.

4.4.1 Sampling theory and maximum likelihood estimators

The following introduction of the elementary concepts of probability theory is heavily based on [53].
Central for the application of probability theory to practice is the concept of a random experiment. We do some experiment, such as tossing a coin or counting the number of scattered x-ray photons, that yields some *event* A from a given set. We can assign each event a probability $P(A)$ that tells us how frequently this event turns up in the experiment.
Let us assume for convenience that there are uncountably infinite possible events, and let us further associate each event with a real number. For example, different outcomes of some measurement (events) can be labelled by their measured value. Then each event is

characterized by a possible value of a *random variable* $\tilde{x}$. We now introduce a *cumulative distribution function* of $\tilde{x}$ by

$$F(x) = P(\tilde{x} < x) \ . \tag{4.24}$$

$F(x)$ gives the probability of obtaining an event that is associated with a real number smaller than x. Forming the derivative of F (if possible) yields the *probability density* $f(x) = \mathrm{d}F(x)/\mathrm{d}x$, which gives the probability of obtaining an event $x \leq \tilde{x} < x + \mathrm{d}x$. For what follows, it is useful to think of a random variable as the set of all possible outcomes of the random experiment, or equivalently, as a placeholder for the actual result of the random experiment.
We can also introduce functions of random variables

$$\tilde{H} = H(\tilde{x}) \ , \tag{4.25}$$

which are again random variables, but with a different probability density. In addition to the normal properties of a function, we can define the *expectation value* of H as

$$\overline{H(\tilde{x})} = \overline{\tilde{H}} = \int H(x) f(x) \ \mathrm{d}x \tag{4.26}$$

with f the probability distribution of $\tilde{x}$. This expectation value gives us the average value that we obtain when doing the random experiment often and calculating the value of H of the resulting event. As a crude measure of the squared average deviation of the value of H from the expectation value, we introduce the *variance*

$$\sigma^2(H(\tilde{x})) = \sigma^2(\tilde{H}) = \left(\overline{H(\tilde{x}) - \overline{H(\tilde{x})}} \right)^2 \ . \tag{4.27}$$

With these basic elements introduced, we can fast-forward to the foundations of sampling theory. We define a *sample of size* K as a set of K random variables $\tilde{\mathbf{x}} = (\tilde{x}_1, \ldots, \tilde{x}_K)$ with distribution function $f(\mathbf{x})$. Let us assume that the single variables are uncorrelated, that is, $f(\mathbf{x}) = f_1(x_1) \cdot \cdots \cdot f_K(x_K)$ (although this is not strictly required, and we will drop it in section 4.4.3).
For example, repeating a random experiment K times would give us a sample of size K. In many cases of practical interest, we are doing measurements, whose outcome is the exact value of the measured parameter plus some random error, and it is our task to make an educated guess for the exact value. Put in a more abstract form, this leads to the concept of parameter estimation.
Let us assume that the form of the probability density is known, but the exact function depends on some parameter $\boldsymbol{\lambda}_0 = (\lambda_1, \ldots, \lambda_p)$, that is $f(\mathbf{x}) = f(\mathbf{x}; \boldsymbol{\lambda}_0)$. A set of functions $\{\xi_K(\tilde{\mathbf{x}})\}_{K \in \mathbb{N}}$ that try to infer the value of $\boldsymbol{\lambda}_0$ from a sample of size K is called an *estimator*.

An estimator is *unbiased* if, for any K,

$$\overline{\tilde{\xi}_K} = \boldsymbol{\lambda}_0 \ , \tag{4.28}$$

that is, on average over all possible samples, the estimator returns the true value of $\boldsymbol{\lambda}_0$. We call an estimator *consistent* if

$$\lim_{K\to\infty} \sigma^2(\tilde{\xi}_K) = 0 \ . \tag{4.29}$$

It can be shown that there is a lower limit to the variance $\sigma^2(\tilde{\xi}_K)$ depending on the bias of the estimator. Estimators that fulfill this lower limit are called *minimum variance estimators*.
For many problems, we are interested in unbiased, minimum variance estimators. Unfortunately, finding such estimators is often difficult. To create estimators that are approximately unbiased with minimum variance, let us assume we have some sample $\tilde{\mathbf{x}}$. Then, in hindsight, the probability of drawing this sample is

$$\mathrm{d}\tilde{P} = f(\tilde{\mathbf{x}};\boldsymbol{\lambda}_0)\ \mathrm{d}^K x \ , \tag{4.30}$$

which requires the knowledge of $\boldsymbol{\lambda}_0$. However, in a twist of thought, we can reinterpret this equation, if we allow an arbitrary value for $\boldsymbol{\lambda}$. In this case, $\mathrm{d}\tilde{P}$ gives the "likelihood" of getting exactly this sample given a certain value for the parameters. We can then introduce a *likelihood function* for the possible parameters

$$L(\boldsymbol{\lambda};\tilde{\mathbf{x}}) = f(\tilde{\mathbf{x}};\boldsymbol{\lambda}) = \prod_{i=1}^{K} f_i(\tilde{x}_i;\boldsymbol{\lambda}) \ . \tag{4.31}$$

Although the likelihood function is at first just an arbitrary function, it has a very intuitive interpretation. Imagine, we had to decide between two parameters. For $\lambda = 0$, the probability densities $f_i(x)$ are strongly peaked around $x = 0$, for another value $\lambda = 1$, the $f_i(x)$ are only significant around 1. Now we perform the random experiment, and get a specific sample, i.e., set of numbers $\mathbf{x}$ that are all close to 1. Intuitively, we would consider this as a definite proof for $\lambda = 1$. If we formally calculate the likelihood function, it is easily seen that $L(1;\mathbf{x}) \gg L(0;\mathbf{x})$.
If we play around with some other configurations (only zeros, half zeros and half ones etc.), it becomes clear that we can interpret the likelihood function as some sort of "quantifiable gut feeling". We could then take the value of $\boldsymbol{\lambda}$ that maximizes the likelihood function as a guess for $\boldsymbol{\lambda_0}$. If such a maximum exists, we can thus introduce a *maximum likelihood estimator*

$$\xi_K^{\mathrm{ML}}(\tilde{\mathbf{x}}) = \arg\max_{\boldsymbol{\lambda}} \; L(\boldsymbol{\lambda};\tilde{\mathbf{x}}) = \arg\max_{\boldsymbol{\lambda}} \; l(\boldsymbol{\lambda};\tilde{\mathbf{x}}) \tag{4.32}$$

$$l(\boldsymbol{\lambda};\tilde{\mathbf{x}}) = \ln L(\boldsymbol{\lambda};\tilde{\mathbf{x}}) = \sum_{i=1}^{K} \ln f_i(\tilde{x}_i;\boldsymbol{\lambda}) \; . \tag{4.33}$$

Since the logarithm is a monotonous function, it does not matter if we consider the likelihood function or its logarithm. Furthermore, we can scale the likelihood function by a function $G(\tilde{\mathbf{x}})$, or equivalently add constants $g = \ln G$ to the logarithmic likelihood function without changing the estimator. We will generously exploit this property later by dropping terms independent of $\boldsymbol{\lambda}$.
Under quite general conditions, the maximum likelihood estimator is an unbiased, minimum variance estimator in the limit $K \to \infty$ [54]. In practice, however, we always deal with finite samples; so we can only hope that that ξ_K^{ML} is sufficiently unbiased with a reasonably low variance.
Last, it should be mentioned that it is usually not feasible to calculate the variance $\sigma^2(\tilde{\xi}_K^{\mathrm{ML}})$ explicitly. As a workaround, we can report the width of the likelihood function, which can serve as a quantitative measure of the faith that we have in the estimate.

4.4.2 Extracting the scattering curves

Now let us apply these concepts to x-ray diffraction. We scatter an x-ray beam from N_0 identical systems, measure the resulting diffraction pattern with a pixelated area detector, and subtract the diffraction pattern without pump pulse from that with pump pulse. Our sample is then formed by the difference photon count at each pixel.
If we add some counting "noise", the difference photon count y of some pixel is a random number that can be written as the theoretically predicted count rate plus some random error $\tilde{\varepsilon}$.

$$\tilde{y} = \Delta \frac{\mathrm{d}\sigma}{\mathrm{d}\Omega}(q,\theta_q) \; N_0 \; I_0 \, \Delta\Omega_{\mathrm{pixel}} + \tilde{\varepsilon} \; , \tag{4.34}$$

where $\Delta \mathrm{d}\sigma/\mathrm{d}\Omega$ is given by (4.16), I_0 is the number of incoming photons, and $\Delta\Omega_{\mathrm{pixel}}$ is the solid angle covered by the detector pixel (we assume that each pixel is small enough that the cross section is constant over its area). As a first step, we divide by all the uninteresting constants

$$\tilde{y}' = \frac{\tilde{y}}{I_0 N_0 \Delta\Omega_{\mathrm{pixel}} 2(2\pi)^2 \sigma_T} = S_0(q) - P_2(\cos\theta_q) S_2(q) + \tilde{\varepsilon}' \; . \tag{4.35}$$

In the following, we will only work with the primed quantities, but drop the prime for ease of notation. For definiteness, and to allow a simple analytic treatment of this problem, we introduce a couple of idealizing assumptions:

1. We assume that the difference photon count can take any real number to avoid complications associated with discrete random variables.

2. For definiteness, we assume that the positions of the pixels form a rectangular grid. That is, each detector pixel can be assigned a double index (i, j) with $1 \leq i \leq Z$ and $1 \leq j \leq N$, so that it represents the position with $q = q_i$, $\phi = 2\pi i/N$. With (4.23), we can alternatively assign each pixel a value of $x_{ij} = P_2(\cos\theta_q(q_i, \phi_j))$. This allows us to rewrite (4.35) in the form

$$\tilde{y}_{ij} = S_0(q_i) - x_{ij} S_2(q_i) + \tilde{\varepsilon}_{ij} = S_{0i} - x_{ij} S_{2i} + \tilde{\varepsilon}_{ij} \ , \tag{4.36}$$

   and declare the set $\tilde{y}_{ij}$ as our sample of size NZ.

3. We assume that the error depends only on the value of q, that is, $\tilde{\varepsilon}_{ij} = \tilde{\varepsilon}_i$. The background of this idea is that the fraction of molecules that we excite is small [46], and that the main source of the error are counting statistics. Consequently, both the diffraction pattern with and without laser excitation are approximately isotropic, as should be the counting errors. Note, however, that the Thomson cross section in (4.35) contains polarization terms that depend on the value of ϕ and might modify this argument; for simplicity we will assume that the x-ray beam is unpolarized, in which case this dependence vanishes. We further assume that the $\tilde{\varepsilon}_i$ have a Gaussian distribution with a variance of $\sigma^2(\tilde{\epsilon}_i) = \sigma_i^2$ and a mean value of zero.

The parameters we want to estimate now are the isotropic and anisotropic curves, that is the Z values of S_{0i}, and those of S_{2i}. For a given guess, we can write down the likelihood function as

$$L\Big(\{S_{0i}, S_{2i}\}; \{\tilde{y}_{ij}\}\Big) = \prod_{i=1}^{Z} \prod_{j=1}^{N} \exp\Big(-\frac{(S_{0i} - x_{ij} S_{2i} - \tilde{y}_{ij})^2}{2\sigma_i^2}\Big) \ , \tag{4.37}$$

and the logarithmic likelihood function as

$$l\Big(\{S_{0i}, S_{2i}\}; \{\tilde{y}_{ij}\}\Big) = -\sum_{i=1}^{Z} \frac{1}{2\sigma_i^2} \sum_{j=1}^{N} (S_{0i} - x_{ij} S_{2i} - \tilde{y}_{ij})^2 \ . \tag{4.38}$$

By forming the derivatives, we find that this function is maximized for

$$S_{0i}^{\mathrm{ML}} = \sum_j c_{ij}\, \tilde{y}_{ij} \tag{4.39}$$

$$S_{2i}^{\mathrm{ML}} = \frac{1}{\sum_j x_{ij}} \left(N S_{0i}^{\mathrm{ML}} - \sum_j \tilde{y}_{ij} \right) \ , \tag{4.40}$$

where the c_{ij} are defined as

$$c_{ij} = \frac{\sum_k x_{ik}(x_{ij} - x_{ik})}{(\sum_k x_{ik})^2 - N\sum_k x_{ik}^2} \ . \tag{4.41}$$

They fulfill a number of useful properties:

$$\sum_j c_{ij} = 1 \tag{4.42}$$

$$\sum_j x_{ij} c_{ij} = 0 \tag{4.43}$$

$$\frac{\sum_j c_{ij}^2}{N\sum_j c_{ij}^2 - 1} = \frac{\sum_j x_{ij}^2}{(\sum_j x_{ij})^2} \ . \tag{4.44}$$

Equations (4.39) and (4.40), understood as functions of the random variables $\tilde{y}_{ij}$, are then the maximum likelihood estimators for the diffraction curves. Note, though, that they are only well-defined if the denominators in (4.40), (4.41) are nonzero, which we silently assume in the following. [1]

Because the sampling problem (4.36) and the estimators (4.39), (4.40) have such a simple form, we can analytically calculate the expectation values, variances, and covariances:

$$\overline{\tilde{S}_{0i}^{\mathrm{ML}}} = \Big(\sum_j c_{ij}\Big) S_{0i} - \Big(\sum_j c_{ij} x_{ij}\Big) S_{2i} + \Big(\sum_j c_{ij}\Big)\overline{\tilde{\varepsilon}_i} = S_{0i} \tag{4.45a}$$

$$\overline{\tilde{S}_{2i}^{\mathrm{ML}}} = S_{2i} \tag{4.45b}$$

$$\sigma^2(\tilde{S}_{0i}^{\mathrm{ML}}) = \sum_j c_{ij}^2 \sigma_i^2 \tag{4.45c}$$

$$\sigma^2(\tilde{S}_{2i}^{\mathrm{ML}}) = \Big(\frac{1}{\sum_j x_{ij}}\Big)^2 \Big(N^2 \sum_j c_{ij}^2 - N\Big)\sigma_i^2 \tag{4.45d}$$

$$\mathrm{cov}(\tilde{S}_{0i}^{\mathrm{ML}}, \tilde{S}_{2i}^{\mathrm{ML}}) = \overline{(\tilde{S}_{0i}^{\mathrm{ML}} - \overline{\tilde{S}_{0i}^{\mathrm{ML}}})(\tilde{S}_{2i}^{\mathrm{ML}} - \overline{\tilde{S}_{2i}^{\mathrm{ML}}})} = \frac{1}{\sum_j x_{ij}}\Big(N\sum_j c_{ij}^2 - 1\Big)\sigma_i^2 \ . \tag{4.45e}$$

With these final results, we are in a position to determine which experimental geometry is "best". Obviously, we would like to have a minimal variance of the estimated scattering curves, so we just have to calculate these variances for different values of q_i and δ. The result of such a calculation is displayed in figure 4.10.

Overall, the variance of the estimator for the isotropic curve is largely independent of the experimental setup as long as we avoid parallel or almost parallel setups $\delta < 40°$. If, in addition, we want to minimize the variance of the estimated anisotropic curve, we should always use a perpendicular setup $\delta = 90°$.

[1] One important case where this method fails is the parallel setup. It is easily seen that, if the incoming beam is parallel to the laser polarization, the value of x_{ij} is independent of j. As a direct consequence, the denominator of c_{ij} in (4.41) is zero, that is, we cannot decompose the difference diffraction pattern into the diffraction curves.

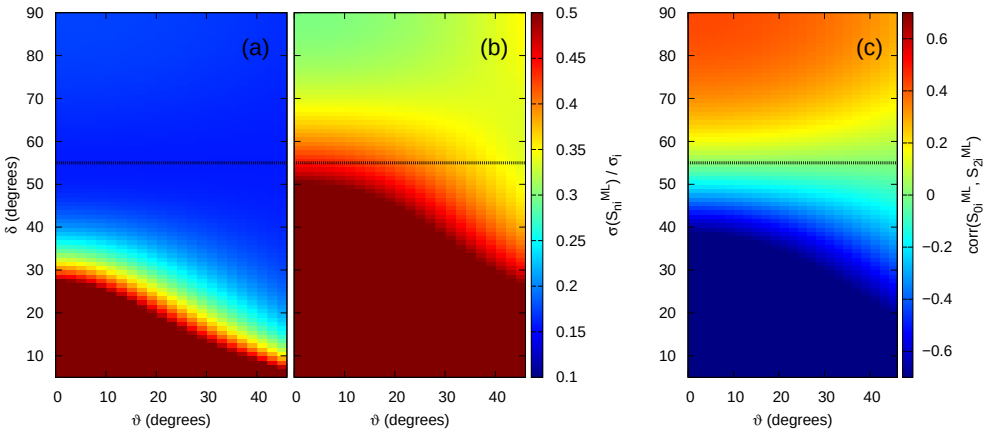

Figure 4.10: Plot of the standard deviation $\sigma(\tilde{x}) \equiv \sqrt{\sigma^2(\tilde{x})}$ of the estimator for (a) the isotropic signal $\tilde{S}_0^{\mathrm{ML}}$, and (b) the anisotropic signal $\tilde{S}_2^{\mathrm{ML}}$ as a function of the scattering angle ϑ, and the angle δ between laser polarization axis and wave vector of the incoming photons. (c): Plot of the correlation $\mathrm{corr}(\tilde{S}_0^{\mathrm{ML}}, \tilde{S}_2^{\mathrm{ML}}) = \mathrm{cov}(\tilde{S}_0^{\mathrm{ML}}, \tilde{S}_2^{\mathrm{ML}})/\sigma(\tilde{S}_0^{\mathrm{ML}})\sigma(\tilde{S}_2^{\mathrm{ML}})$. For all calculations, $N = 40$; however, different values of N show the same qualitative behavior. The horizontal line shows the position of the "magic angle" setup $\delta = \mathrm{acos}\sqrt{1/3} \approx 55°$

So far, we found that we should use a perpendicular setup if we want to use both the isotropic and the anisotropic curve for data fitting. If we only want to use the isotropic curve, for example because we have not upgraded our fitting algorithm, and it only implements the Debye-formula (i.e., calculation of S_0), we only need to make sure that the angle δ is not too small.

However, there is a third graph in figure 4.10 that shows the correlation of the two estimates. This quantity is a crude measure for the probability that an overestimation of S_0 coincides with an overestimation of S_2 (or underestimation for negative correlation). One important consequence is that for correlated random variables, the variance of the single variables is a poor measure of how much they actually deviate from their expectation values.

As can be seen in figure 4.10, the correlation between the two scattering curves differs from zero except for the "magic angle" setup. We therefore recommend doing experiments either in the perpendicular geometry if both scattering curves are used for structure determination, or, as the inferior solution, the magic angle geometry if only the isotropic scattering curve is used further.

4.4.3 Extracting the structural information

In the last section, we only estimated the scattering curves without taking into account that they encode information about the system's structure, that is, about the internal difference density distribution $\Delta\bar{\varrho}_{\mathrm{vib}}$ and rotational coefficients c_2 in (4.18)). To correct this, let us now discuss how to set up a maximum likelihood estimator for the structure. We will not go through all the derivation, but just write down the equations for the likelihood function.

The two-dimensional problem

First, we write down the likelihood function for the case where we estimate the structure directly from the two-dimensional diffraction pattern. We start with (4.36), but take into account explicitly that the scattering curves are functions of the rotational coefficients and the $\Delta\bar{\varrho}_{\mathrm{vib}}$ [2]

$$\tilde{y}_{ij} = S_0(\Delta\bar{\varrho}_{\mathrm{vib}}; q_i) - x_{ij} S_2(\Delta\bar{\varrho}_{\mathrm{vib}}, c_2; q_i) + \tilde{\varepsilon}_i = S_{0i} - x_{ij} S_{2i} + \tilde{\varepsilon}_i \ , \tag{4.46}$$

where the second shorthand notation will be used in the following. We can immediately write down the likelihood function as

$$L(\Delta\bar{\varrho}_{\mathrm{vib}}, c_2; \tilde{y}_{ij}) = \prod_{i=1}^{Z} \prod_{j=1}^{N} \exp\left(\frac{(S_{0i} - x_{ij} S_{2i} - \tilde{y}_{ij})^2}{2\sigma_i^2} \right) \ , \tag{4.47}$$

and the logarithmic likelihood function becomes after dropping all terms that are independent of c_2, $\Delta\bar{\varrho}_{\mathrm{vib}}$

$$\begin{aligned} l(\Delta\bar{\varrho}_{\mathrm{vib}}, c_2; \tilde{y}_{ij}) = &- \sum_i \frac{N}{2\sigma_i^2} \ S_{0i}^2 - \sum_i \frac{\sum_j x_{ij}^2}{2\sigma_i^2} \ S_{2i}^2 + \sum_i \frac{\sum_j x_{ij}}{\sigma_i^2} \ S_{0i} S_{2i} \\ &+ \sum_i \frac{\sum_j \tilde{y}_{ij}}{\sigma_i^2} \ S_{0i} - \sum_i \frac{\sum_j x_{ij} \tilde{y}_{ij}}{\sigma_i^2} \ S_{2i} \ . \end{aligned} \tag{4.48}$$

So the generic way for estimating the structure $\Delta\bar{\varrho}_{\mathrm{vib}}$ and the rotational coefficient c_2 is to calculate for each value q_i the isotropic and anisotropic scattering curves S_{0i}, S_{2i}, calculate the logarithmic likelihood function via (4.48), and pick those structures and coefficients where the likelihood is maximized. Due to the non-trivial dependence of the logarithmic likelihood on the parameters, we can in general not use an analytic formula, but have to maximize the likelihood with some numerical scheme.

[2] In fact, they are functionals; but let us assume that the difference density is parameterized within some model, then the scattering curves are functions of these parameters. To avoid this additional layer of formalism, we will always talk about $\Delta\bar{\varrho}_{\mathrm{vib}}$ when we actually mean "the set of parameters $\boldsymbol{\lambda}$ that specify $\Delta\bar{\varrho}_{\mathrm{vib}}$ in our model"

The one-dimensional problem

Alternatively, we can study another closely related problem, where we obtain two sets of random variables

$$\tilde{S}_{0i} = S_0(\Delta\bar{\varrho}_{\mathrm{vib}}; q_i) + \tilde{\eta}_{0i} \tag{4.49}$$

$$\tilde{S}_{2i} = S_2(\Delta\bar{\varrho}_{\mathrm{vib}}, c_2; q_i) + \tilde{\eta}_{2i}\ , \tag{4.50}$$

where the probability density of the $\tilde{\eta}$ is

$$f(\eta_{0i}, \eta_{2i}) = A \exp\left(-\frac{N}{2\sigma_i^2}\ \eta_{0i}^2 - \frac{\sum_k x_{ik}^2}{2\sigma_i^2}\ \eta_{2i}^2 + \frac{\sum_k x_{ik}}{\sigma_i^2}\ \eta_{0i}\eta_{2i} \right) \tag{4.51}$$

with A some normalization constant, and all other variables defined as before. The probability density has been chosen such that $\tilde{\eta}_{0i}, \tilde{\eta}_{2i}$ have the same variance and covariance as the maximum likelihood estimators in (4.39), (4.40).
Analogous to all the occurrences before, we can again calculate the logarithmic likelihood function for a given difference density and rotational coefficient. After dropping all terms that do not depend on $\Delta\bar{\varrho}_{\mathrm{vib}}$, c_2, we obtain

$$\begin{aligned} l(\Delta\bar{\varrho}_{\mathrm{vib}}.c_2; \{\tilde{S}_{0i}\}, \{\tilde{S}_{2i}\}) = &-\sum_i \frac{N}{2\sigma_i^2}\ S_{0i}^2 - \sum_i \frac{\sum_j x_{ij}^2}{2\sigma_i^2} S_{2i}^2 + \sum_i \frac{\sum_j x_{ij}}{\sigma_i^2} S_{0i} S_{2i} \\ &+ \sum_i \left(\frac{N}{\sigma_i^2}\ \tilde{S}_{0i} - \frac{\sum_j x_{ij}}{\sigma_i^2} \tilde{S}_{2i} \right) S_{0i} + \sum_i \left(\frac{\sum_j x_{ij}^2}{\sigma_i^2} \tilde{S}_{2i} - \frac{\sum_j x_{ij}}{\sigma_i^2} \tilde{S}_{0i} \right) S_{2i}\ . \end{aligned} \tag{4.52}$$

If we now insert for $\tilde{S}_{0i}, \tilde{S}_{2i}$ the expressions for the maximum likelihood estimators, equations (4.39), (4.40), we recover after some algebra the likelihood function (4.48).

Conclusion

Now let us step back a bit and ponder what we have shown. The ultimate goal of the data evaluation procedure is to extract the "best fit" for $\Delta\bar{\varrho}_{\mathrm{vib}}$ and c_2; we have chosen to use the maximum likelihood method, where we assign a likelihood value to each possible structure and rotational constant.
The generic way to do so is to start with the difference diffraction pattern, (4.46), which ultimately leads to the logarithmic likelihood function (4.48). Alternatively, we calculate from the diffraction pattern two new sets of random variables, (4.39), (4.40), and treat the thus calculated numbers as if we had drawn them from the random experiment described by equations (4.49), (4.50), (4.51). Applying the maximum likelihood method yields for each diffraction pattern and each set $\Delta\bar{\varrho}_{\mathrm{vib}}$, c_2 the same likelihood up to constant factors.

This leads to two results. First and foremost, the variances and covariances that we used in section 4.4.2 to argue for optimal experimental setups are not just arbitrary numbers, but they can be assigned an actual meaning within the alternative random experiment in (4.51). As a side result, we have introduced a simple way (4.48), and a complicated way (equations (4.39), (4.40), (4.52)) for calculating the same logarithmic likelihood.
So why should we prefer one or the other way? Obviously, calculating the logarithmic likelihood function directly from the difference diffraction pattern is more robust as it does not involve denominators that might become zero. If, for example, we decide for some strange reason to perform a diffraction experiment in the parallel geometry, (4.48) is the way to go for calculating the likelihood function.
On the other hand, the first step in the complicated procedure, equations (4.39), (4.40), condenses the NZ data points of the diffraction image into the two scattering curves, each of which consists of Z data points with "error bars" (plus the covariances). With these curves, it becomes much easier to judge the quality of the scattering data or the impact of further data processing intuitively than if we have to deal with the whole two-dimensional diffraction pattern.

Appendix A

Proof that n-photon absorption produces 2n-th order Legendre polynomials

In this appendix, I want to prove some relations for symmetric tops excited by an electric field (i.e., laser pulse). After introducing the topic of the rotation of symmetric tops, I will prove that exciting a symmetric top molecule along the symmetry axis by an electric field gives, in first order, a rotational distribution that is a second order polynomial of $\cos\theta$. The core of this proof is given in [55], we only need to go beyond some random phase approximation used in the reference. After that, we will discuss the extension of the proof to higher order excitations.
I would like to point out that I have used a simple brute-force approach that involves expanding the wave function in rotational eigenstates, and showing that each term gives an appropriate polynomial. The advantage is that this approach requires few formal arguments from angular momentum theory; at the same time, it is rather inelegant and requires a lot of bookkeeping.
One of the consequences is that I will not extend this proof to the case where the transition dipole moment is perpendicular to the symmetry axis. While playing around with the formulas suggests that the end result will be the same, a detailed treatment becomes rather forbidding; it involves multiple rotation matrices in the interaction Hamiltonian as well as multiple degenerate electronic transitions.

A.1 Introduction

To simplify the notation, we write out only the rotational coordinates of the molecule, that is, we drop electronic and vibrational coordinates; they are not required for the arguments presented here. Similar to section 4.2, we then define a laboratory-fixed coordinate system, whose z-axis is defined by the laser polarization axis, and a molecule-fixed coordinate system, whose z-axis is defined by the symmetry axis of the symmetric top. The other two axes can be defined arbitrarily. The orientation of the molecular frame with respect to the laboratory frame is determined by the Euler angles α, θ, γ also introduced in section 4.2.
The molecule is now subject to a Hamiltonian

$$\hat{H} = \hat{H}_0 + \hat{H}_{\text{int}} \tag{A.1}$$

consisting of the Hamiltonian $\hat{H}_0$ of the field-free molecule, and the molecule-field interaction $\hat{H}_{\text{int}}$. Initially, the molecule is in some eigenstate of $\hat{H}_0$

$$\hat{H}_0|JKM\rangle = E_{JK}|JKM\rangle \ . \tag{A.2}$$

Each rotational eigenstate is characterized by three quantum numbers: the total angular momentum J, a quantum number M associated with a rotation around the laser polarization axis, and K associated with a rotation around the symmetry axis. Note that the energy does not depend on the quantum number M, which we will exploit later. Up to normalization, the eigenstates are the Wigner rotation matrices D, and can also be expressed by the reduced rotation matrices d

$$\sqrt{\frac{8\pi^2}{2J+1}}\ \langle\alpha\theta\gamma|JKM\rangle = D^J_{MK}(\alpha,\theta,\gamma) = \mathrm{e}^{-\mathrm{i}M\alpha}\mathrm{e}^{-\mathrm{i}K\gamma}d^J_{MK}(\theta) \ . \tag{A.3}$$

For the interaction Hamiltonian, we use the dipole approximation with a semi-classical laser field, and obtain

$$\hat{H}_{\text{int}}(t) = -\mathbf{E}(t)\hat{\boldsymbol{\mu}} = -E(t)\mu\ \cos\theta = -E(t)\mu\ D^1_{00}(\alpha,\theta,\gamma) \ . \tag{A.4}$$

Note that the electric field vector $\mathbf{E}$ is parallel to the laboratory frame's z-axis, while the transition dipole moment $\boldsymbol{\mu}$ is parallel to the z-axis in the molecule-fixed frame. The dependence on the orientation of the molecule can be trivially found and expressed as a rotation matrix. We assume that the molecule stays a symmetric top throughout the interaction with the laser pulse, which is reasonable for a pump pulse that is short compared to the molecular dynamics.

We are interested in the n-th order perturbative regime, where the time evolution can be approximated by applying $\hat{H}_{\text{int}}$ n times to the system state (see equation (3.32)).

Eventually, we want to prove that the density is a $2n$-th order polynomial of $\cos\theta$, so we also introduce the density

$$\varrho_{\text{rot}}(\alpha,\theta,\gamma,t) = \sum_{J,K} g^J_K\ \varrho^J_K(\alpha,\theta,\gamma,t) = \sum_{J,K} g^J_K\ \sum_M \left|\psi^J_{KM}(\alpha,\theta,\gamma,t)\right|^2 \ . \tag{A.5}$$

The g^J_K are the Boltzmann factors, which are the population of the initial states $|JKM\rangle$ in thermal equilibrium, and ψ^J_{KM} are the time-dependent wave functions that arise from the initial state $|JKM\rangle$.

We will finally use some relations for the rotation matrices: [48]

$$\sum_M D^{J*}_{MK} D^J_{MK'} = \delta_{KK'} \tag{A.6}$$

$$D^{J*}_{MK} = (-1)^{M-K} D^J_{-M-K} \tag{A.7}$$

$$d^1_{00}(\theta) = \cos\theta \qquad d^1_{01}(\theta) = -d^1_{0-1}(\theta) = \frac{\sin\theta}{\sqrt{2}} \tag{A.8}$$

$$D^1_{00} D^J_{MK} = (-1)^{M-K} \sum_{C=J-1}^{J+1} (2C+1) \begin{pmatrix} 1 & J & C \\ 0 & M & -M \end{pmatrix} \begin{pmatrix} 1 & J & C \\ 0 & K & -K \end{pmatrix} D^C_{MK} \tag{A.9}$$

$$D^C_{MK} \begin{pmatrix} 1 & J & C \\ 0 & M & -M \end{pmatrix} = (-1)^{M-K} \sum_n \begin{pmatrix} 1 & J & C \\ n & K-n & -K \end{pmatrix} D^1_{0n} D^J_{M\,K-n} \ , \tag{A.10}$$

where the 3-j symbols in equations (A.9), (A.10) are real-valued numbers. I want to point out that (A.10) corresponds to equation (B.2) in [55] for $q = 0$ and expressed with 3j-symbols instead of Clebsch-Gordan coefficients.

A.2 First-order perturbation

First, we consider only a single occurrence of the interaction Hamiltonian (A.4). We obtain for the time-dependent wave functions

$$\begin{aligned} \psi^J_{KM}(\alpha,\theta,\gamma,t) &= \langle \alpha\theta\gamma| - \frac{i}{\hbar} \int \mathrm{d}t' \hat{U}_0(t-t') \hat{H}_{\mathrm{int}}(t') \hat{U}_0(t'-t_0) |JKM\rangle \\ &= \sum_{C=J-1}^{J+1} a_{CJK}(t) \begin{pmatrix} 1 & J & C \\ 0 & M & -M \end{pmatrix} D^C_{MK}(\alpha,\theta,\gamma) \ . \end{aligned} \tag{A.11}$$

The first field-free propagation $\hat{U}_0$ produces a complex phase that depends on the quantum numbers J, K, the interaction Hamiltonian (A.4) multiplies the result with another Wigner matrix, which we can contract with (A.9), and the remaining unperturbed time evolution gives another phase depending on the quantum numbers C, K. In consequence, we can expand the wave function into products of a time-dependent coefficient independent of M, a 3j-symbol that depends explicitly on M, and a rotation matrix.
When we next calculate the density (A.5), we obtain

$$\begin{aligned} \varrho^J_K(\alpha,\theta,\gamma,t) = \sum_{C,C'} a^*_{C'JK}(t) a_{CJK}(t) \sum_M \\ \times D^{C'*}_{MK}(\alpha,\theta,\gamma) \begin{pmatrix} 1 & J & C' \\ 0 & M & -M \end{pmatrix} \begin{pmatrix} 1 & J & C \\ 0 & M & -M \end{pmatrix} D^C_{MK}(\alpha,\theta,\gamma) \ . \end{aligned} \tag{A.12}$$

We can repeatedly use the contraction (A.10) to get rid of the 3j-symbols, and reduce the expression to

$$\varrho_K^J(\alpha,\theta,\gamma,t) = \sum_{C,C'} a^*_{C'JK}(t)\; a_{CJK}(t) \sum_{n_1,n_2} b_{JKC'Cn_1n_2} D^{1*}_{0n_1}(\alpha,\theta,\gamma) D^1_{0n_2}(\alpha,\theta,\gamma) \times \sum_M D^{J*}_{M\,K-n_1}(\alpha,\theta,\gamma) D^J_{M\,K-n_2}(\alpha,\theta,\gamma)\ , \quad \text{(A.13)}$$

where we absorbed all the M-independent 3j-symbols in another coefficient b. Using (A.6), the summation over M can be reduced to $\delta_{n_1n_2}$. If we expand the remaining Wigner rotation matrices with (A.3), we find that the γ-dependent phases cancel, and from (A.8), the remaining reduced rotation matrices $|d^1_{0n}|^2$ give either $\cos^2\theta$ or $0.5\sin^2\theta$, which is in any case a second order polynomial of $\cos\theta$.

A.3 Higher-order perturbation

The argument is easily extended to higher-order perturbations. To obtain a detailed insight into this, it is sufficient to go to second-order perturbation theory. So we use the part of the propagator (3.32) with two applications of $\hat{H}_{\text{int}}$, and in the same way as before obtain for the time-dependent wave function

$$\psi^J_{KM}(\alpha,\theta,\gamma,t) = \sum_{C_1=J-1}^{J+1} \sum_{C_2=C_1-1}^{C_1+1} a_{JKC_1C_2}(t) \times \begin{pmatrix} 1 & J & C_1 \\ 0 & M & -M \end{pmatrix} \begin{pmatrix} 1 & C_1 & C_2 \\ 0 & M & -M \end{pmatrix} D^{C_2}_{MK}(\alpha,\theta,\gamma) \quad \text{(A.14)}$$

with M-independent coefficients a. Again, we can calculate the density components

$$\varrho_K^J(\alpha,\theta,\gamma,t) = \sum_{C_1'=J-1}^{J+1} \sum_{C_2'=C_1'-1}^{C_1'+1} \sum_{C_1=J-1}^{J+1} \sum_{C_2=C_1-1}^{C_1+1} a^*_{JKC_1'C_2'}(t) a_{JKC_1C_2}(t) \times \sum_M D^{C_2'*}_{MK}(\alpha,\theta,\gamma) \begin{pmatrix} 1 & C_1' & C_2' \\ 0 & M & -M \end{pmatrix} \begin{pmatrix} 1 & J & C_1' \\ 0 & M & -M \end{pmatrix} \times \begin{pmatrix} 1 & J & C_1 \\ 0 & M & -M \end{pmatrix} \begin{pmatrix} 1 & C_1 & C_2 \\ 0 & M & -M \end{pmatrix} D^{C_2}_{MK}(\alpha,\theta,\gamma)\ . \quad \text{(A.15)}$$

To keep things simple, let us consider only a single summand C_i, C_i', and drop the first line of (A.15). We can apply (A.10) multiple times, and obtain

$$\sum_{\substack{n_1,n_1'\\ n_2,n_2'}} b\; D^{1*}_{0n_1'} D^{1*}_{0,n_2'} D^{1}_{0n_2} D^{1}_{0n_1} \;\sum_{M} D^{J*}_{M\,K-n_2'-n_1'} D^{J}_{M\,K-n_2-n_1}\;, \tag{A.16}$$

where b holds all constant factors, and we have suppressed the angle arguments of the rotation matrices.

Before we simplify this term, let us briefly reflect what we have done. We have first applied the interaction Hamiltonian n times on the wave function, which in general, changes the rotational quantum number J, and adds some factors from the field-free propagation (A.14). However, when we need to calculate the density, we can use the contraction (A.10) to sort of invert this change in the rotational quantum number. As a side effect, each contraction (i.e., each application of $\hat{H}_{\text{int}}$ in first place) leaves some rotation matrix D^1_{0n} or the appropriate complex conjugate.

Now if $n = 0$, this matrix just reduces to a $\cos\theta$. If $n = \pm 1$, the matrix gives some phase $\exp(\mp \mathrm{i}\gamma)$, and a $\sin\theta$. However, when we use the sum rule (A.6), we get $\delta_{n_1+n_2,n_1'+n_2'}$ in (A.16). That is, each contribution $D^1_{0\pm1}$ must be matched by the same complex conjugate, which removes the γ-dependent complex exponential, and ensures that we always have products of two $\sin\theta$-terms.

It is not difficult to perceive that these arguments are not limited to the lowest order perturbation, but also hold for higher orders, or when mixing different orders (e.g. first order for the bra, and second order for the ket) in the density calculation. The order of the polynomial of $\cos\theta$ depends on the number of interactions of the ket plus the bra. For a general n-th order perturbation on the wave function level, we obtain then a polynomial of $\cos\theta$ of order $2n$.

Appendix B

Wave packet methods

Here, I want to present some details on the wave packet calculation of NaI. This appendix is divided into three parts. The first is a brief introduction into the DVR method. Implementing this method has been my major contribution to the `WavePacket` code [22], and it forms the natural basis for propagating the wave function and evaluating diffraction patterns later on. In the second part, we will briefly study the propagation of the wave packet for the case of the NaI molecule. The third part presents the numerical details of the calculation of the diffraction pattern of NaI.

B.1 The DVR method

The DVR method is an efficient method for evaluating the action of special operators on a wave function, and is in principle applicable for an arbitrary basis expansion [56]. Though it can be discussed in the more general context of a pseudo-spectral basis [18], we will only discuss the simplest version, in which we expand the wave function in a basis of Legendre polynomials.
The fundamental building block for the polynomial DVR method is the Gaussian quadrature [18]. It states that for each interval $[a, b]$, weight function $w(x)$ and order N, we can find N points x_i and weights w_i such that

$$\int_a^b w(x) f(x) \mathrm{d}x = \sum_{i=1}^{N} w_i f(x_i) \tag{B.1}$$

is exact if f is a polynomial of degree up to $2N - 1$. For the simplest case of a Gauss-Legendre quadrature, $w(x) = 1$ and the boundaries are $a = -1, b = 1$.
To apply this theorem, let us assume that we have expanded a one-dimensional wave function $\psi(x)$ into normalized Legendre polynomials

$$\psi(x) = \sum_{l=0}^{L-1} f_l \tilde{P}_l(x) \ , \tag{B.2}$$

where $\tilde{P}_l(x) = \sqrt{(2l+1)/2}\, P_l(x)$, and x can take values from -1 to 1. If we choose $N > L$ grid points, we can calculate the coefficients f_l as

$$f_l = \int_{-1}^{1} \tilde{P}_l(x)\psi(x)\mathrm{d}x = \sum_{i=1}^{N} w_i \tilde{P}_l(x_i)\psi(x_i) \ . \tag{B.3}$$

This relation tells us that there are two equivalent representations of ψ. We can either describe the wave function by the coefficient vector $\mathbf{f} = \{f_l\}_{l=0,\ldots,L-1}$ (called the *finite basis representation*, FBR), or we can use the value of the wave function at the quadrature points $\boldsymbol{\psi} = \{\psi(x_i)\}_{i=1,\ldots,N}$ (called the *discrete variable representation*, DVR). Equation (B.2) with $x = x_i$ and equation (B.3) provide the transformation between these two representations.
Now let us go a step further and apply an operator $\hat{A} = A(\hat{x})$ to the wave function. We obtain a new wave function $\psi' = \hat{A}\psi$. Now the DVR method is the relation

$$\psi'(x_i) = A(x_i)\psi(x_i) \ , \tag{B.4}$$

that is, I obtain the DVR of ψ' by multiplying the value of A with the wave function ψ at each grid point. The underlying approximation can be easily seen if we look at ψ' in the FBR

$$\psi'(x) = \sum_l f'_l \tilde{P}_l(x) \ . \tag{B.5}$$

Within the DVR method, I calculate the coefficients f'_l by a combination of (B.3) and (B.4), which yields

$$f'_l = \sum_i w_i \tilde{P}_l(x_i)\psi'(x_i) = \sum_i w_i \tilde{P}_l(x_i)A(x_i)\psi(x_i) \ . \tag{B.6}$$

On the other hand, I can also calculate the f'_l without any approximation as

$$f'_l = \int_{-1}^{1} \tilde{P}_l(x)\psi'(x)\mathrm{d}x = \int_{-1}^{1} \tilde{P}_l(x)\hat{A}\psi(x)\mathrm{d}x = \int_{-1}^{1} \tilde{P}_l(x)A(x)\psi(x)\mathrm{d}x \ . \tag{B.7}$$

So within the DVR method, we replace

$$\int_{-1}^{1} \tilde{P}_l(x)A(x)\psi(x)\mathrm{d}x \quad \longrightarrow \quad \sum_i w_i \tilde{P}_l(x_i)A(x_i)\psi(x_i) \ . \tag{B.8}$$

Since $\tilde{P}_l$ and ψ are by definition polynomials of order $L-1$, the DVR method is exact if $A(x)$ is a polynomial of order $2N - 2L + 1$. In this case, applying the operator $\hat{A}$ in the form of (B.4) is much more convenient than explicitly calculating the matrix elements (B.7), and gives the same results.

As a side note, the DVR method can be easily extended to use various other polynomials. For example, we can rewrite an expansion of a rotational wave function in spherical harmonics $Y_{nm}(\theta, \varphi)$ with fixed quantum number m as an expansion in normalized associated Legendre functions $\tilde{P}_n^m(x = \cos\theta)$. These can be written as [57]

$$\tilde{P}_n^m(x) = (x^2 - 1)^{m/2} f_{n,m}(x) \ , \tag{B.9}$$

where f is a polynomial of order $n - m$. The factor $(x^2 - 1)^m$ forms the weight function when applying the Gaussian quadrature, leading to the Gauss-Jacobi quadrature.
Also, we can also expand the wave function in plane waves, which leads to the Fourier method [58]. This method is also a special DVR method, where the Gaussian quadrature is replaced by analogous properties of the discrete Fourier transformation, and we have to assume that the function $A(x)$ is sufficiently band-limited.
The original `WavePacket` code [59] implemented only the Fourier method. The Gauss-Jacobi quadrature was implemented by Martin Winter, Burkhard Schmidt and me in 2007, which ultimately required a major rewrite of the code.

B.2 NaI calculation

To calculate the dynamics of the NaI molecule, we first set up the Schrödinger equation for the nuclear coordinates as described in section 2.1, especially equation (2.5). If we drop the nuclear center-of-mass motion, we are left with the relative position vector $\mathbf{R}$, which we can express with the internuclear distance R, the angle θ between the molecular axis and the laser polarization vector, and the angle φ that describes the rotation of the molecular axis around the laser polarization vector. Furthermore, we modified the Scrödinger equation (2.5) in two ways.
First, we did not use an adiabatic electronic basis, but the diabatic basis. In this basis, the non-adiabatic couplings are replaced by diabatic, potential-like couplings [18]. Second, we did not propagate the nuclear wave functions Λ_i^{dia}, but made a contact transformation $\Phi_i = R\Lambda_i^{\mathrm{dia}}$. The Schrödinger equation for the Φ_i is then

$$\begin{aligned} \mathrm{i}\hbar\dot{\Phi}_i(R,\theta,\varphi,t) = &\left[-\frac{\hbar^2}{2m}\frac{\mathrm{d}^2}{\mathrm{d}R^2} + \frac{\hat{L}^2}{2mR^2} + V_{ii}^{\mathrm{dia}}(R)\right]\Phi_i(R,\theta,\varphi,t) \\ &+ \sum_j \left[V_{ij}^{\mathrm{dia}}(R) - \varepsilon(t) D_{ij}^{\mathrm{dia}}(R)\cos\theta\right)\Phi_j(R,\theta,\varphi,t) \ . \end{aligned} \tag{B.10}$$

m is the reduced mass of the molecule, $\hat{L}$ is the angular momentum operator, $\varepsilon(t)$ the electric field of the laser. The polarization axis has been chosen to be parallel to the z-axis, and the transition dipole moment is parallel to the molecular axis. The diabatic potentials are defined by

$$V_{ij}^{\mathrm{dia}}(R) = \langle \lambda_i^{\mathrm{dia}}(R) | \, \hat{h} \, | \lambda_j^{\mathrm{dia}}(R) \rangle_{\mathbf{r}} \ , \tag{B.11}$$

and the dipole moments are

$$D_{ij}^{\mathrm{dia}}(R) = \langle \lambda_i^{\mathrm{dia}}(R) | \, \hat{\mu} \, | \lambda_j^{\mathrm{dia}}(R) \rangle_{\mathbf{r}} \ . \tag{B.12}$$

The diabatic potentials and dipole moments were taken from [60]. Only two diabatic states have been included in the calculation; they are coupled by a transition dipole moment parallel to the molecular axis.
As a first step in solving (B.10), we expand the wave functions in a set of plane waves (with periodic boundary conditions) and spherical harmonics

$$\Phi_i(R, \theta, \varphi, t) = \sum_{k.l} c_{ikl}(t) \, \mathrm{e}^{\mathrm{i}kR} \, Y_{lm}(\theta, \varphi) \ . \tag{B.13}$$

In this basis, the kinetic energy operators are diagonal

$$\frac{\mathrm{d}^2}{\mathrm{d}R^2} \, \mathrm{e}^{\mathrm{i}kR} = -k^2 \mathrm{e}^{\mathrm{i}kR} \qquad\qquad \hat{L}^2 Y_{lm}(\theta, \varphi) = l(l+1) Y_{lm}(\theta, \varphi) \ . \tag{B.14}$$

Note that m is a conserved quantum number. For NaI excited from the rotational ground state, we have $m = 0$, and there is no explicit φ-dependence Up to constant factors, we can then replace $Y_{l0}(\theta, \varphi)$ by the normalized Legendre polynomials $\tilde{P}_l(\cos\theta)$.
To summarize, the Φ_i can now be expressed with plane waves and normalized Legendre polynomials, in which basis the kinetic energy is diagonal, and they can also be transformed in the appropriate DVR (discrete points $(R_i, \cos\theta_j)$), where the potentials and dipole moments are trivially applied by the DVR method.
To avoid the implicit periodic boundary conditions when expanding the wave function in plane waves, we added a negative imaginary term to the radial potential that absorbed the wave function before it hit the boundary.
For the actual propagation, we used the symmetric split operator method, changing between the FBR and DVR depending on which part of the Hamiltonian we evaluate. The details of the propagation are explained in [61].

B.3 Calculation of diffraction patterns

Finally, we can calculate the difference diffraction pattern. The derivation is similar to that in section 4.2, however, I choose to redo it for two reasons.
In chapter 4, we discussed the problem of how to deduce the structural information from the diffraction pattern. To simplify this problem, we uncoupled the internal from the rotational degrees of freedom, and dropped the latter. When we do the wave packet calculation, we are in a different situation where we already know the correct (full) difference density, and it is actually difficult to impose the approximation (4.2), so we want to avoid the notion of rotational coefficients, and use the full expansion of (4.5) instead. Also, with little effort, we obtain formulas where the propagated wave function can be directly plugged in.

The starting point is equation (3.58) with the form factor (2.25). Using real atomic form factors [4], we get for NaI

$$\Delta\frac{\mathrm{d}\sigma}{\mathrm{d}\Omega}(\tau) = \sigma_T f_{\mathrm{Na}}(q) f_{\mathrm{I}}(q) \int \mathrm{d}^3R\ \Delta\bar{\varrho}(\mathbf{R},\tau)\Big(\mathrm{e}^{\mathrm{i}\mathbf{q}\mathbf{R}} + \mathrm{e}^{-\mathrm{i}\mathbf{q}\mathbf{R}}\Big)\ . \tag{B.15}$$

The exponentials can be directly transformed as [57]

$$\mathrm{e}^{\mathrm{i}\mathbf{q}\mathbf{R}} = \mathrm{e}^{\mathrm{i}qR\cos\theta'} = \sum_{n=0}^{\infty}(2n+1)(-1)^{n/2}P_n(\cos\theta')j_n(qR)\ , \tag{B.16}$$

where $\cos\theta'$ is the angle between the vectors $\mathbf{q}$ and $\mathbf{R}$. The Legendre polynomial can be further rewritten using the addition theorem for spherical harmonics

$$P_n(\cos\theta') = \frac{4\pi}{2n+1}\sum_{m=-n}^{n} Y^*_{nm}(\theta_q,\varphi_q)Y_{nm}(\theta,\varphi) \tag{B.17}$$

with θ_q, φ_q as the angular coordinates of $\mathbf{q}$. If we now plug (B.16), (B.17) into (B.15), and write out the integration over the spherical coordinates, we get

$$\begin{aligned}\Delta\frac{\mathrm{d}\sigma}{\mathrm{d}\Omega} = 2\sigma_T f_{\mathrm{Na}}(q) f_{\mathrm{I}}(q) \sum_{n\ \mathrm{even}}(-1)^{n/2}(2n+1)\int_0^\infty \mathrm{d}R\int_0^\pi \mathrm{d}\theta\ \sin\theta\, R^2\Delta\bar{\varrho}(R,\theta,\tau)\\ \times j_n(qR)\ \frac{4\pi}{2n+1}\sum_{m=-n}^{n} Y^*_{nm}(\theta_q,\varphi_q)\ \int_0^{2\pi}\mathrm{d}\varphi\ Y_{nm}(\theta,\varphi)\ .\end{aligned} \tag{B.18}$$

Note that terms with odd n cancel during the expansion (B.16). The integration over φ returns $2\pi Y_{n0}(\theta,0)\delta_{m0}$. With some more algebra, and replacing $x = \cos\theta$, we then obtain the final result

$$\begin{aligned}\Delta\frac{\mathrm{d}\sigma}{\mathrm{d}\Omega} = 4\pi\sigma_T f_{\mathrm{Na}}(q) f_{\mathrm{I}}(q) \sum_{n\ \mathrm{even}}(-1)^{n/2}(2n+1)P_n(\cos\theta_q)\\ \times\int_0^\infty \mathrm{d}R\int_{-1}^{1}\mathrm{d}x\ R^2\Delta\bar{\varrho}(R,x,\tau)P_n(x)j_n(qR)\ .\end{aligned} \tag{B.19}$$

For the evaluation of this expression, we note that the difference density at each DVR grid point (R_i, x_j) can be easily obtained from the absolute square of the wave function via (see (3.57))

$$R^2\Delta\bar{\varrho}(R_i,x_j,\tau) = \int \mathrm{d}t\ I(t-\tau)\sum_m\Big(\Big|\Phi_m(R_i,x_j,t)\Big|^2 - \Big|\Phi_m^{\mathrm{ref}}(R_i,x_j)\Big|^2\Big) \tag{B.20}$$

with $I(t)$ describing the shape of the x-ray pulse intensity. The difference density is a polynomial of x, and a band-limited function of R. If we have chosen enough grid points, it is therefore possible to reuse the DVR grid, and evaluate the integrals in (B.19) by the DVR method. The value of q and θ_q can be calculated for each detector pixel from equations (4.22), (4.23).
I finally want to point out that the scripts used for the calculation of the difference diffraction signal are rather generous with all the prefactors. Especially, the Thomson cross section σ_T, equation (3.19), is not included in the calculated cross sections. As it contains products of polarization vectors of the incoming and scattered photon, adding it would slightly distort the diffraction signals in; however, this contribution can easily be removed from an experimental signal.

Bibliography

[1] J. A. Schmidt, M. S. Johnson, U. Lorenz, Y. Jung, and S. Nanbu. Photolysis of N_2O: The dynamics of the N-N mode reveal production of vibrationally excited N_2. *J. Chem Phys*, submitted, 2010.

[2] M. Fischer, U Lorenz, B Schmidt, and R Schmidt. "Centrifugal fragmentation" in the photodissociation of H_2^+ in intense laser fields. *in preparation*, 2007-20xx.

[3] W. Friedrich, P. Knipping, and M. Laue. Interferenzerscheinungen bei Röntgenstrahlen. *Ann. Phys.*, 346:971, 1913.

[4] J.A. Ibers and W.C. Hamilton, editors. *International Tables for X-ray Crystallography*. The Kynoch Press, 1974.

[5] J. Als-Nielsen and D. McMorrow. *Elements of Modern X-Ray Physics*. John Wiley & Sons, 2001.

[6] M. Dantus, M. J. Rosker, and A. H. Zewail. Real-time femtosecond probing of "transition states" in chemical reactions. *J. Chem. Phys.*, 87:2395, 1987.

[7] T. S. Rose, M. J. Rosker, and A. H. Zewail. Femtosecond real-time observation of wave packet oscillations (resonance) in dissociation reactions. *J. Chem. Phys.*, 88:6672, 1988.

[8] H. Stapelfeldt, E. Constant, H. Sakai, and P. B. Corkum. Time-resolved Coulomb explosion imaging: A method to measure structure and dynamics of molecular nuclear wave packets. *Phys. Rev. A*, 58:426, 1998.

[9] C. Z. Bisgaard, O. J. Clarkin, G. Wu, A. M. D. Lee, O. Geßner, C. C. Hayden, and A. Stolow. Time-Resolved Molecular Frame Dynamics of Fixed-in-Space CS_2 Molecules. *Science*, 323:1464, 2009.

[10] J. Arthur et al. Linac Coherent Light Source (LCLS) Conceptual Design Report. Technical Report SLAC-R-593, Stanford Linear Accelerator Center, 2002.

[11] L. F. DiMauro, J. Arthur, N. Berrah, J. Bozek, J. N. Galayda, and J. Hastings. Progress report on the LCLS XFEL at SLAC. *J. Phys.: Conf. Ser.*, 88:012058, 2007.

[12] T. Tanaka and T. Shintake (eds). SCSS X-FEL Conceptual Design Report. Technical report, Riken, 2005.

[13] M. Altarelli et al. The European X-Ray Free-Electron Laser - Technical design report. Technical Report DESY 2006-097, DESY, 2007.

[14] M. Born and R. Oppenheimer. Zur Quantentheorie der Molekeln. *Ann. Phys.*, 389:457, 1927.

[15] M. Born and K. Huang. *Dynamical Theory of Crystal Lattices*. Oxford University Press, 1954.

[16] S. Chelkowski, A. Conjusteau, T. Zuo, and A. D. Bandrauk. Dissociative ionization of H_2^+ in an intense laser field: Charge-resonance-enhanced ionization, Coulomb explosion, and harmonic generation at 600 nm. *Phys. Rev. A*, 54:3235, 1996.

[17] A. D. Bandrauk, S. Chelkowski, and I. Kawata. Molecular above-threshold-ionization spectra: The effect of moving nuclei. *Phys. Rev. A*, 67:013407, 2003.

[18] D. J. Tannor. *Introduction to Quantum Mechanics: A Time-Dependent Perspective*. University Science Books, 2007.

[19] R. Schinke. *Photodissociation Dynamics: Spectroscopy and Fragmentation of Small Polyatomic Molecules*. Cambridge University Press, 1993.

[20] V. Engel and H. Metiu. A quantum mechanical study of predissociation dynamics of NaI excited by a femtosecond laser pulse. *J. Chem. Phys.*, 90:6116, 1989.

[21] M. Grønager and N.E. Henriksen. Real-time control of electronic motion: Application to nai. *J. Chem. Phys.*, 109:4335, 1998.

[22] U. Lorenz and B. Schmidt. WavePacket 4.7.2: A program package for quantum-mechanical wavepacket propagation and time-dependent spectroscopy. Available via http://wavepacket.sourceforge.net, 2010.

[23] T. Helgaker, P. Jørgensen, and J. Olsen. *Molecular Electronic-Structure Theory*. John Wiley & Sons, 2000.

[24] J. Cao and K.R. Wilson. Ultrafast X-ray Diffraction Theory. *J. Phys. Chem. A*, 102:9523, 1998.

[25] N.E. Henriksen and K.B. Møller. On the Theory of Time-Resolved X-ray Diffraction. *J. Phys. Chem. B*, 112:558, 2008.

[26] R. Santra. Concepts in x-ray physics. *J. Phys. B*, 42:023001, 2009.

[27] C. Cohen-Tanoudji, J. Dupont-Roc, and G. Grynberg. *Atom-Photon Interactions*. John Wiley & Sons, 1992.

[28] H. Wagenfeld. Theoretical Computations of X-ray Dispersion Corrections. In S. Ramaseshan and S. C. Abrahams, editors, *Anomalous scattering*. International Union of Crystallography, Munksgaard International Publishers, 1975.

[29] D. T. Cromer and D. Liberman. Relativistic Calculation of Anomalous Scattering Factors for X Rays. *J. Chem. Phys.*, 53:1891, 1970.

[30] P. J. Ho and R. Santra. Theory of x-ray diffraction from laser-aligned symmetric-top molecules. *Phys. Rev. A*, 78:053409, 2008.

[31] T. Rozgonyi, R. Sauerbrey, and T. Feurer. Time-resolved x-ray diffraction in a molecular crystal. *J. Appl. Phys*, 97:013537, 2004.

[32] W.-K. Liu and S. H. Lin. Theory of gas-phase time-resolved ultrafast electron diffraction. *Phys. Rev. A*, 55:641, 1997.

[33] J. H. Hubbell, Wm. J. Weigele, E. A. Briggs, R. T. Brown, D. T. Cromer, and K. J. Howerton. Atomic Form Factors, Incoherent Scattering Functions, and Photon Scattering Cross Sections. *J.Phys.Chem.Ref.Data*, 4:471, 1975.

[34] H. Hayashi, N. Watanabe, and Y. Udagawa. Optical spectra of liquid water in vacuum uv region by means of inelastic x-ray scattering spectroscopy. *J. Chem. Phys.*, 108:823, 1998.

[35] P. Abbamonte, K. D. Finkelstein, M. D. Collins, and S. M. Gruner. Imaging Density Disturbances in Water with a 41.3-Attosecond Time Resolution. *Phys. Rev. Lett.*, 92:237401, 2004.

[36] L. Van Hove. Correlations in Space and Time and Born Approximation Scattering in Systems of Interacting Particles. *Phys. Rev.*, 95:249, 1954.

[37] M. Ben-Nun, T. J. Martínez, P. M. Weber, and K. R. Wilson. Direct imaging of excited electronic states using diffraction techniques: theoretical considerations. *Chem. Phys. Lett.*, 262:405, 1996.

[38] S. Mukamel. *Principles of Nonlinear Optical Spectroscopy.* Oxford University Press, 1995.

[39] R. Loudon. *The Quantum Theory of Light.* Oxford University Press, 2000.

[40] D. A. Kohl and E. J. Shipsey. Elastic electron scattering from state-selected molecules I. Intensities. *Z. Phys. D*, 24:33, 1992.

[41] J. S. Baskin and A. H. Zewail. Oriented Ensembles in Ultrafast Electron Diffraction. *ChemPhysChem*, 7:1562, 2006.

[42] B. Friedrich and D. Herschbach. Alignment and Trapping of Molecules in Intense Laser Fields. *Phys. Rev. Lett.*, 74:4623, 1995.

[43] H. Stapelfeldt and T. Seideman. Colloquium: Aligning molecules with strong laser pulses. *Rev. Mod. Phys.*, 75:543, 2003.

[44] P. J. Ho, D. Starodub, D. K. Saldin, V. L. Shneerson, A. Ourmazd, and R. Santra. Molecular structure determination from x-ray scattering patterns of laser-aligned symmetric-top molecules. *The Journal of Chemical Physics*, 131:131101, 2009.

[45] P. Debye. Zerstreuung von Röntgenstrahlen. *Ann. Phys.*, 351:809, 1915.

[46] T. K. Kim, J. H. Lee, M. Wulff, Q. Kong, and H. Ihee. Spatiotemporal Kinetics in Solution Studied by Time-Resolved X-Ray Liquidography (Solution Scattering). *ChemPhysChem*, 10:1958, 2009.

[47] J. S. Baskin and A. H. Zewail. Ultrafast Electron Diffraction: Oriented Molecular Structures in Space and Time. *ChemPhysChem*, 6:2261, 2005.

[48] D. M. Brink and G. R. Satchler. *Angular Momentum.* Oxford University Press, 1968.

[49] I. S. Gradshteyn and I. M. Ryzhik. *Table of Integrals, Series, and Products.* Academic Press, 1965. formula 7.333-1.

[50] M. Christensen, K. Haldrup, K. Bechgaard, R. Feidenhans'l, Q. Kong, M. Cammarata, M. Lo Russo, M. Wulff, N. Harrit, and M. M. Nielsen. Time-Resolved X-ray Scattering of an Electronically Excited State in Solution. Structure of the $^3A_{2u}$ State of Tetrakis-μ-pyrophosphitodiplatinate(II). *J. Am. Chem. Soc.*, 131:502, 2009.

[51] K. Haldrup, M. Christensen, M. Cammarata, Q. Kong, M. Wulff, S. O. Mariager, K. Bechgaard, R. Feidenhans'l, N. Harrit, and M. M. Nielsen. Structural Tracking of a Bimolecular Reaction in Solution by Time-Resolved X-Ray Scattering. *Angew. Chem.*, 121:4244, 2009.

[52] K. Haldrup, M. Christensen, and M. M. Nielsen. Analysis of time-resolved X-ray scattering data from solution-state systems. *Acta Cryst. A*, 66:261, 2010.

[53] S. Brandt. *Statistical and Computational Methods in Data Analysis.* North-Holland Publishing Company, 1970.

[54] G. A. Korn and T. M. Korn. *Mathematical handbook for scientist and engineers.* McGraw-Hill, 1968.

[55] E. H. van Kleef and I. Powis. Anisotropy in the preparation of symmetric top excited states. I. One-photon electric dipole excitation. *Molecular Physics*, 96:757, 1999.

[56] J. C. Light, I. P. Hamilton, and J. V. Lill. Generalized discrete variable approximation in quantum mechanics. *J. Chem. Phys.*, 82:1400, 1985.

[57] M. Abramowitz and I. A. Stegun (eds). *Handbook of Mathematical Functions with Formulas, Graphs, and Mathematical Tables.* Dover Publications, 1972.

[58] D. Kosloff and R. Kosloff. A Fourier Method Solution for the Time Dependent Schrödinger Equation as a Tool in Molecular Dynamics. *Journal of Computational Physics*, 52:35, 1983.

[59] B. Schmidt. Wavepacket 4.4: A program package for quantum-mechanical wavepacket propagation and time-dependent spectroscopy. Free University Berlin, 2007.

[60] G. H. Peslherbe, R. Bianco, J. T. Hynes, and B. M. Ladanyi. On the photodissociation of alkali-metal halides in solution. *J. Chem. Soc. Faraday Trans.*, 93:977, 1997.

[61] M. R. Hermann and J. A. Fleck Jr. Split-operator spectral method for solving the time-dependent Schrödinger equation in spherical coordinates. *Phys. Rev. A*, 38:6000, 1988.

Paper I

Theory of time-resolved inelastic x-ray diffraction

Theory of time-resolved inelastic x-ray diffraction

Ulf Lorenz,* Klaus B. Møller,† and Niels E. Henriksen‡
CMM, Department of Chemistry, Building 207, Technical University of Denmark, DK-2800 Kgs. Lyngby, Denmark
(Received 23 October 2009; published 24 February 2010)

Starting from a general theory of time-resolved x-ray scattering, we derive a convenient expression for the diffraction signal based on a careful analysis of the relevant inelastic scattering processes. We demonstrate that the resulting inelastic limit applies to a wider variety of experimental conditions than similar, previously derived formulas, and it directly allows the application of selection rules when interpreting diffraction signals. Furthermore, we present a simple extension to systems simultaneously illuminated by x rays and a laser beam.

DOI: 10.1103/PhysRevA.81.023422 PACS number(s): 34.80.Qb, 32.80.Wr, 33.80.−b, 42.50.Ct

I. INTRODUCTION

Since its discovery, x-ray diffraction has become a major tool for studying the structure of matter. Its key virtue is that, in a time-independent framework [1], the differential cross section for elastic scattering is just the Fourier transform of the electronic density ϱ_e,

$$\frac{d\sigma}{d\Omega} = \left| \int d^3r \; \varrho_e(\mathbf{r}) \, e^{i\mathbf{qr}} \right|^2, \tag{1}$$

where we neglected the weak scattering from the nuclei and expressed the cross section in units of the scattering of a free electron. This gives almost direct access to real-space information of the electronic structure. In contrast to optical photons, x rays interact with all electrons, which makes the cross section insensitive to minor variations of valence orbitals. One can therefore often go further and use the independent atom model (IAM), in which one models ϱ_e by the density of the isolated atoms. Within this approximation, the diffraction pattern becomes a function of the atomic positions in the probed system.

It is therefore not surprising that currently, much work is spent on the development of intense, pulsed, femtosecond x-ray sources, namely, free electron lasers (FELs). After exciting a system with an optical pump pulse, the subsequent dynamics can be followed in time by a femtosecond x-ray pulse with variable time delay. If the time-resolved scattering can be described by a formula similar to Eq. (1), this allows us to directly follow atomic rearrangements without the need for complex electronic structure calculations that link the experimental signal to the molecular dynamics. However, similar to modern ultrafast optical pump-probe experiments, we require an extension of the conventional static theory.

The previous work on the theoretical foundations of time-resolved x-ray diffraction (TRXD) can be roughly divided into two categories. In one approach, the conventional expression (1) is used as the starting point [2–8]. Essentially, the electronic density gets an additional time variable, and the result is convoluted with the time-dependent intensity of the x-ray beam to obtain the signal as a function of the delay time. However, Eq. (1) is typically derived from Fermi's Golden Rule [1,6]. In the derivation of the Golden Rule, the initial state is assumed to be an eigenstate of the unperturbed Hamiltonian, that is, to have no intrinsic time dependence. An alternative derivation of (1) uses classical electromagnetic theory for the treatment of the x-ray field [4]. Here, it is assumed that the electric current in the target system is exclusively induced by the incoming x-ray field, which again requires a negligible time evolution. Furthermore, the (classical) x-ray field and the (quantum) target system are coupled via the dielectric constant. This quantity, however, is obtained from time-independent perturbation theory and can therefore be assigned only to time-independent states, not to wave packets. Strictly speaking, formulas obtained by these derivations are thus not valid for describing ultrafast, coherent wave-packet motion. However, they have been applied successfully to subpicosecond TRXD experiments [8], which suggests that, though the derivation is different, the formulas for TRXD should have a form similar to that of the time-independent theory.

In another approach, one evaluates the interaction between the studied nonstationary quantum system and the x-ray photon field, usually within first-order perturbation theory. This has been done with a wave-packet [9,10] or density-operator formalism [11–13].

In general, the interaction between the x rays and the target system can be either elastic, leaving the state of the target systems unchanged, or inelastic, thereby changing the population of the individual energy eigenstates. With the exception of [12,13], previous work focused on a hybrid "electronically elastic" scattering. It was assumed that the scattering process is inelastic with respect to nuclear modes but elastic with respect to electronic states, or that contributions to electronically inelastic diffraction can be removed by special experimental setups. It is interesting to note that the same approximation of electronically elastic scattering has also been used in the closely related field of time-resolved electron diffraction (e.g., [14]). However, this approach is different from the earliest treatments on x-ray diffraction [15], which explicitly considered electronically inelastic components. In this paper, we want to review the theory for TRXD without such a hybrid scheme. We obtain a less restrictive, more general formulation, which also permits the use of symmetry arguments in the evaluation of the diffraction signal.

In Sec. II, we outline and discuss the general system-independent formulation. We then focus on molecular systems in Sec. III, and connect our results to those derived previously.

*ulf.lorenz@kemi.dtu.dk
†klaus.moller@kemi.dtu.dk
‡neh@kemi.dtu.dk

Section IV summarizes our findings and provides an outlook on further research. In the appendices, we discuss an extension of the theory to systems with time-dependent Hamiltonians,and discuss in more detail some of the approximations used in the derivations.

II. GENERAL THEORY

The key quantity of interest in x-ray diffraction is the differential signal strength $dS/d\Omega$, which we define as the number of scattered photons arriving in a certain solid angle. If we allow these photons to have frequencies ω_s that are different from the central frequency ω_0 of the incoming beam, we can write

$$\frac{dS}{d\Omega} = \int_{\omega_1}^{\omega_2} d\omega_s \frac{d^2S}{d\Omega d\omega_s}, \tag{2}$$

to express it in terms of the double-differential signal strength. This quantity is then defined as

$$\frac{d^2S}{d\Omega d\omega_s} = \rho(\omega_s) \lim_{t\to\infty} \langle \Xi_0 | \hat{U}^\dagger(t,t_0) \hat{n}_{\mathbf{k}_s,\epsilon_s} \hat{U}(t,t_0) | \Xi_0 \rangle. \tag{3}$$

The initial state Ξ_0 is a direct product consisting of a target in a prepared nonstationary state Ψ and a photon state ψ_{uk_0} that describes the x-ray pulse on its way to the target. They interact, and after essentially infinite time, the scattered photons hit a detector that is modeled by the photon number operator $\hat{n}_{\mathbf{k}_s,\epsilon_s}$, and counts the number of photons with wave vector $\mathbf{k}_s$ and optionally polarization ϵ_s. Multiplication by the density of photon states ρ yields the number of scattered photons per solid angle. If the propagation is carried out with first-order perturbation theory for the interaction between the target and the x rays, we obtain (see [10] for the details)

$$\frac{d^2S}{d\Omega d\omega_s} = \left(\frac{d\sigma}{d\Omega}\right)_{\mathrm{Th}} \frac{\omega_s}{\omega_0} s(\mathbf{q}, \omega_0 - \omega_s), \tag{4}$$

where

$$s(\mathbf{q},\omega) = \frac{1}{2\pi} \int dt\ I(t) \int d\delta\ C(\delta) e^{i\omega\delta} \times \left\langle \Psi\left(t+\frac{\delta}{2}\right) \middle| \hat{L}^\dagger \hat{U}\left(t+\frac{\delta}{2}, t-\frac{\delta}{2}\right) \hat{L} \middle| \Psi\left(t-\frac{\delta}{2}\right) \right\rangle. \tag{5}$$

Here, $(d\sigma/d\Omega)_{\mathrm{Th}}$ is the classical Thomson cross section of a free electron,

$$I(t) = \frac{2\epsilon_0 c}{\hbar\omega_0} \left\langle \psi_{uk_0} \middle| \hat{E}^{(-)} \hat{E}^{(+)} \middle| \psi_{uk_0} \right\rangle \tag{6}$$

is the photon number intensity of the incoming beam,

$$\hat{L} = \sum_{i=1}^{\#\mathrm{electrons}} e^{i\mathbf{q}\hat{\mathbf{r}}_i} \tag{7}$$

is the scattering operator with $\mathbf{q} = \mathbf{k_0} - \mathbf{k_s}$ being the scattering vector, and

$$C(\delta) = \int d\omega' F(\omega_0 + \omega') e^{i\omega'\delta} \tag{8}$$

defines the coherence function of the x-ray beam in terms of the normalized power spectrum F, which is centered around ω_0. The typical decay time T_c of the coherence function is inversely proportional to the width $\Delta\omega_0$ of F. Note that the convention for some of the symbols differs from [10] for convenience, and to be more in line with the classic literature.

As discussed in [10], the result is also valid for the important practical case where the x-ray beam is not a coherent photon state but described by incoherent ensembles. This result was derived using two important assumptions. We assumed that the beam is fully characterized by its intensity and power spectrum. This only holds for special cases, such as FELs in the linear regime [16] or ensembles of identical Gaussian pulses. Furthermore, we have neglected wave-vector dispersion of the x-ray beam. In the classical limit, this translates to the substitution of the electric field

$$\mathbf{E}(\mathbf{r},t) = \mathbf{E}_0 h(\mathbf{r},t) e^{i(\mathbf{k_0 r} - \omega_0 t)} \approx \mathbf{E}_0 h(\mathbf{R},t) e^{i(\mathbf{k_0 r} - \omega_0 t)}, \tag{9}$$

that is, the envelope function h is only evaluated at the position $\mathbf{R}$ of the target system. The incoming beam is thus assumed to have a fixed wave vector $\mathbf{k_0}$, but varying frequencies. The idea is that the wave vector of the incoming photon only enters through the scattering vector $\mathbf{q}$, whose variations can be neglected. We discuss this approximation in the next subsection when we also vary the length of the wave vector of the scattered photon, $\mathbf{k}_s$.

In the following, we will discuss the limit of inelastic diffraction in more detail, using an analysis similar to the work of Cao and Wilson [9]. For more convenient manipulation, we start by transforming (5) to an energy eigenstate representation. If the Hamiltonian $\hat{H}$ of the probed system is time independent (for time-dependent systems, see Appendix A), the wave function can be expanded as

$$\Psi(t) = \sum_i c_i \varphi_i e^{-iE_i t/\hbar}, \quad \hat{H}\varphi_i = E_i \varphi_i. \tag{10}$$

Inserting this and performing standard manipulations yields

$$s(\mathbf{q}, \omega_0 - \omega_s) = \int dt\ I(t) \sum_{ijk} c_i^* c_j\ e^{-i(E_j - E_i)t/\hbar} L_{ki}^* L_{kj} \times F\left(\omega_s + \frac{1}{\hbar}\left(E_k - \frac{E_i + E_j}{2}\right)\right), \tag{11}$$

with $L_{ik} = \langle \varphi_i | \hat{L} | \varphi_k \rangle$.

A. Inelastic limit

Let us first consider the limit of elastic diffraction $L_{ij} = \delta_{ij} L_{ii}$. Equation (11) simplifies to

$$s(\mathbf{q}, \omega_0 - \omega_s) = \sum_i |c_i|^2 |L_{ii}|^2 F(\omega_s) \int dt I(t), \tag{12}$$

and the diffraction image becomes independent of time. The reason is that the interference terms $i \neq j$ in (11) hold the information about the time evolution of the quantum system, but they do no contribute here. We conclude thus that we are *not* interested in purely elastic scattering, but we have to include inelastic terms.

To do so, we insert (11) and (4) into (2) and change the order of integration and summation, which yields

$$\frac{dS}{d\Omega} = \left(\frac{d\sigma}{d\Omega}\right)_{\mathrm{Th}} \int dt\, I(t) \sum_{ijk} c_i^* c_j e^{-i(E_j - E_i)t/\hbar} \times \int_{\omega_1}^{\omega_2} d\omega_s\, L_{ki}^* L_{kj}\, \frac{\omega_s}{\omega_0}\, F\left(\omega_s + \frac{1}{\hbar}\left(E_k - \frac{E_i + E_j}{2}\right)\right). \tag{13}$$

This expression is difficult to simplify because the summation over i, j, k, and the integration over ω_s are entangled. This happens through the argument of F, but also through the scattering operator $\hat{L}$, since $\mathbf{k}_s$, and thus $\mathbf{q}$, is a function of the frequency ω_s. However, this problem is not unique to time-resolved diffraction. For systems in their stationary ground state, $c_i = c_j = \delta_{i0}$, Eq. (13) corresponds to time-independent diffraction, and the entanglement of the remaining k summation and the ω_s integration is still in there. In this context, a solution for this problem is well known under the name "static approximation" [15,17]. To get an insight into the approximations and limitations when applying this to TRXD, we shall go through the derivation in some detail.

The probed target system is in a nonstationary state whose energy spread is at most a few eV, that is, $|E_i - E_j| \ll \hbar\omega_0$. Furthermore, the basis of the static approximation is the assumption that the matrix elements L_{ik} can be neglected unless $|E_k - E_i| \ll \hbar\omega_0$, which we discuss in detail in Appendix B. Thus, although we formally retain the unrestricted sums over i, j, k, only those summands with $|\Delta E| = |E_k - (E_i + E_j)/2| \ll \hbar\omega_0$ contribute to the signal.

To exploit this relation, we require the interval $[\omega_1, \omega_2]$ to include ω_0. We also assume that the power spectrum F has a not too large width $\Delta\omega_0 \ll \omega_0$. The integrand is then dominated by contributions with $|\omega_s - \omega_0| \lesssim |\Delta E|/\hbar + \Delta\omega_0 \ll \omega_0$, otherwise, either F or the matrix elements L_{ki}, L_{kj} vanish.

As a result of this, we find that the scattering vector remains almost constant when integrating over ω_s. For example, we find from geometric relations that

$$\left|\frac{q^2}{q_0^2} - 1\right| \leqslant \left|\frac{\Delta E}{\hbar\omega_0}\right| + \left|\frac{\Delta\omega_0}{\omega_0}\right|^2 + \left|\frac{\Delta\omega_0 \Delta E}{\hbar\omega_0^2}\right| + \left(\frac{|\Delta E| + 2\hbar\Delta\omega_0}{\hbar c q_0}\right)^2, \tag{14}$$

where q_0 is the magnitude of the scattering vector for elastic scattering $k_s = k_0$, and c is the speed of light. For typical FEL parameters $\hbar\omega_0 \approx 10$ keV, $\Delta\omega_0/\omega_0 = 10^{-3}$ [18], and assuming $|\Delta E| \leqslant 100$ eV (see Appendix B), and $q_0 = 0.5$–8 Å^{-1}, the relative variation $|q/q_0|$ is less than 3%.

Since the length of the scattering vector stays almost constant, and diffraction patterns are usually not overly sensitive to the value of $\mathbf{q}$ (see, e.g., examples in [1] and discussion in [10]), we now replace the scattering operator $\hat{L}$ by the elastic version $\hat{L}_0 = \hat{L}(\mathbf{q}|k_s = k_0)$, and move its matrix elements outside of the integral. Using all the approximations so far, and setting $\omega_s/\omega_0 \approx 1$, the remaining integral

$$\int_{\omega_1}^{\omega_2} d\omega_s\, F\left(\omega_s + \frac{1}{\hbar}\left(E_k - \frac{E_i + E_j}{2}\right)\right) \tag{15}$$

gives a constant of unity for all i, j, k, if $\omega_1 \to 0$ and $\omega_2 \to \infty$, i.e., if the detector collects all photons. We can then rewrite the differential signal strength as

$$\frac{dS}{d\Omega} = \left(\frac{d\sigma}{d\Omega}\right)_{\mathrm{Th}} \int dt\; I(t) \langle \Psi(t)|\hat{L}_0^\dagger \hat{L}_0|\Psi(t)\rangle. \tag{16}$$

This is the inelastic limit of x-ray diffraction. A similar expression has been derived in the context of TRXD before [9,10]. However, the previous works do not stress its fundamental importance for time-resolved diffraction. As our more detailed derivation shows, (16) is the relevant limit if the static approximation is valid, and the following experimental conditions hold:

1. The system evolves freely during the scattering process.
2. Only states with low energies are excited, that is, $|E_i - E_j| \ll \hbar\omega_0$, which should be fulfilled for all but a few exotic experiments.
3. The incoming x-ray beam has a sufficiently narrow bandwidth $\Delta\omega_0 \ll \omega_0$.
4. We collect all scattered photons, $\omega_1 \to 0$, $\omega_2 \to \infty$.

Since these resemble typical experimental conditions, we conclude that the inelastic limit should be generally chosen as the starting point for further theory. This limit also has properties that are of special importance in the context of time-resolved diffraction.

First, it is not restricted to a special representation of the wave function. This allows us to use the same basic formula (16) for different tasks such as mapping atomic orbitals [2] or measuring atomic rearrangements within a molecule. We can also trivially recast the result using a density operator $\hat{\varrho}$. If we neglect decoherence (i.e., statistical mixing with a thermal bath) during the interaction with the x-ray pulse, we can write directly

$$\frac{dS}{d\Omega} = \left(\frac{d\sigma}{d\Omega}\right)_{\mathrm{Th}} \int dt\, I(t) \mathrm{Tr}[\hat{\varrho}(t)\hat{L}_0^\dagger \hat{L}_0]. \tag{17}$$

For completeness, we want to point out that a more detailed derivation would show that this density-operator formulation holds as long as we can neglect decoherence during the coherence time of the x-ray pulse, which is at most about a femtosecond [19]. For this, we first rewrite (5) with a density operator [see also Eq. (42) in [12]]. If decoherence can be neglected during the coherence time, an expansion equivalent to (10) can be performed. The rest of the discussion about the static approximation only involved matrix elements of $\hat{L}$, and it is equally valid for all representations of the quantum state.

The only restriction we had to put on the target system is a time-independent Hamiltonian. By examining carefully why and how we did this, we can find a simple extension of the theory to systems irradiated by lasers if the laser parameters change sufficiently slowly. This is detailed in Appendix A.

Finally, the operator $\hat{L}_0^\dagger \hat{L}_0$ is symmetric under space inversion, which allows the use of symmetry arguments in the evaluation of expectation values. This is in contrast to the operator $\hat{L}$ that has no trivial symmetry properties.

B. Symmetry considerations

In many experiments, we study systems whose total Hamiltonian is symmetric under space inversion, for example, free molecules in the gas phase. The energy eigenstates, which are typically the initial states for the pump-probe experiments, also obey this symmetry. If we assume that spin is a good quantum number, they are either even or odd functions with respect to the inversion of all (nuclear and electronic) space coordinates.

The same argument holds for systems in contact with a thermal bath, such as small sections in a liquid sample. In thermal equilibrium, the density operator of the system commutes with the Hamiltonian $[\hat{H}, \hat{\rho}] = 0$. In the absence of degeneracies, and for Hamiltonians symmetric under inversion, each eigenstate of this density operator (or, equivalently, each member of the thermal ensemble) is then an even or odd function of the coordinates.

The excitation of the system with a linearly polarized pump laser involves the dipole operator $\hat{\mu}$, which is odd under space inversion. It is known from elementary group theory that each application then changes the symmetry of the state. If we excite the system by absorption of an odd number of photons, we thus create a coherent superposition of a ground state Ψ_g and an excited state wave packet Ψ_e

$$|\Psi(t)\rangle = |\Psi_g(t)\rangle + |\Psi_e(t)\rangle, \tag{18}$$

with Ψ_g, Ψ_e transforming differently under space inversion. When calculating (16), contributions of the form

$$\langle\Psi_g(t)|\hat{L}_0^\dagger \hat{L}_0|\Psi_e(t)\rangle = \langle\Psi_g(t)|\sum_{i\neq j}^{N_e} e^{i\mathbf{q}(\hat{\mathbf{r}}_i-\hat{\mathbf{r}}_j)}|\Psi_e(t)\rangle \tag{19}$$

are zero, because the operator $\hat{L}_0^\dagger \hat{L}_0$ is invariant under space inversion. The diffraction image is thus an *incoherent* sum of the images of the ground and excited state wave function.

However, this argument does not hold under certain circumstances:

1. If the Hamiltonian is not symmetric under inversion, the eigenstates have no symmetry properties, and the previous argument is void. The typical example here are molecules at interfaces.
2. For systems that are oriented prior to the arrival of the pump pulse, the symmetry of the initial state is destroyed by the orientation.
3. If the excitation includes an even number of photons, Ψ_g, Ψ_e have the same symmetry properties.

In these cases, the interference terms (19) also show up in the diffraction pattern, which is now the *coherent* sum of the two states. We thus have the possibility to include or exclude specific contributions to the signal.

III. APPLICATION TO MOLECULES

We use the well-known Born-Huang representation [20] to apply the theory to molecules. For this, we decompose the system into nuclei and electrons and denote their collective coordinates as $\mathbf{R}$ and $\mathbf{r}$. The total wave function is factorized into "nuclear" and "electronic" wave functions

$$\Psi(\mathbf{R}, \mathbf{r}, t) = \sum_m \Lambda_m(\mathbf{R}, t)\lambda_m(\mathbf{r}; \mathbf{R}). \tag{20}$$

For each $\mathbf{R}$, the electronic states λ_m are chosen to form an orthonormal basis set in the electronic subsystem

$$\langle\lambda_m(\mathbf{R})|\lambda_n(\mathbf{R})\rangle_r = \delta_{mn}. \tag{21}$$

Here and in the following, we use the subscript r to denote an integration over only the electronic coordinates. Furthermore, we will drop the explicit $\mathbf{R}$ dependence of λ_m. For most applications, only a few electronic states need to be considered, which greatly reduces the dimensionality of the quantum system.

We can directly insert the Born-Huang representation (20) into (16) and obtain the diffraction signal of a molecule. Writing out the integration over the nuclear coordinates explicitly, we obtain

$$\frac{dS}{d\Omega} = \left(\frac{d\sigma}{d\Omega}\right)_{\text{Th}} \int dt\ I(t) \sum_{n,m} \times \int d\mathbf{R}\ \Lambda_m^*(\mathbf{R}, t)\Lambda_n(\mathbf{R}, t)\ s_{mn}(\mathbf{R}), \tag{22}$$

$$s_{mn}(\mathbf{R}) = \langle\lambda_m|\hat{L}_0^\dagger \hat{L}_0|\lambda_n\rangle_r. \tag{23}$$

For density operators, the Born-Huang representation corresponds to the expansion

$$\hat{\varrho}(t) = \sum_{mn} \hat{\varrho}_{mn}(t)|\lambda_n\rangle\langle\lambda_m|, \tag{24}$$

where the operators $\hat{\varrho}_{mn}$ act on the nuclear degrees of freedom only. We write out the trace over the electronic degrees of freedom explicitly and evaluate the trace over the nuclear coordinates in a local basis. Equation (17) becomes then

$$\frac{dS}{d\Omega} = \left(\frac{d\sigma}{d\Omega}\right)_{\text{Th}} \int dt I(t) \sum_{m,n} \int d\mathbf{R}\varrho_{mn}(\mathbf{R}, t)s_{mn}(\mathbf{R}), \tag{25}$$

$$\varrho_{mn}(\mathbf{R}, t) = \langle\mathbf{R}|\hat{\varrho}_{mn}(t)|\mathbf{R}\rangle. \tag{26}$$

The terms $\varrho_{mm}(\mathbf{R})$ are the nuclear densities and define the probability density of finding a nuclear configuration $\mathbf{R}$ with a certain electronic state $|\lambda_m\rangle$. The nondiagonal terms $\varrho_{mn}(\mathbf{R})$ are the nuclear coherences; the corresponding terms describe interferences between the different electronic states in the diffraction pattern.

For practical use, and to gain more insight, we shall now consider additional approximations to connect the general result (25) to those derived previously [9–11].

A. Connection to other derivations

While the results so far are applicable to an arbitrary electronic basis λ_m, we now restrict our choice to the adiabatic basis. If we write the Hamiltonian as a sum

$$\hat{H} = \hat{T}_R + \hat{h} \tag{27}$$

of the kinetic energy $\hat{T}_R$ of the nuclei and an "electronic Hamiltonian" $\hat{h}$, the adiabatic basis are those electronic states

that diagonalize $\hat{h}$. This is a common choice and has been selected by other authors we wish to compare our results to.

We start by having a closer look at the coherences $\varrho_{mn}(\mathbf{R})$. For slow nuclear motion, they oscillate with a frequency of roughly the inverse electronic energy spacing. If the length of the x-ray pulse and the timing jitter between the pump and probe pulses are small enough to resolve these oscillations, the coherences show up as "beating" patterns in the diffraction image.

However, these terms can often be neglected. For well-separated electronic states, the time resolution needs to be on the order of single femtoseconds to measure them. If one of the states m, n is populated through excitation from the other state by absorbing an odd number of photons, the coherence terms between these two states will not contribute due to the symmetry arguments outlined earlier. Most importantly, we argue in Appendix B that for many systems, the matrix elements s_{mn} are significantly smaller than the diagonal terms s_{mm}, thus reducing the contribution from the coherences.

If we drop the contributions of the nuclear coherences, only a single sum in (25) is left. To simplify the evaluation of the remaining matrix elements $s_{mm}(\mathbf{R})$, we use a resolution of identity $\mathbb{1}_r = \sum_n |\lambda_n\rangle\langle\lambda_n|$ to formally separate them into an elastic and a purely inelastic contribution

$$s_{mm} = |\langle\lambda_m|\hat{L}_0|\lambda_m\rangle_r|^2 + \sum_{n\neq m} |\langle\lambda_n|\hat{L}_0|\lambda_m\rangle_r|^2. \tag{28}$$

Inserting this into (25) yields, after neglecting the nuclear coherence terms,

$$\frac{dS}{d\Omega} = \left(\frac{d\sigma}{d\Omega}\right)_{\mathrm{Th}} \int dt\, I(t) \sum_m \times \int d\mathbf{R}\, \varrho_{mm}(\mathbf{R}, t) |\langle\lambda_m|\hat{L}_0|\lambda_m\rangle_r|^2 + S_{\mathrm{inel}}. \tag{29}$$

The first term gives the "electronically elastic" scattering and has a simple interpretation. The matrix element $\langle\lambda_m|\hat{L}_0|\lambda_m\rangle$ is the Fourier transform of the electronic density of state m. Thus, the first term is similar to the standard result of x-ray diffraction [see Eq. (1)] weighted by a time-averaged distribution of nuclear geometries. S_{inel} denotes the purely inelastic contribution to the signal. Its interpretation and evaluation is much more cumbersome, so we wish to remove it in one way or the other.

Two solutions have been proposed in the literature. In one approach [5], it is assumed that the inelastic contribution can be neglected because the nondiagonal elements $\langle\lambda_n|\hat{L}_0|\lambda_m\rangle_r$ are small compared to the diagonal terms. This general result stems from the fact that only a single orbital contributes to the matrix element (see Appendix B), while all electrons contribute to the elastic scattering. However, this argument is problematic because, even though the *single* matrix elements are small (see Appendix B), the sum in (28), and thus S_{inel} includes many terms. For atoms, this inelastic scattering contribution has been tabulated (e.g., [21]). Even for heavy species, such as iodine, the elastic and inelastic contributions are similar in magnitude for $q \gtrsim 6$ Å^{-1}, so this seems too crude an approximation.

Other references suggested an energy-scale separation (vaguely described in [9], implicitly used in [10], and explicitly pointed out in [11]). For this, we note that (11) only gives a significant contribution if the argument of F is approximately ω_0. The intuitive picture that emerges is that each excitation of the system leads to a corresponding energy loss of the outgoing photon. For a nearly monochromatic source, $F(\omega) \approx \delta(\omega - \omega_0)$, the energy of the outgoing photons exhibits a peak for each resonance. We can now use the Born-Oppenheimer approximation, and we assume that energy levels corresponding to an excitation of nuclear modes (which we wish to include) have much smaller energy spacing than the electronic states (which we want to remove). By filtering out the latter contributions (i.e., photons deviating from ω_0 by more than, say, 1 eV) before they reach the detector, we can remove all electronically inelastic components from the diffraction pattern, so that $S_{\mathrm{inel}} = 0$.

However, this argument has several problems as well. The energy-scale separation becomes meaningless for close-lying electronic states. Thus, this line of thought excludes nonadiabatic transitions, which are very common in photochemistry. Furthermore, the required excessive filtering of the incoming and outgoing photons might reduce the signal by orders of magnitude, which makes this setup somewhat unattractive.

However, we note that practical experiments often use difference diffraction techniques for TRXD (e.g., [4,22]). That is, two diffraction images are taken, one with the pump laser turned on and off, respectively, and the two signals are subtracted to yield a difference signal. If we are interested in the difference signal, we do not have to require that the inelastic contribution *vanishes*. If it is independent of the atomic arrangement, and the electronic state, the corresponding terms cancel already due to norm conservation. Furthermore, in many experiments, the scattering signal is evaluated using the independent atom model (IAM) (e.g., [1,9,10]) for the description of the electronic densities. The IAM approximates the electronic structure of a molecule by that of its independent constituent atoms. It does therefore not describe the reorganization of electronic densities due to chemical binding. As detailed in Appendix B, we can show that S_{inel} is roughly independent of the molecular structure within the limit of the IAM, and it can thus be ignored in difference diffraction images. A similar argument has been used previously for the case of gas-phase electron diffraction by Liu and Lin [23]. This solution allows us to approximate the scattering with molecular targets as being electronically elastic, solves all of the problems mentioned earlier, but still allows us to employ, for example, symmetry rules derived in the inelastic limit.

We finally assume that the scattering from all electronic states is similar, as only a few valence orbitals are rearranged, and replace the matrix elements by the IAM form factor (see, e.g., [9,10], and Appendix B3)

$$\langle\lambda_m|\hat{L}_0|\lambda_m\rangle_r \approx f_{\mathrm{IAM}}(\mathbf{q};\mathbf{R}) = \sum_{\alpha}^{\#\mathrm{atoms}} f_\alpha(\mathbf{q})\, e^{i\mathbf{q}\mathbf{R}_\alpha}, \tag{30}$$

with the atomic form factors

$$f_\alpha(\mathbf{q}) = \int d^3r\, \varrho_\alpha(\mathbf{r}) e^{i\mathbf{q}\mathbf{r}}, \tag{31}$$

and ϱ_α and $\mathbf{R}_\alpha$ the ground-state electronic density and position of atom α. Since we deal with difference patterns, we

further denote by $\Delta\varrho_{mm}$ the difference densities between our diffraction pattern and a reference pattern (e.g., obtained by turning the excitation laser off). Equation (29) gives

$$\frac{d\Delta S}{d\Omega} = \left(\frac{d\sigma}{d\Omega}\right)_{\mathrm{Th}} \int dt\, I(t) \times \int d\mathbf{R} \left[\sum_m \Delta\varrho_{mm}(\mathbf{R}, t)\right] |f_{\mathrm{IAM}}(\mathbf{q}; \mathbf{R})|^2. \quad (32)$$

The quantity in brackets is the difference in the probability density of finding a certain nuclear geometry $\mathbf{R}$ at time t. Within the limit of the IAM and neglect of coherence terms, the diffraction signal is therefore just the product of the "time-averaged difference distribution of geometries," $\int I(t) \sum_m \Delta\varrho_{mm}(\mathbf{R}, t)\, dt$, and the IAM form factor, integrated over all geometric configurations $\mathbf{R}$. This final result closely resembles the time-independent theory but with a distribution function that depends on the pump-probe delay time.

IV. CONCLUSIONS AND OUTLOOK

In this paper, we reviewed the general result of our previous work on time-resolved x-ray diffraction for nonstationary systems [10] and reformulated it in a form that is more in line with the standard results for time-independent systems.

We argued that in the context of scattering on nonstationary systems, it is essential to allow for inelastic scattering processes in the target system but that the scattering operator only connects states whose energy difference is small compared to the energy of the incoming photons (the "static approximation"). Furthermore, under typical experimental conditions, we can replace the scattering operator by its elastic version. This leads to the central result for the differential signal strength given in Eq. (16).

We applied this formalism to molecules and obtained expressions that contain nuclear coherences between different electronic states. This implies that the diffraction patterns are not equal to the classical incoherent sum of signals from each of the involved electronic states, but involve fast-oscillating "beating" contributions [9]. We argued, however, that in many situations, these coherences can be neglected, even for closely spaced electronic states. Employing further results from the widely used independent atom model, the calculation of difference diffraction patterns can be condensed into a simple and appealing form, Eq. (32).

Having established the formalism allows future investigation of new questions. It is, for example, well known that wave packets created by ultrashort laser pulses can show strong dispersion. In contrast to vibrational ground states typically encountered in stationary systems, these wave packets can easily span distances of several Ångströms. The impact of this on the obtainable information from diffraction patterns is basically unknown. Furthermore, we argued that the nuclear coherence terms can be usually neglected. For systems composed of light atoms, however, they might show up in diffraction patterns. Identifying promising systems and describing the resulting diffraction patterns requires a more detailed quantitative analysis.

ACKNOWLEDGMENTS

This work was supported by the Danish National Research Foundation's Center for Molecular Movies (CMM). We thank Stephan P. A. Sauer for useful discussions.

APPENDIX A: SYSTEMS WITH TIME-DEPENDENT HAMILTONIAN

In the course of our formal derivations, we required that the system evolves under a time-independent Hamiltonian, Eq. (10). In this appendix, we review this restriction. As it turns out, this restriction can be relaxed to encompass systems driven by a laser with slowly varying parameters. We first employ Floquet theory to formally remove the periodic oscillation of the electric field, then we use the adiabatic theorem to treat nonperiodic (pulsed) laser fields.

The limit of an overlapping laser and x-ray pulse is important for two reasons. First, by illuminating molecules with a laser, we can create nonequilibrium structures that can then be probed by the x-ray beam. For example, it has been proposed to align gas-phase molecules with a laser while scattering off them [11]. Since the distribution of molecular orientations is then no longer isotropic, this would yield additional information about the structure. Second, we find that the final result has the same basic form as in the case of time-independent Hamiltonians, so if the x-ray pulse and the excitation pulse happen to overlap, the corresponding diffraction images do not need to be discarded or treated in any special way.

1. Floquet theory

Within semiclassical theory and electric-dipole approximation, the Hamiltonian of a system under the influence of a continuous-wave laser with amplitude ε_0 is

$$\hat{H}(t; \theta) = \hat{H}_0 + \hat{\mu}\varepsilon_0 \cos(\omega t + \theta), \quad (A1)$$

where $\hat{H}_0$ is the time-independent Hamiltonian of the unperturbed system, and $\hat{\mu}$ the dipole operator. Our goal is to transform this time-dependent problem into a time-independent description by using Floquet theory [24–27]. As the basic idea, the Schrödinger equation with Hamiltonian (A1) is solved for all initial phases θ simultaneously. For this, one first defines an enlarged Floquet space [26]

$$\mathcal{K} = \mathcal{H} \otimes L_2(\mathbb{S}^1; d\theta/2\pi) \quad (A2)$$

as the direct product of the original Hilbert space $\mathcal{H}$ and the space of square-integrable, 2π-periodic functions of θ. This space is equipped with a natural scalar product

$$\langle\langle \xi | \eta \rangle\rangle = \frac{1}{2\pi} \int_0^{2\pi} d\theta\ \langle \xi(\theta) | \eta(\theta) \rangle\,. \quad (A3)$$

The single brackets $\langle | \rangle$ denote the scalar product in $\mathcal{H}$. We now lift the initial state that we wish to propagate, $\varphi_0(x) = \varphi(x, t_0)$, to $\mathcal{K}$ by

$$\xi_0(\theta) = \varphi_0 \otimes \mathbb{1}_\theta, \quad (A4)$$

and propagate ξ_0 such that

$$\varphi(x, t; \theta_0) \equiv \xi\big(x, \theta_0 + \omega(t - t_0), t\big) \quad (A5)$$

is the solution when propagating φ_0 with the Hamiltonian $\hat{H}(t;\theta_0)$ from (A1). It can be shown [26] that the propagator $\hat{U}_K$ of ξ is generated by a time-independent Floquet Hamiltonian

$$\hat{K}(\theta) = \hat{H}(t=0;\theta) - i\hbar\omega\partial_\theta. \tag{A6}$$

The time dependence of the original Hamiltonian is hidden in the mapping $\mathcal{K} \to \mathcal{H}$ for fixed initial phase. To formally remove this time dependence, we can evaluate expectation values directly in $\mathcal{K}$. Any operator $\hat{A}$ that is independent of the phase θ can be trivially lifted to the Floquet space. Calculating the expectation value then gives

$$\langle\langle\xi(t)|\hat{A}|\xi(t)\rangle\rangle = \frac{1}{2\pi}\int_0^{2\pi} d\theta\ \langle\varphi(t;\theta)|\hat{A}|\varphi(t;\theta)\rangle. \tag{A7}$$

Thus, by using Floquet theory, we can formally remove any periodic time dependence in the Hamiltonian at the cost of an integration over all initial phases. The scattering of x-ray photons is described by the scattering operator $\hat{L}$, which is not correlated with the excitation laser, so Eq. (5) can be retained with all scalar products evaluated in $\mathcal{K}$, and propagators replaced by the Floquet propagators $\hat{U}_K$.

This leaves open the problem of evaluating the phase average (A7). Qualitatively, the averaging removes laser-induced oscillations $\sim \cos n\omega t$ ($n \in \mathbb{Z}$), and is therefore often referred to as averaging over a period of the laser (e.g., [28], where the derived Hamiltonian can also be obtained from Floquet perturbation theory [25]).

2. Adiabatic Hamiltonians

Floquet theory itself removes only the periodic time dependence. In practice, however, we encounter lasers with a time-dependent amplitude and possibly a chirp, which are not strictly periodic. In this case, we can separate out the central frequency as periodicity and write the Hamiltonian in (A1) with a time-dependent field strength $\varepsilon_0 = \varepsilon_0(t)$. While we can still evaluate Eq. (5) in the Floquet space, and thereby remove oscillations $\sim \cos n\omega t$, the Floquet Hamiltonian is now time-dependent $\hat{K}(\theta, t)$. This leads to a problem, because the discussion leading to the inelastic result (16) revolved around an expansion of the wave function in the basis of energy eigenstates.

To solve this problem, we make use of the adiabatic theorem [29]. For this, we first expand the wave function in the basis of instantaneous eigenstates of $\hat{K}$ in analogy to (10)

$$|\Psi(t)\rangle\rangle = \sum_i c_i(t)|\varphi_i(t)\rangle\rangle \tag{A8}$$

with

$$\hat{K}(t)|\varphi_i(t)\rangle\rangle = E_i(t)|\varphi_i(t)\rangle\rangle. \tag{A9}$$

The transformation to an eigenstate basis was done by inserting various resolutions of identity into (5). The instantaneous eigenstates also form a complete set of eigenstates, so we can do the same here to obtain

$$\begin{aligned}\sum_{ijkl} c_i^*(t)c_j(t)\left\langle\langle\varphi_i(t)|\ \hat{U}_K\left(t, t+\frac{\delta}{2}\right)\ \hat{L}^\dagger\ \middle|\varphi_k\left(t+\frac{\delta}{2}\right)\right\rangle\right\rangle \\ \times\left\langle\left\langle\varphi_k\left(t+\frac{\delta}{2}\right)\middle|\ \hat{U}_K\left(t+\frac{\delta}{2}, t-\frac{\delta}{2}\right)\ \middle|\varphi_l\left(t-\frac{\delta}{2}\right)\right\rangle\right\rangle \\ \times\left\langle\left\langle\varphi_l\left(t-\frac{\delta}{2}\right)\middle|\ \hat{L}\ \hat{U}_K\left(t-\frac{\delta}{2}, t\right)\ |\varphi_j(t)\rangle\right\rangle\right\rangle.\end{aligned} \tag{A10}$$

If the laser parameters, and thus the Floquet Hamiltonian $\hat{K}(t)$ change slowly in time with respect to the coherence time of the beam (i.e., the value of δ), we can use the adiabatic approximation [29]

$$\begin{aligned}\hat{U}_K(t\pm\delta, t)|\varphi_i(t)\rangle\rangle &\approx |\varphi_i(t\pm\delta)\rangle\rangle e^{\mp i E_i(t)\delta/\hbar} \\ &\approx |\varphi_i(t)\rangle\rangle e^{\mp i E_i(t)\delta/\hbar}.\end{aligned} \tag{A11}$$

Inserting (A10) and (A11) into (5) yields

$$\begin{aligned}s(\mathbf{q}, \omega_0-\omega_s) = \int dt\ I(t)\sum_{ijk} c_i^*(t)c_j(t) \\ \times\langle\langle\varphi_i(t)|\hat{L}^\dagger|\varphi_k(t)\rangle\rangle\langle\langle\varphi_k(t)|\hat{L}|\varphi_j(t)\rangle\rangle \\ \times F\left(\omega_s + \frac{1}{\hbar}\left[E_k(t) - \frac{E_i(t)+E_j(t)}{2}\right]\right),\end{aligned} \tag{A12}$$

which is just Eq. (11) lifted to the Floquet space, and with time-dependent energies and states. If the intensity of the laser is not too strong, and the photon energy not too high, we can expect the instantaneous Floquet states to be "well-behaved" and fulfill all important restrictions (e.g., the static approximation). All derivations can be performed as in the time-independent case with all expectation values or traces evaluated in $\mathcal{K}$. Especially, Eqs. (17) and (32) maintain their form and interpretation.

Note, however, that formally *all* eigenstates in (A12) have to change adiabatically, those that are occupied as well as those that can be occupied due to inelastic scattering events. Because of the energy scales involved in these scattering events, the adiabatic approximation (A11) cannot be rigorously validated in practice but has to be assumed to hold. Also, we want to point out that although (A12) uses a formally inconvenient time-dependent expansion of the wave function, the final representation-independent result (16) still holds.

X-ray scattering from laser-aligned molecules has been described previously by Ho and Santra [11], who implicitly used adiabatic Floquet theory by employing the alignment Hamiltonian of Friedrich and Herschbach [28]. As our formal approach demonstrates, for the special cases of periodic and adiabatic perturbations, the scattering theory is not different from that for time-independent Hamiltonians. Furthermore, we want to point out that because of our more general formulation of the diffraction process, we do not need any further assumptions about the Hamiltonian as in [11]; specifically, the formalism is equally valid for resonant and nonresonant laser parameters.

APPENDIX B: QUALITATIVE EVALUATION OF MATRIX ELEMENTS

In this appendix, we review the static approximation, consider the electronic cross terms of Eq. (23), and discuss how the basic ideas of the IAM can simplify the evaluation of the inelastic matrix elements in Eq. (28). We use the formalism of second quantization [30] and drop nuclear and spin coordinates for easier notation. Given a single-electron basis ϕ_p, denoting the usual creation and annihilation operators in this basis as $\hat{a}_p^\dagger$ and $\hat{a}_p$, and the vacuum state as $|0\rangle$, the set of Slater determinants

$$|\Phi_\mathbf{I}\rangle = \hat{a}_{I_1}^\dagger \cdots \hat{a}_{I_{N_e}}^\dagger |0\rangle \tag{B1}$$

forms an orthonormal basis in the space of N_e electrons. We can expand electronic states in this basis

$$|\lambda_m\rangle = \sum_\mathbf{I} c_\mathbf{I}^{(m)} |\Phi_\mathbf{I}\rangle. \tag{B2}$$

The scattering operators can be written as [30]

$$\hat{L}_0 = \sum_{pq} L_{pq} \hat{a}_p^\dagger \hat{a}_q, \tag{B3}$$

$$\hat{L}_0^\dagger \hat{L}_0 = N_e + \sum_{pqrs} L_{pqrs} \hat{a}_p^\dagger \hat{a}_r^\dagger \hat{a}_s \hat{a}_q, \tag{B4}$$

with

$$L_{pq} = \int d^3x \phi_p^*(\mathbf{x}) e^{i\mathbf{qx}} \phi_q(\mathbf{x}), \tag{B5}$$

$$L_{pqrs} = L_{pq} L_{sr}^*. \tag{B6}$$

We suppress the summand N_e in (B4) in the following because it only gives rise to a homogeneous background signal. We also suppress the subindex 0 from the scattering operators unless explicitly referring to the elastic scattering operator.

1. Static approximation

In the course of the derivation of the inelastic limit, we have assumed that matrix elements $\langle\lambda_k|\hat{L}|\lambda_i\rangle$ are zero unless the energy difference $|E_k - E_i|$ is sufficiently small. This static approximation can be deduced from qualitative considerations and inferred from somewhat limited experimental and theoretical data (e.g., [31–35]).

For the qualitative discussion, we assume that each energy eigenstate is made up of a single Slater determinant. Using the second quantization prescriptions (B1) and (B3), we obtain for two different eigenstates or Slater determinants

$$\langle\Phi_\mathbf{K}|\hat{L}|\Phi_\mathbf{I}\rangle = \begin{cases} L_{ki}, & \text{if} \quad |\Phi_\mathbf{K}\rangle = \hat{a}_k^\dagger \hat{a}_i |\Phi_\mathbf{I}\rangle, \\ 0, & \text{otherwise}, \end{cases} \tag{B7}$$

since the single-particle operator $\hat{L}$ can only change one electronic orbital at a time. We can thus restrict the discussion to properties of the single-electron basis. As a side note, we want to point out that each of these inelastic matrix elements is typically much smaller than the corresponding elastic term $\langle\Phi_\mathbf{K}|\hat{L}|\Phi_\mathbf{K}\rangle$. That is because Eq. (B7) only contains contributions from a single electron, while the elastic matrix element is the sum of the scattering from all occupied orbitals.

If we choose $E_\mathbf{I} < E_\mathbf{K}$, the orbital ϕ_i typically represents a bound state, while ϕ_k is some excited orbital. If $E_\mathbf{K} - E_\mathbf{I}$ is much larger than the binding energy E_i of the bound (core or valence) orbital ϕ_i, then ϕ_k is essentially a plane wave with kinetic energy $p^2/2m_e \sim E_\mathbf{K} - E_\mathbf{I} - E_\text{ion}$. The matrix element

$$L_{ki} = \int d^3r e^{i(\mathbf{p}+\mathbf{q})\mathbf{r}} \phi_i(\mathbf{r}) \tag{B8}$$

is the high-momentum component of the bound orbital ϕ_i, which decays exponentially on a typical scale $\propto \sqrt{m_e E_\text{ion}}$. As the density of states only grows with the energy according to a power law ($\propto E^{1/2}$ for plane waves), the contribution of states ϕ_k to the summation in (13) decreases exponentially in the limit of high energies.

In the extreme case, the vectors $\mathbf{q}$ and $\mathbf{p}$ can point in opposite directions, from which we obtain a qualitative estimate for the cutoff

$$|E_\mathbf{K} - E_\mathbf{I}|_\text{max} = \frac{q^2}{2m_e} + 2E_i. \tag{B9}$$

For typical values of q, the right-hand side of Eq. (B9) varies from tens to a few hundreds of eV. However, we can obtain more accurate and reliable values from experimental data or more elaborate calculations. As these are usually done for the ground state, we have to assume tacitly that the results will not change drastically for optically excited states.

The matrix elements $|\langle\lambda_k|\hat{L}|\lambda_0\rangle|^2$ occur in the context of generalized oscillator strengths (e.g., [36] and references therein) and are observables for inelastic scattering methods, such as electron energy loss spectroscopy [31]. However, the focus is often not on convergence properties, and the experimental data are somewhat scattered. Nevertheless, the available literature (e.g., [31–35]) also suggests a cutoff of at most a few 100 eV, which decreases for smaller values of q.

2. Nondiagonal matrix elements of $\hat{L}_0^\dagger \hat{L}_0$

After we introduced molecular systems, we rapidly dropped the coherence terms that connect different electronic states. Here, we want to discuss the specific argument that nondiagonal terms s_{mn} defined in (23) are much smaller than the diagonal terms s_{mm}.

We first calculate the matrix elements of $\hat{L}_0^\dagger \hat{L}_0$ for single Slater determinants. The result is

$$\langle\Phi_\mathbf{K}|\hat{L}_0^\dagger \hat{L}_0|\Phi_\mathbf{I}\rangle = \begin{cases} \sum_{q,r,q\neq r} L_{qqrr} - L_{qrrq}, & |\Phi_\mathbf{K}\rangle = |\Phi_\mathbf{I}\rangle, \\ \sum_{q\neq i} L_{kiqq} + L_{qqki} - L_{kqqi} - L_{qikq}, & |\Phi_\mathbf{K}\rangle = \hat{a}_k^\dagger \hat{a}_i |\Phi_\mathbf{I}\rangle, \quad k \neq i, \\ L_{k_1 i_1 k_2 i_2} + L_{k_2 i_2 k_1 i_1} - L_{k_1 i_2 k_2 i_1} - L_{k_2 i_1 k_1 i_2}, & |\Phi_\mathbf{K}\rangle = \hat{a}_{k_1}^\dagger \hat{a}_{k_2}^\dagger \hat{a}_{i_2} \hat{a}_{i_1} |\Phi_\mathbf{I}\rangle, \quad k_{1/2} \neq i_{1/2}, \\ 0, & \text{otherwise}, \end{cases} \tag{B10}$$

where the sums run over all occupied orbitals of determinant $\Phi_{\mathbf{I}}$. From this equation, we can deduce that the sum for the case $\mathbf{K} = \mathbf{I}$ contains N_e^2 terms, while for different determinants, we only sum at most over N_e terms. This can be understood intuitively because at least one pair of creation and annihilation operators has to lift an electron from an orbital occupied in $\Phi_{\mathbf{I}}$ to another one solely occupied in $\Phi_{\mathbf{K}}$.

We can then calculate the nondiagonal matrix elements for the electronic states, which might consist of multiple determinants (B2). We also introduce two further approximations based on (B10):

1. If we assume that the matrix L_{pqrs} is well balanced, matrix elements $\langle\Phi_{\mathbf{K}}|\hat{L}_0^\dagger\hat{L}_0|\Phi_{\mathbf{I}}\rangle$ with $\mathbf{I} = \mathbf{K}$ will be significantly larger than for different determinants. Under this assumption, we can choose to retain only matrix elements that involve the same determinants $\mathbf{I}$, $\mathbf{K}$. The error that we introduce by this approximation should then compare to the signal as $1/N_e$.
2. We assume that all Slater determinants give the same contribution $\langle\Phi_{\mathbf{I}}|\hat{L}_0^\dagger\hat{L}_0|\Phi_{\mathbf{I}}\rangle = F$. The underlying idea is that all important Slater determinants differ only by a rearrangement of a few valence electrons, which is insignificant compared to the contribution of the core electrons. Correspondingly, we would expect the error to be of the order of the ratio between the number of valence electrons and the total number of electrons.

With these approximations, we obtain

$$s_{mn} = \langle\lambda_m|\hat{L}_0^\dagger\hat{L}_0|\lambda_n\rangle = \sum_{\mathbf{I},\mathbf{K}} c_{\mathbf{K}}^{(m)*} c_{\mathbf{I}}^{(n)} \langle\Phi_{\mathbf{K}}|\hat{L}_0^\dagger\hat{L}_0|\Phi_{\mathbf{I}}\rangle$$
$$= F\sum_{\mathbf{I}} c_{\mathbf{I}}^{(m)*} c_{\mathbf{I}}^{(n)} = 0, \tag{B11}$$

since the latter expression is just the scalar product between the two orthogonal electronic states.

We can therefore expect the nondiagonal elements to be small compared to the diagonal contributions s_{mm} unless the approximations made earlier fail. The approximations might fail especially for molecules built of light atoms, which have a large fraction of valence electrons.

3. Independent atom model

The IAM is usually used in the context of elastic scattering. To apply it to the inelastic contributions, we first point out the underlying approximations in more detail. For simplicity, we ignore rotational averaging of the single atomic shells. To simplify notation, we also drop the index of the electronic state.

Obviously, as a first step, we have to assign the electrons to specific atoms. For this, we assume that the single-electron Hilbert space can be split up into subspaces $\mathcal{H}_i$ that are large enough to hold the wave function of the isolated atom i. We also assume that all these subspaces can be chosen to be orthogonal.

It should be pointed out that these two requirements are mutually exclusive. For practical molecular geometries, orbitals of different atoms have nonzero overlap. The corresponding subspaces can then not be chosen to be orthogonal *and* contain the wave function of the isolated atoms. However, assuming nonorthogonal subspaces significantly complicates the following algebra, and as we discuss at the end of this section, this overlap must be negligible for most orbitals anyway if the IAM is valid, so we will ignore this detail for simplicity.

We now introduce an orthonormal basis $\{\phi_p\}_{p\in\mathbb{N}}$, where the orbital ϕ_p shall belong to the subspace or atom $\mathcal{H}_i$ if p is the element of some set $S_i \subseteq \mathbb{N}$. The orbitals are understood to have a fixed form and to move around with their respective atoms. That is,

$$\phi_p(\mathbf{r}) = g_p(\mathbf{r} - \mathbf{R}_i), \quad p \in S_i, \tag{B12}$$

where $\mathbf{R}_i$ is the position of the ith atom, and g_p is the fixed functional form of the atomic orbital.

Next, we define states of the independent atoms as

$$|\xi_i\rangle = \hat{C}_i^\dagger|0\rangle, \tag{B13}$$

where $\hat{C}_i^\dagger$ is a (sum of) strings of creation operators $\hat{a}_p^\dagger$ ($p \in S_i$). The electronic structure of the independent atom i shall be independent of the position of the atom, which requires $\hat{C}_i^\dagger$ to be independent of $\mathbf{R}_i$ as well.

With the notation fixed, the IAM can now be formulated as

$$|\lambda\rangle \approx |\lambda'\rangle = \left(\prod_{i=1}^{N_a} \hat{C}_i^\dagger\right)|0\rangle. \tag{B14}$$

Here, N_a is the number of atoms in the molecule. Writing out the scattering amplitude and using the orthonormality of the atomic subspaces, we can bring this approximation into a more instructive form

$$\langle\lambda|\hat{L}_0|\lambda\rangle \approx \sum_{i=1}^{N_a}\langle\xi_i|\hat{L}_0|\xi_i\rangle, \tag{B15}$$

that is, the molecular form factor [left-hand side of (B15)] is the sum of the atomic form factors, where we have not factored out the atomic coordinates explicitly. Within the IAM, we thus neglect electronic correlations between different atoms, which would lead to atomic cross terms.

Some identities that may help with the preceding and further manipulations are

$$L_{pq}(\mathbf{R}_i) = L_{pq}(\mathbf{R}_i = 0)e^{i\mathbf{q}\mathbf{R}_i}, \quad p,q \in S_i, \tag{B16}$$
$$[\hat{C}_i^\dagger, \hat{a}_p]_+ = \hat{C}_i^\dagger\hat{a}_p + \hat{a}_p\hat{C}_i^\dagger = 0, \quad p \notin S_i, \tag{B17}$$
$$[\hat{C}_i^\dagger, \hat{C}_j]_+ = 0, \quad i \neq j. \tag{B18}$$

The first identity uses (B12) to factor out the geometry-dependent complex phase from matrix elements; the second and third relations follow from the orthogonality of the atomic subspaces.

We now employ (B4), (B5), and (B14) to evaluate directly the matrix elements s_{mm} in Eq. (28):

$$\langle\lambda|\hat{L}_0^\dagger\hat{L}_0|\lambda\rangle \approx \langle\lambda'|\hat{L}_0^\dagger\hat{L}_0|\lambda'\rangle$$
$$= \left(\sum_i \sum_{p,q,r,s\in S_i} + \sum_{i\neq j}\sum_{\substack{p,q\in S_i\\ r,s\in S_j}} + \sum_{i\neq j}\sum_{\substack{p,s\in S_i\\ r,q\in S_j}}\right)$$
$$\times L_{pq}L_{sr}^*\langle\lambda'|\hat{a}_p^\dagger\hat{a}_r^\dagger\hat{a}_s\hat{a}_q|\lambda'\rangle, \tag{B19}$$

where we used the orthogonality relation (B17). It ensures that only those matrix elements contribute, where the creation operators act on the same subspaces as the annihilation operators.

The first summand in (B19) only involves orbitals around a single atom. The geometry-dependent phases of L_{pq} and L^*_{sr} then cancel, so that this contribution is independent of the nuclear geometry.

The second summand can be shown to be identical to the elastic term $|\langle\lambda'|\hat{L}_0|\lambda'\rangle|^2$ [i.e., the first term in (28)] apart from geometry-independent contributions. To demonstrate this, use (B15) together with (B17), and compare this to the second summand in (B19) after insertion of (B14) and extensive use of the commutation relations (B17) and (B18).

The last summand in (B19) contains matrix elements of orbitals around different atoms. It is therefore sensitive to the nuclear geometry but cannot be evaluated without detailed knowledge of the orbital shapes and the electronic structure of the single atoms. However, if it would contribute appreciably to the diffraction pattern, then matrix elements of the form (B6) and thus products $\phi^*_p(\mathbf{x})\phi_q(\mathbf{x})$ with $p \in S_i$, $q \in S_j$ have to be significant for many occupied orbitals. In this case, mutual Coulomb repulsion between electrons of different atoms is also significant, leading to strong correlations between many electrons of different atoms and hence to a breakdown of the IAM. If the IAM level of theory is sufficient to fit the elastic part of Eq. (29), these correlations can be neglected, usually because the scattering is dominated by tightly bound, uncorrelated core electrons. As a consequence, the third summand in (B19) can then be neglected for the purpose of x-ray diffraction. The inelastic part of the diffraction pattern S_{inel} in Eq. (29) is thus roughly independent of the nuclear geometry.

[1] J. Als-Nielsen and D. McMorrow, *Elements of Modern X-Ray Physics* (Wiley, New York, 2001).
[2] M. Ben-Nun, T. J. Martínez, P. M. Weber, and K. R. Wilson, Chem. Phys. Lett. **262**, 405 (1996).
[3] M. Ben-Nun, J. Cao, and K. R. Wilson, J. Phys. Chem. A **101**, 8743 (1997).
[4] S. Bratos, F. Mirloup, R. Vuilleumier, and M. Wulff, J. Chem. Phys. **116**, 10615 (2002).
[5] T. Rozgonyi, R. Sauerbrey, and T. Feurer, J. Appl. Phys. **97**, 013537 (2005).
[6] C. H. Chao, S. H. Lin, W.-K. Liu, and P. Rentzepis, in *Time-Resolved Diffraction*, edited by J. Helliwell and P. Rentzepis (Oxford University, New York, 1997), p. 260.
[7] A. Debnarova, S. Techert, and S. Schmatz, J. Chem. Phys. **125**, 224101 (2006).
[8] S. L. Johnson, P. Beaud, E. Vorobeva, C. J. Milne, E. D. Murray, S. Fahy, and G. Ingold, Phys. Rev. Lett. **102**, 175503 (2009).
[9] J. Cao and K. R. Wilson, J. Phys. Chem. A **102**, 9523 (1998).
[10] N. E. Henriksen and K. B. Møller, J. Phys. Chem. B **112**, 558 (2008).
[11] P. J. Ho and R. Santra, Phys. Rev. A **78**, 053409 (2008).
[12] S. Tanaka, V. Chernyak, and S. Mukamel, Phys. Rev. A **63**, 063405 (2001).
[13] S. Tanaka, S. Volkov, and S. Mukamel, J. Chem. Phys. **118**, 3065 (2003).
[14] D. A. Kohl and E. J. Shipsey, Z. Phys. D **24**, 39 (1992).
[15] I. Waller and D. R. Hartree, Proc. R. Soc. London A **124**, 119 (1929).
[16] E. L. Saldin, E. A. Schneidmiller, and M. V. Yurkov, Opt. Commun. **148**, 383 (1998).
[17] L. Van Hove, Phys. Rev. **95**, 249 (1954).
[18] M. Altarelli *et al.*, Tech. Rep., DESY, 2007 (unpublished), http://xfel.desy.de/tdr/tdr.
[19] T. Tschentscher, Chem. Phys. **299**, 271 (2004).
[20] M. Born and K. Huang, *Dynamical Theory of Crystal Lattices* (Clarendon, Oxford, 1954).
[21] J. H. Hubbell, Wm. J. Veigele, E. A. Briggs, R. T. Brown, D. T. Cromer, and R. J. Howerton, J. Phys. Chem. Ref. Data **4**, 471 (1975).
[22] M. Christensen, K. Haldrup, K. Bechgaard, R. Feidenhansl, Q. Kong, M. Cammarata, M. L. Russo, M. Wulff, N. Harrit, and M. M. Nielsen, J. Am. Chem. Soc. **131**, 502 (2008).
[23] W.-K. Liu and S. H. Lin, Phys. Rev. A **55**, 641 (1997).
[24] J. H. Shirley, Phys. Rev. **138**, B979 (1965).
[25] H. Sambe, Phys. Rev. A **7**, 2203 (1973).
[26] S. Guérin, F. Monti, J.-M. Dupont, and H. R. Jauslin, J. Phys. A **30**, 7193 (1997).
[27] K. Drese and M. Holthaus, Eur. Phys. J. D **5**, 119 (1999).
[28] B. Friedrich and D. Herschbach, Phys. Rev. Lett. **74**, 4623 (1995).
[29] A. Messiah, *Quantum Mechanics II* (North-Holland, Amsterdam, 1962).
[30] T. Helgaker, P. Jørgensen, and J. Olsen, *Molecular Electronic-Structure Theory* (Wiley, New York, 2000).
[31] M. Takahashi, N. Watanabe, Y. Wada, S. Tsuchizawa, T. Hirosue, H. Hayashi, and Y. Udagawa, J. Electron Spectrosc. Relat. Phenom. **112**, 107 (2000).
[32] J. F. Ying and K. T. Leung, J. Chem. Phys. **100**, 7120 (1994).
[33] R. C. Ulsh, H. F. Wellenstein, and R. A. Bonham, J. Chem. Phys. **60**, 103 (1974).
[34] R. S. Barbieri and R. A. Bonham, Phys. Rev. A **44**, 7361 (1991).
[35] S. P. A. Sauer (private communication).
[36] M. Inokuti, Rev. Mod. Phys. **43**, 297 (1971).

Paper II

On the interpretation of time-resolved anisotropic diffraction patterns

On the interpretation of time-resolved anisotropic diffraction patterns

U Lorenz, K B Møller and N E Henriksen

CMM, Department of Chemistry, Building 207, Technical University of Denmark, DK-2800 Kgs. Lyngby, Denmark

E-mail: ulf.lorenz@kemi.dtu.dk, klaus.moller@kemi.dtu.dk, neh@kemi.dtu.dk

Abstract. We review existing systematic treatments for the interpretation of anisotropic diffraction patterns from partially aligned symmetric top molecules. Such patterns arise in the context of time-resolved diffraction experiments. We calculate diffraction patterns for ground state NaI excited with an uv-laser. The results are interpreted with the help of a qualitative analytic model, and general recommendations for the analysis and interpretation of anisotropic diffraction patterns are given.

PACS numbers: 34.80.Bm, 34.80.Qb, 33.80.-b

Submitted to: *New Journal of Physics*

1. Introduction

Almost 100 years ago, Friedrich, Knipping, and Laue published an article [1] in which they described intensity maxima after sending an x-ray beam through crystals, and interpreted these in terms of diffraction of x-rays at the atomic sites. Ever since, x-ray diffraction has been an indispensable tool in determining the atomic structure of matter. To a good approximation, x-ray diffraction patterns are simple functions of the atomic species and the relative positions of the nuclei with respect to each other, that is, they directly encode the nuclear geometry. This is a big advantage of diffraction over most other techniques, e.g., optical spectroscopy; these usually measure properties of the electronic structure, and infer the nuclear geometry indirectly from models or extensive electronic structure calculations.

For a chemist, the natural next step after resolving the structure of reactants and products in a chemical reaction would be to "film" the reaction itself, which leads to Time-Resolved X-ray Diffraction (TRXD). In this field, the commonly used technique is pump–probe difference diffraction. A pump laser initiates the chemical reaction, and after a specific delay time, the x-ray probe pulse produces a diffraction pattern. From this time-dependent diffraction pattern, a reference pattern of the unexcited sample is subtracted to yield a difference pattern; this technique removes all contributions that

do not depend on the time-dependent nuclear geometry, such as incoherent scattering, or the scattering from the major portion of the molecules that have not been excited. The difference patterns, or rather their encoded structures, can then be ordered by the pump-probe delay time to produce a "molecular movie" of the chemical reaction. While the use of a pump laser means that only photochemical processes can be studied, this is to some extend unavoidable; for most reactions, only laser technology provides a fast enough clocking mechanism.

Alas, up to date, there was a distinct lack of suitable x-ray sources for ultrafast TRXD experiments. Existing synchrotron sources produce pulses of about 50 picoseconds; this is fast enough to study, for example, short-lived transient states in liquid ([2, 3] and references therein) or crystalline samples ([4] and references therein). However, many processes require a sub-picosecond time resolution. While such a time resolution can be obtained with slicing [5, 6] or plasma sources [7, 8], they only yield a low photon flux, making such setups unattractive for many experiments.

This situation is expected to change with the availability of X-Ray Free Electron Lasers over the next few years [9–12]. They will provide x-ray pulses of 100 femtoseconds duration or less, and with intensities exceeding that of current synchrotron facilities by orders of magnitude. With the experimental facilities soon to be available, it is the task of the theoretician to provide support in the design of experiments and interpretation of results. This aid can take various forms.

On a fundamental level, we can study what information is encoded in time-resolved diffraction patterns. While this may seem at first like a purely academic exercise, the need for such studies becomes apparent if we recall that standard textbook derivations are only applicable for time-independent systems; for example, they employ time-independent scattering expressions, or assume negligible electric currents (i.e., stationary systems). Studies of the theoretical foundations of TRXD have been conducted by various authors [13–21], and mainly differ in the type of systems studied, description of the interaction, and thoroughness of the derivation.

Most of the results for the difference cross section can be cast into the form

$$\Delta\frac{\mathrm{d}\sigma}{\mathrm{d}\Omega}(\mathbf{q},\tau) = \sigma_T \int \mathrm{d}^{3N}R\ \Delta\bar{\varrho}(\mathbf{R}^{(3N)},\tau)\ |F_{\mathrm{mol}}(\mathbf{R}^{(3N)},\mathbf{q})|^2 \tag{1}$$

with σ_T being the classical Thomson scattering cross section from a free electron. $\mathbf{q}$ is the scattering vector (difference of wave vectors of incoming and outgoing photon) and $\mathbf{R}$ denotes the manifold of nuclear coordinates. As a convention throughout this article, we notate an n-dimensional vector x as $\mathbf{x}^{(n)}$, and drop the superscript for $n = 3$. N specifies the number of atoms in the molecule. The time-averaged difference density of nuclear geometries $\Delta\bar{\varrho}$ as a function of the pump–probe delay time τ is the convolution of the difference density $\Delta\varrho$ with the intensity profile I of the x-ray pulse,

$$\Delta\bar{\varrho}(\mathbf{R}^{(3N)},\tau) = \int \mathrm{d}t\ I(t-\tau)\Delta\varrho(\mathbf{R}^{(3N)},t)\ . \tag{2}$$

For brevity, we will use the term difference density to denote both of them. Physically, $\Delta\varrho(\mathbf{R}_0^{(3N)},t)\mathrm{d}^{3N}R$ is the difference probability of finding a molecule whose molecular

geometry is in an infinitesimal volume $\mathrm{d}^{3N}R$ around $\mathbf{R}_0^{(3N)}$. The squared molecular form factor $|F_{\mathrm{mol}}|^2$ specifies the signal for a fixed nuclear geometry. Within the independent atom model, it can be written in terms of the atomic form factors f_a and bond vectors $\mathbf{R}_{ab}$ as

$$|F_{\mathrm{mol}}(\mathbf{R}^{(3N)}, \mathbf{q})|^2 = \sum_{a,b}^{N} f_a^*(q) f_b(q)\ \mathrm{e}^{\mathrm{i}\mathbf{q}\mathbf{R}_{ab}} \tag{3}$$

Equation (1) has a close resemblance to ordinary x-ray diffraction; the result from time-independent theory can essentially be obtained by replacing the time-dependent difference density with the time-independent density of the stationary system. However, there are distinct differences in the interpretation of the results.

In stationary molecules, the electronic potential energy surface usually exhibits one (or more) deep wells that correspond to stable geometries, and the nuclear density is strongly localized at these minima. It is then permissible to replace the density distribution by a delta-function (or sum thereof); this removes the integration in (1), and the diffraction pattern is basically the molecular form factor (or a sum of such form factors) for *the* well-defined molecular structure(s). This approximation is not always possible, though. In bulk liquids, for example, the distance between two atoms of the same species is not well-defined, and it is more useful to operate with distribution functions instead (see, e.g., [3]).

In general, we expect the approximation of well-defined molecular geometries to fail in TRXD experiments, even at $T = 0$K. One reason is apparent from (2): the finite duration of the x-ray pulse smears out all dynamics. On a more fundamental level, however, the wave function of the nuclear coordinates that has been excited by the pump laser is no longer in the minimum of a deep potential well. As a result, we observe quantum-mechanical wavepacket dispersion (see for example [22–24]); the difference density becomes delocalized, and an x-ray diffraction measurement yields a whole distribution of molecular structures.

Another wave function aspect that is different from typical time-independent diffraction is alignment of molecules, where for example the pump laser preferentially excites molecules that are aligned with respect to the polarisation axis. Typical difference densities on ultrashort timescales then consist of contributions from the excited wave function, and from the "hole" due to the depletion of the ground state, both of which are partially aligned with respect to the laser polarisation axis.

In section 2, we review and discuss the processing of anisotropic diffraction patterns. Sections 3 and 4 presents the details and the results of our calculation on NaI excited from the ground state by a uv laser. These calculations serve to illustrate the procedures and caveats detailed before. Our findings are summarized in section 5, and an outlook for further research is presented.

2. Anisotropic distributions

Anisotropic diffraction patterns have been analysed in several previous studies. For diatomic molecules, the inversion of the diffraction pattern has been studied by Ben-Nun et al. [14]. In another paper, Cao and Wilson [15] studied the inversion from a cylindrically symmetric sample assuming constant atomic form factors. Several formulas in these articles are related to those we present here. However, for polyatomic molecules, it is rather difficult to generalise the procedure in [14], or the approximations are too crude, and it is difficult to assign a simple physical picture to the internuclear distribution function in [15].

Alternatively, we note that the formalism of x-ray and electron diffraction is identical within the independent atom model. For a systematic treatment of the class of symmetric top molecules, we can then draw on experience from the field of ultrafast electron diffraction. Kohl and Shipsey [25] calculated diffraction patterns from molecules selected to be in specific rotational quantum states. Similar to our own interest, the Zewail group studied diffraction patterns arising from aligned ensembles [26, 27], which resulted in a systematic description of the anisotropies [28]. In the following, we summarize their derivations, and discuss the obtained results in some depth.

Throughout this text, we will use the integral notation (1). This is in contrast to [25–28], where the averaging procedure is mostly hidden in brackets. Although this introduces some overhead in the notation, we think that the manipulations in this section are more transparent when formally applied to a density distribution.

We restrict our attention to symmetric tops (which includes linear molecules as a special case) that are excited by a linearly polarized laser pulse from a thermal ensemble. This already encompasses experiments on a range of symmetric molecules, see for example [2, 4, 25, 28]. We further only consider the case where the transition dipole moment (i.e., the molecule-fixed vector that is aligned) is parallel to the symmetry axis. The difference density can then be decomposed exactly as (see the appendix)

$$\Delta\bar{\varrho}(\mathbf{R}^{(3N)},\tau) = \Delta\bar{\varrho}(\theta,\mathbf{r}^{(3N-6)},\tau) = \sum_{n\ \text{even}} P_n(\cos\theta)\ \Delta\bar{\varrho}_n(\mathbf{r}^{(3N-6)},\tau) \tag{4}$$

where P_n are the Legendre polynomials, and $\mathbf{r}$ denotes the internal coordinates of the molecule (i.e., excluding centre of mass (CM), and rotational coordinates) in a molecule-fixed frame. For linear molecules, there are 5 CM and rotational coordinates; to keep the discussion simple, we only consider the general nonlinear case in the following. The angle θ is defined in figure 1. Note that the difference density depends only on one of the three Euler angles. Terms with odd n are antisymmetric under space inversion, and give no contribution when calculating the diffraction pattern (1), so we drop them. Using the orthogonality of the Legendre polynomials, the inverse relation reads

$$\Delta\bar{\varrho}_n(\mathbf{r}^{(3N-6)},\tau) = \frac{2n+1}{2}\int_0^\pi \mathrm{d}\theta\ \sin\theta\ \Delta\bar{\varrho}(\theta,\mathbf{r}^{(3N-6)},\tau)\ P_n(\cos\theta) \tag{5}$$

Note that here and in the following, we always drop the integration over the two remaining Euler angles, and the CM coordinates. As the difference density is

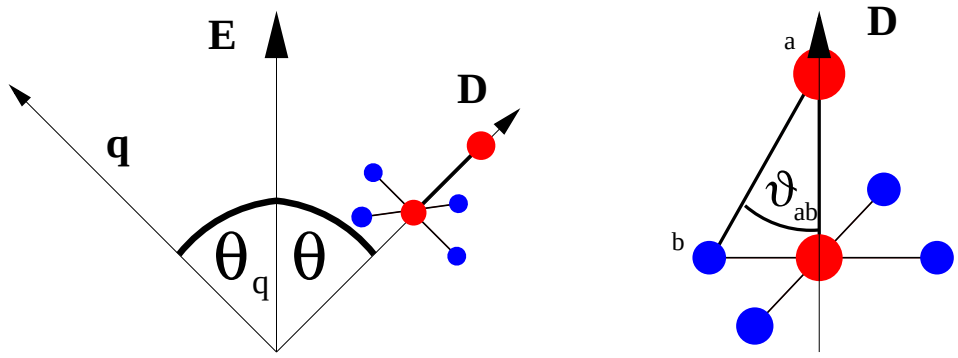

Figure 1. Definition of the various angles used in the formulas. Left image: angles defined in the laboratory-fixed frame. The z-axis is defined by the laser polarisation vector **E**. Right image: angles defined in the molecule-fixed frame. The z-axis in this frame is given by the transition dipole vector **D**, which is assumed to be parallel to the symmetry axis of the symmetric top.

independent of them, these integrations just give rise to additional normalisation factors; however, we always have to carry the $\sin\theta$-factor from the Jacobi determinant around. As detailed in [25,28], a difference density of the form (4) leads to a difference diffraction signal (1) of the form

$$\Delta\frac{\mathrm{d}\sigma}{\mathrm{d}\Omega}(\mathbf{q},\tau)=\Delta\frac{\mathrm{d}\sigma}{\mathrm{d}\Omega}(q,\theta_q,\tau)=2(2\pi)^2\sigma_T\sum_{n\ \mathrm{even}}(-1)^{n/2}P_n(\cos\theta_\mathrm{q})S_n(q,\tau) \quad (6)$$

with

$$S_n(q,\tau)=\sum_{a,b}^{N}f_a^*(q)f_b(q)\int\mathrm{d}^{3N-6}r\ \Delta\bar{\varrho}_n(\mathbf{r}^{(3N-6)},\tau)\ P_n(\cos\vartheta_{ab})j_n(qr_{ab}) \quad (7)$$

in terms of spherical Bessel functions j_n, and with r_{ab} as the distance between atoms a and b and ϑ_{ab} the angle between the ab-vector and the transition dipole moment as defined in figure 1. At this point, the link between the integration and the variables r_{ab}, ϑ_{ab} is somewhat opaque; we will detail the integration scheme later on.

In the simplest anisotropic case, we only consider the terms $n=0,2$, and the density is a second-order polynomial of $\cos\theta$. This is what we get whenever we excite molecules from thermal equilibrium by one-photon absorption [29]. The diffraction pattern (6) is then a simple sum of S_0 (the "isotropic" curve), and S_2 (the "anisotropic" curve). If we consider a fixed delay time τ and a fixed length of the scattering vector q, we can assign each detector pixel on the resulting circle a value of $P_2(\cos\theta_\mathrm{q})$ and a value of $\Delta\mathrm{d}\sigma/\mathrm{d}\Omega$. The decomposition of $\Delta\mathrm{d}\sigma/\mathrm{d}\Omega$ into S_0 and S_2 turns into a simple linear fitting problem, whose slope gives the anisotropic, and whose y-intercept gives the isotropic curve [14]. Alternatively, we can obtain the isotropic signal by "magic angle detection" [28]. If the angle α between the incoming x-ray beam and the laser polarisation axis fulfills $\cos^2\alpha=\frac{1}{3}$, the isotropic signal can be obtained by directly integrating over the azimuthal angle on the detector plate.

Up to now, we have merely rewritten the general equation (1). To grasp the full potential of (6), (7), we now turn our attention to the density components $\Delta\bar{\varrho}_n$ and their relation to some "fundamental" density distributions.

2.1. Density distributions

Whenever a molecule interacts with a photon, its rotational quantum number changes. During the laser-matter interaction, a molecule that starts out with a well-defined rotational quantum number becomes an ensemble (coherent superposition) of states with different rotational quantum numbers. These quantum numbers influence the subsequent time evolution through ro-vibrational coupling (e.g., centrifugal distortion). However, in many practical applications, this coupling can be neglected. That is, the rotational motion of the molecule and its internal evolution are uncoupled, and we can approximate

$$\Delta\bar{\varrho}(\theta, \mathbf{r}^{(3N-6)}, \tau) = \varrho_{\mathrm{rot}}(\theta, \tau)\ \Delta\bar{\varrho}_{\mathrm{vib}}(\mathbf{r}^{(3N-6)}, \tau) \tag{8}$$

We have to extend this ansatz in the case of multiple species, where we understand species as well-defined, mutually distinguishable configurations that contribute to the signal. For example, there might be a "hole" term (depletion of the stable ground state) and an excited state wavepacket, both of which exhibit different rotational motion due to different moments of inertia (see also the example of NaI in the subsequent sections). We assume in analogy to (8) that for each well-defined species S, the rotational motion and internal evolution are uncoupled, so that we can write

$$\begin{aligned}\Delta\bar{\varrho}(\theta, \mathbf{r}^{(3N-6)}, \tau) &= \sum_S \varrho^S_{\mathrm{rot}}(\theta, \tau)\ \Delta\bar{\varrho}^S_{\mathrm{vib}}(\mathbf{r}^{(3N-6)}, \tau) \\ &= \sum_S \sum_{n\ \mathrm{even}} P_n(\cos\theta) c^S_n(\tau)\ \Delta\bar{\varrho}^S_{\mathrm{vib}}(\mathbf{r}^{(3N-6)}, \tau)\ .\end{aligned} \tag{9}$$

Comparison with (4) show that each density component $\Delta\bar{\varrho}_n$ is built up from fundamental "vibrational" difference densities $\Delta\bar{\varrho}^S_{\mathrm{vib}}$ that describe the time-dependent structure of the single species, and (real-valued) coefficients c^S_n that arise from an expansion of the angular distribution in Legendre polynomials, and thus describe the angular distribution of the species. If we do not know the exact angular distribution, these coefficients appear as additional fitting parameters.

With this in mind, we can construct a general analysis procedure for the class of anisotropic diffraction patterns presented here. We first use (6) to decompose the two-dimensional diffraction pattern $\Delta\mathrm{d}\sigma/\mathrm{d}\Omega$ into a set of one-dimensional diffraction curves S_n. In a second step, we guess the vibrational difference densities and coefficients, and build up the single density components $\Delta\bar{\varrho}_n$ via (9). This guess is compared to the diffraction curves (7), and subsequently improved through some iterative scheme. For the special case of diatomics, the scattering curves can be directly inverted, see (19) below.

We point out that (6), (7) contains the special case of isotropic densities, where only the $n = 0$ term contributes. The diffraction pattern (6) is isotropic, and if we write out the Legendre polynomial and spherical Bessel function in (7), the isotropic scattering curve is given by

$$S_0(q,\tau) = \int \mathrm{d}^{3N-6}r\ \Delta\bar{\varrho}_0(\mathbf{r}^{(3N-6)},\tau)\ \sum_{a,b}^{N} f_a^*(q) f_b(q) \frac{\sin(qr_{ab})}{qr_{ab}} \tag{10}$$

which is the well-known Debye formula for isotropic ensembles [30] (where again the integration is often suppressed).

From the case of purely isotropic signals we can extract a number of relations that are also useful for anisotropic patterns. Using distributions ϱ^S_{rot} with norm 1 and the orthogonality of the Legendre polynomials, we obtain

$$c_0^S(\tau) = \frac{1}{2}\int_0^\pi \mathrm{d}\theta\ \sin\theta\ \varrho^S_{\mathrm{rot}}(\theta,\tau) P_0(\cos\theta) = \frac{1}{2} \tag{11}$$

This is just the trivial result that for an isotropic distribution, we do not have to care about molecular rotation. Furthermore, we can calculate the difference probability density $\Delta\Gamma$ of finding a specific molecular structure, that is, a certain value of $\mathbf{r}^{(3N-6)}$, by integrating $\Delta\bar{\varrho}$ over the remaining angular degree of freedom

$$\Delta\Gamma(\mathbf{r}^{(3N-6)},\tau) = \int_0^\pi \mathrm{d}\theta\ \sin\theta\ \Delta\bar{\varrho}(\theta,\mathbf{r}^{(3N-6)},\tau) = \sum_S\ \Delta\bar{\varrho}^S_{\mathrm{vib}}(\mathbf{r}^{(3N-6)},\tau) \tag{12}$$

where we used (5), (9) (with $P_0(x) = 1$), and (11). The vibrational difference densities $\Delta\bar{\varrho}^S_{\mathrm{vib}}$ are thus exactly the difference probability distributions of the molecular structures for the corresponding species S.

Equations (11), (12) are, in fact, valid for arbitrary difference densities. The orthogonality of the Legendre polynomials ensures that all but the isotropic components $(c_0^S, \Delta\bar{\varrho}_0)$ vanish during the θ-integration. This leads to an important conclusion: If we decompose the signal according to (6), and focus only on the isotropic component S_0, we can ignore the rotational coefficients, and interpret the resulting density as a (difference) probability distribution, that is, *we can process the curve S_0 and interpret the results as if we had an isotropic ensemble in the first place.*

In the theory involving isotropic ensembles, (10) is often recast in a form that involves atom-pair–distribution functions (see, e.g., [3]), which removes the cumbersome integration over $\mathbf{r}^{(3N-6)}$. We first calculate the difference probability density $\Delta\Gamma_{ab}$ for the distance between atoms a, b being r_0. In the spirit of (12), we take the probability density of finding some structure $\mathbf{r}^{(3N-6)}$, and integrate it over all internal coordinates except the ab distance. Formally, we choose the internal coordinates to be the spherical coordinates $\vartheta_{ab}, \phi_{ab}, r_{ab}$ of the ab vector, and some $3N-9$ other internal coordinates x_{ab}, and obtain

$$\begin{aligned}\Delta\Gamma_{ab}(r_0,\tau) \quad &= r_0^2\left(\int_0^\pi \mathrm{d}\vartheta_{ab}\ \sin\vartheta_{ab}\int_0^{2\pi}\mathrm{d}\phi_{ab}\int \mathrm{d}^{3N-9}x_{ab}\sum_S \Delta\bar{\varrho}^S_{\mathrm{vib}}(\vartheta_{ab},\phi_{ab},\mathbf{x}_{ab}^{(3N-9)},\tau;r_{ab}=r_0)\right)\\ &= r_0^2\ \Delta g_{ab}(r_0,\tau)\end{aligned} \tag{13}$$

thereby defining a difference pair distribution Δg_{ab} of the ab distance. The same integration scheme can be used to evaluate (10), and we can express the signal through the pair-distribution functions as

$$S_0(q,\tau) = \sum_{a,b}^{N} f_a^*(q) f_b(q) \int_0^\infty \mathrm{d}r\ r^2\ \Delta g_{ab}(r,\tau) \frac{\sin(qr)}{qr}\ . \tag{14}$$

Note that pair-distribution functions can be defined in different ways. To reduce the number of summands, the sum sometimes only runs over all atom *types*, and the distribution function is defined per pair of atom types. In liquid scattering experiments, it is more convenient to convert the pair distribution into a dimensionless quantity called the radial distribution function [3].
The concept of using the spherical coordinates of the ab vector for the integration, and hiding most integrations in the definition of some distribution function can be extended to the anisotropic components. From (7) and (9), we obtain

$$\begin{aligned} S_n(q,\tau) = \sum_{a,b}^{N} f_a^*(q) f_b(q) \int_0^\infty \mathrm{d}r\ r^2 \int_0^\pi \mathrm{d}\vartheta\ \sin\vartheta \\ \times \left(\sum_S c_n^S(\tau)\ \Delta g_{ab}^S(r,\vartheta,\tau) \right) P_n(\cos\vartheta) j_n(qr) \end{aligned} \tag{15}$$

where the species-dependent angle-resolved difference pair distributions Δg_{ab}^S are

$$\Delta g_{ab}^S(r,\vartheta,\tau) = \int_0^{2\pi} \mathrm{d}\phi_{ab} \int \mathrm{d}^{3N-9} x_{ab}\ \Delta\bar{\varrho}_{\mathrm{vib}}^S(\phi_{ab}, \mathbf{x}^{(3N-9)}, \tau; r_{ab} = r, \vartheta_{ab} = \vartheta) \tag{16}$$

Note that we now have one pair distribution per species in (15), while we had a single pair distribution in (13). This is caused by the different species having different angular distributions, which we account for by the rotational coefficients. Only if all species have the same angular distribution, or if all rotational coefficients are identical, can we sum up the species-dependent pair distributions to a global pair distribution.
Finally, we want to remark that the method presented here might only be feasible for weak alignment, as induced by few photon absorption. The stronger the alignment, the higher the order of the Legendre polynomials that appear in the decomposition (4), (6). Especially in the case of multiple species, this leads to a large number of rotational coefficients that, in general, have to be guessed.

2.2. Direct inversion

In the following, we study the behaviour of the single density components $\Delta\bar{\varrho}_n$ of NaI. NaI has the internuclear distance r as the single internal coordinate, which greatly reduces the complexity. Also, the relevant transition dipole moment is parallel to the molecular axis, so that $P_n(\cos\vartheta_{\mathrm{NaI}}) = 1$. Choosing real atomic form factors for convenience, (7) simplifies to

$$S_n(q,\tau) = 2 f_1(q) f_2(q) \int \mathrm{d}r\ r^2\ \Delta\bar{\varrho}_n(r,\tau)\ j_n(qr)\ . \tag{17}$$

For a diatomic, it is possible to invert the scattering curves directly to obtain $\Delta\bar{\varrho}_n(r,\tau)$. The spherical Bessel functions have an orthogonality relation [33]

$$\int_0^\infty \mathrm{d}q\; q^2 j_n(uq) j_n(vq) = \frac{\pi}{2u^2}\;\delta(u-v), \tag{18}$$

so that, up to constant factors,

$$\Delta\bar{\varrho}_n(r,\tau) = \int_0^{q_\mathrm{max}} \mathrm{d}q\; q^2 \frac{S_n(q,\tau)}{f_1(q) f_2(q)}\; j_n(qr)\; \mathrm{e}^{-kq^2} \tag{19}$$

(a related formula is (30) in [15]). Since real-world data is only collected for $q \leq q_\mathrm{max} < \infty$, the inverted density using $[0, q_\mathrm{max}]$ for the integral boundaries exhibits high-frequency oscillations, which are here suppressed by applying the exponential factor with $k > 0$. Again, applying this to the isotropic contribution ($n = 0$) gives the well-known inversion formula for isotropic samples [26].

For isotropic distributions, the inversion formula can also be used for studying polyatomic molecules [26–28, 34]. Let us assume that all atomic form factors have the same functional form, $f_a(q) = Z_a f(q)$, with Z_a the number of electrons of atom a, insert (14) into (19) and use (18). We obtain up to constants the expression $\sum_{a,b} Z_a Z_b \Delta g_{ab}(r,\tau)$. This function has a peak or dip whenever r roughly equals some relevant atom-atom distance that has been established (peak) or removed (dip) during the excitation. While the underlying assumptions are too crude for a quantitative analysis, this inversion is still useful for qualitative estimates of the dynamics.

Direct inversion schemes have also been applied previously to anisotropic diffraction patterns. In [27], a mixture of S_0 and S_2, which is obtained when the laser polarisation axis is parallel to the incoming beam, was inverted using (19) with $n = 0$. In [28], the same procedure was applied to the diffraction pattern along specific lines on the detector (roughly corresponding to different values of θ_q) [28]. As is shown in the references, these procedures can lead to artefacts in the resulting distribution functions, such as predicting breakage of non-existent bonds.

Therefore, we should *always* decompose the diffraction pattern into the single curves S_n, and then invert the isotropic signal using j_0, and the anisotropic signal using j_2, where care has to be taken when interpreting the latter. Comparison with (15) shows that the inversion procedure extracts not only a sum of the angle-resolved difference pair distributions, but also includes contributions from the ϑ-integration and the rotational coefficients, both of which can change the amplitude and sign of the single peaks.

3. The NaI molecule

To illustrate the general decomposition outlined in the last section, we have calculated the dynamics of NaI excited by a uv photon. The relevant potential energy surfaces and nuclear dynamics of NaI after photo-excitation are shown in figure 2. We chose NaI because it is an extensively studied molecule [22–24, 35–37], and because the excited

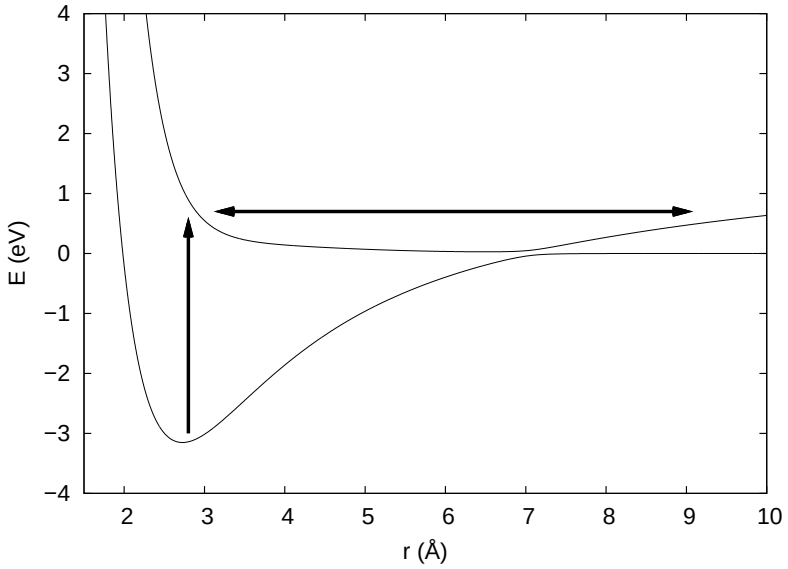

Figure 2. Potential energy surfaces and sketch of the relevant nuclear motion of NaI. By absorbing a uv photon, NaI is vertically excited from the $X^1\Sigma^+$ ground state to the $A^1\Sigma^+$ first excited state, which exhibits a shallow minimum. The nuclei then vibrate on the excited state surface with bond distances ranging from approximately 3 to 12 Å. Through the avoided crossing at 7 Å, parts of the wave packet can make a transition to the electronic ground state, and dissociate.

wave packet oscillates with large amplitudes, so we can easily distinguish the two species, which are the excited state, and the depleted ground state (the "hole").

We used the `WavePacket` program package [38] for the calculation, which comes with potential energy curves, and dipole moments for NaI based on [36]. The wave function as function of the bond vector $\mathbf{R}$ was expanded into radial wave functions ψ_l, and Legendre polynomials as

$$\Psi = \sum_e \Psi_e(\mathbf{R}, t)\ |e\rangle = \sum_{le} \frac{\psi_{le}(r,t)}{r}\ P_l(\cos\theta)\ |e\rangle \tag{20}$$

where the bracket notation is used for the electronic coordinates, or states. The rotational ground state is symmetric under a rotation around the laser polarisation axis, and this symmetry is preserved on excitation with a linearly polarized laser, so we drop the azimuth angle.

From this expansion, we obtain the nuclear density by integrating over the electronic coordinates

$$\varrho(\mathbf{R}, t) = \sum_e |\Psi_e(\mathbf{R}, t)|^2 = \sum_n \varrho_n(r,t) P_n(\cos\theta)\ . \tag{21}$$

which is the form (4) we used for the analysis in the last section. In general, the density components ϱ_n depend on the radial wave functions ψ_{le} in a non-trivial manner. However, for the lowest-order perturbation from the rotational ground state, they can be calculated analytically (see next the section).

In the electric dipole approximation for the molecule-field interaction, the Hamiltonian can be written as

$$\hat{H} = \hat{H}_0 + \varepsilon(t)\hat{\mu}(r)\cos\theta \tag{22}$$

where the field-free Hamiltonian $\hat{H}_0$ conserves the rotational quantum number l, and the dipole operator in the second term is responsible for the initial switching of the electronic state with an amplitude depending on the internuclear distance r and the electric field strength ε.

The molecule was initially placed in the electronic, vibrational, and rotational ground state by a propagation in imaginary time [39]. It was subsequently excited by a laser with a wavelength of 328 nm (this value was taken from previous calculations [23, 24]), a $\sin^2$ shape with 10 fs FWHM, and an intensity of 10^{11} W/cm^2. The propagation was carried out by employing a Gauss-Legendre DVR in θ, and a plane-wave expansion for the radial wave functions, and using the split operator method for the time evolution as detailed in [40]. For simplicity, we carried out the propagation non-perturbatively; however, the laser intensity was chosen such that first-order effects dominate, that is, only the terms with $n = 0, 2$ contribute in (21). The details of the calculation, and the scripts used for data processing can be found in a supplement to this article.

We note in passing that the valence electron in NaI undergoes a substantial reorganisation whenever the internuclear distance passes the avoided crossing [24]. This, however, does not invalidate the independent atom model used to represent the molecular electron density, since the vast majority of the electrons can be considered as core electrons associated with a specific atom.

4. Results

4.1. Dynamics of laser-excited NaI

Figure 3 shows the isotropic and anisotropic difference density of NaI calculated via equation (5). We can immediately identify several features that we discussed earlier. We have two well-defined species: the oscillating excited state wave packet and the ground state "hole", which shows minor vibrations. Qualitatively, both difference densities are similar, and encode the same "fundamental" time evolution. We can also see that the hole contribution changes sign in $\Delta\bar{\varrho}_2$ at $\tau = 1.5$ ps. From the discussion in section 2, especially from comparing (9) with (21), we recall that the density components for each species contain some universal vibrational density, and a rotational coefficient that describes the orientation of the species. In our calculation, the sign change of the anisotropic density component comes from a sign change of c_2^{hole}, that is, a change of the rotational distribution of the hole. This does not happen to the excited state wavepacket, thus emphasizing the need to assign different rotational coefficients to different species. We can deduce from (22) that the excitation is proportional to $\cos\theta$ on the wave function, and $\cos^2\theta$ on a density level. In a simple "classical" picture, we can interpret this such that the laser excites the molecules $\sim \cos^2\theta$, and leaves a "hole" in the ground state

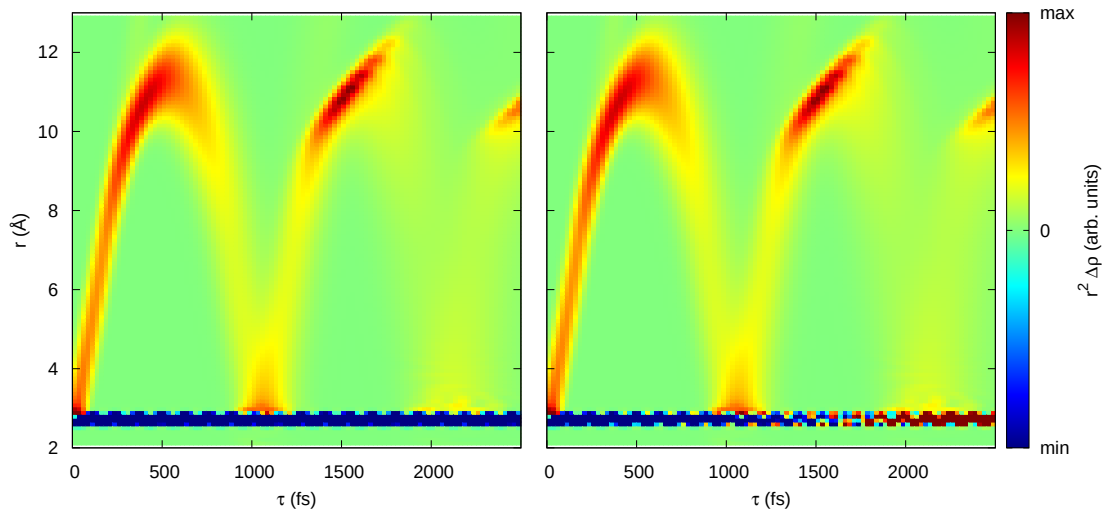

Figure 3. Isotropic $\Delta\bar{\varrho}_0(r,\tau)$ (left) and anisotropic $\Delta\bar{\varrho}_2(r,\tau)$ (right) difference density (in arbitrary units) weighted by r^2 as a function of the pump–probe delay time τ and internuclear distance r.

$\sim -\cos^2\theta$. In the lowest order perturbation, only the states $l \leq l_{\max} = 2$ contribute, which gives a smallest rotational period of $T = 2\pi\hbar/Bl_{\max}(l_{\max}+1) \approx 45$ ps. However, the quantum-mechanical calculation suggests significant rotation of the hole already after 1.5 ps, which demonstrates that this simple picture is wrong.

4.1.1. Interpretation of the dynamics A deeper physical insight into this process can be obtained by analysing the NaI dynamics with an analytic model. In a perturbation theory interpretation, the molecule is always subject to the field-free Hamiltonian, and interacts with the electric field at a random time once, and at two random times for second-order effects. With this in mind, we can explicitly write down expressions for the difference density. For simplicity, we neglect the non-adiabatic transition, so that $\hat{H}_0$ propagates each radial wave function ψ_{le} independently.
If the laser is turned off, the molecule remains in the electronic, vibrational, and rotational ground state, that is

$$\Psi^{\text{off}}(\mathbf{R},t) = \frac{\psi_{\text{GS}}(r,t)}{r}\,|X\rangle\ . \tag{23}$$

ψ_{GS} denotes the vibrational ground state function, whose sole time-dependence is a complex phase. The corresponding nuclear density is

$$r^2\varrho^{\text{off}}(\mathbf{R},t) = |\psi_{\text{GS}}(r)|^2\ P_0(\cos\theta)\ . \tag{24}$$

If the laser is turned on, and we assume no significant rotation during the laser pulse, the wave function at the end of the laser pulse t_e can be written up to second order as

$$\Psi^{\mathrm{on}}(\mathbf{R}, t_e) = \frac{1}{r}\Big[a_0\psi_{\mathrm{GS}}(r, t_e)|X\rangle + a_1\psi_{\mathrm{exc}}(r, t_e)\cos\theta|A\rangle + a_2\psi_{\mathrm{hole}}(r, t_e)\cos^2\theta|X\rangle\Big] . \tag{25}$$

A major portion of the wave function is not excited at all, and stays in the original ground state ψ_{GS}. By absorbing a photon, the molecule can switch to the excited electronic state and move on the corresponding surface, which is described by the wave function ψ_{exc}. Due to the form of the interaction Hamiltonian, it acquires an angular factor of $\cos\theta$. After the molecule is excited, it may become deexcited by emitting a photon, thereby falling back to the electronic ground state. The resulting wave function ψ_{hole} is the result of a two-photon process, and consequently has an orientation dependence of $\cos^2\theta$.

For easier comparison of the magnitude of various terms, we have split up each contribution into a complex-valued, normalized wave function ψ_{i}, and a real-valued coefficient a_i. If the one-photon excitation probability is given by $p \ll 1$, then we would expect $a_0^2 \approx 1 - p$, $a_1^2 = p$, and $a_2^2 \approx p^2$, since the two-photon process arises from deexcitation from the excited subset of the wave function. However, the interference term between ψ_{hole} and ψ_{GS} scales with $a_0 a_2 \approx p$, and thus has the same order of magnitude as the wave function on the excited state surface. In fact, this term describes the detailed dynamics of the created hole in the ground state, and has to be included for a correct treatment.

As the field-free Hamiltonian does not couple states with different rotational quantum numbers, we rewrite (25) using Legendre polynomials, and obtain an expression that is valid for times $t > t_e$

$$\Psi^{\mathrm{on}}(\mathbf{R}, t) = \frac{1}{r}\Big[a_0\psi_{\mathrm{GS}}(r, t)P_0(\cos\theta)|X\rangle + a_1\psi_{\mathrm{exc}}(r, t)P_1(\cos\theta)|A\rangle + \frac{a_2}{3}\psi_{\mathrm{hole},0}(r, t)P_0(\cos\theta)|X\rangle + \frac{a_2}{3}\psi_{\mathrm{hole},2}(r, t)P_2(\cos\theta)|X\rangle\Big] \tag{26}$$

where $\psi_{\mathrm{hole},0}(r, t_e) = \psi_{\mathrm{hole},2}(r, t_e) = \psi_{\mathrm{hole}}(r, t_e)$ from (25), and with separate time dependencies for each radial wave function. Using (24) and (26), we can now calculate the difference density. The expansion (21) into Legendre polynomials can be done analytically, and we obtain the expression

$$r^2\Delta\varrho(\mathbf{R}, t) = r^2\Delta\varrho_0(r, t)P_0(\cos\theta) + r^2\Delta\varrho_2(r, t)P_2(\cos\theta) \tag{27}$$

with the isotropic difference density

$$r^2\Delta\varrho_0(r, t) = \frac{a_1^2}{3}|\psi_{\mathrm{exc}}(r, t)|^2 + (a_0^2 - 1)|\psi_{\mathrm{GS}}(r)|^2 + \frac{2a_2}{3}\Re\Big[\psi^*_{\mathrm{hole},0}(r, t)\psi_{\mathrm{GS}}(r, t)\Big] \tag{28}$$

and the anisotropic difference density

$$r^2\Delta\varrho_2(r, t) = \frac{2a_1^2}{3}|\psi_{\mathrm{exc}}(r, t)|^2 + \frac{4a_2}{3}\Re\Big[\psi^*_{\mathrm{hole},2}(r, t)\psi_{\mathrm{GS}}(r, t)\Big], \tag{29}$$

In deriving these, we only collected terms up to order p, and approximated $a_0 a_2 \approx a_2$. The first term in (28) and (29) describes the wavepacket corresponding to the excited state species. It performs the large amplitude oscillations in figure 3, and one readily observes that the contribution is identical for both difference density components. The remaining terms describe the hole; the second term in (28) describes the static population depletion of the ground state, and gives a negative contribution to the difference density around $r = 3$Å, while the last terms are the coherence or interference terms between the unexcited ground state wave function, and the second-order perturbed wave function. If we assume for the moment that the latter is a real eigenstate ψ_x of the unperturbed Hamiltonian, we can write

$$\begin{aligned}\Re\Big[\psi_x^*(r,t)\psi_{\mathrm{GS}}(r,t)\Big] &= \Re\Big[\psi_x(r)\psi_{\mathrm{GS}}(r)\ \mathrm{e}^{\mathrm{i}\varphi_x+\mathrm{i}(E_x-E_{\mathrm{GS}})t/\hbar}\Big] \\ &= 2\,\psi_x(r)\psi_{\mathrm{GS}}(r)\cos\Big[(E_x-E_{\mathrm{GS}})t/\hbar+\varphi_x\Big]\ . \end{aligned} \tag{30}$$

The product of the two stationary wave functions gives some characteristic density distribution, which then oscillates in time as described by the cosine. The hole wave functions can be expressed as the result of an absorption of a photon from the ground state, propagation on the excited state surface for a certain time, and subsequent emission of the photon. Consequently, the phase φ_x is an arbitrary number that depends on the details of the system and the excitation process.

In general, the hole wave functions $\psi_{\mathrm{hole},i}$ can be written as sums of eigenstates, and the full time-dynamics are a superposition of single interference terms of the form (30). In our calculation, we found the most important contributions to $\psi_{\mathrm{hole},i}$ to be the vibrational ground state and first excited state ψ_0, ψ_1 (we neglect ro-vibrational coupling that would make these states dependent on the rotational quantum number).

Let us first consider the isotropic coherence terms in (28). Since we started in the vibrational ground state, $\psi_0\psi_{\mathrm{GS}} = |\psi_{\mathrm{GS}}|^2$, and $E_0 = E_{\mathrm{GS}}$. Consequently, the coherence term $\sim \psi_0\psi_{\mathrm{GS}}$ is time-independent, has the same form as the depletion of the ground state, and effectively only serves to modify the prefactor of the second term in (28). The product $\psi_1\psi_{\mathrm{GS}}$, in contrast, is a function with one node, and localized around $r = 3$Å. The energy difference $E_1 - E_{\mathrm{GS}}$ is about 32 meV for NaI, corresponding to an oscillation of 130 fs duration. This interference term causes a small oscillation of the difference density around $r = 3$Å in figure 3. However, the overall difference density remains negative at all times due to the ground state depletion.

Essentially the same oscillation is seen in the anisotropic difference density, which we can also trace back to the interference between ψ_{GS} and the first vibrationally excited state in (29). We also find $\psi_0\psi_{\mathrm{GS}} = |\psi_{\mathrm{GS}}|^2$, which gives a contribution similar to the depletion of the ground state in the isotropic difference density. However, since $\psi_{\mathrm{hole},2}$ describes the time evolution of the rotationally excited wave function, the time evolution contains an additional rotational energy term, so that $E_0^{l=2} - E_{\mathrm{GS}}$ is now approximately 0.1 meV, corresponding to a slow oscillation of 45 ps duration.

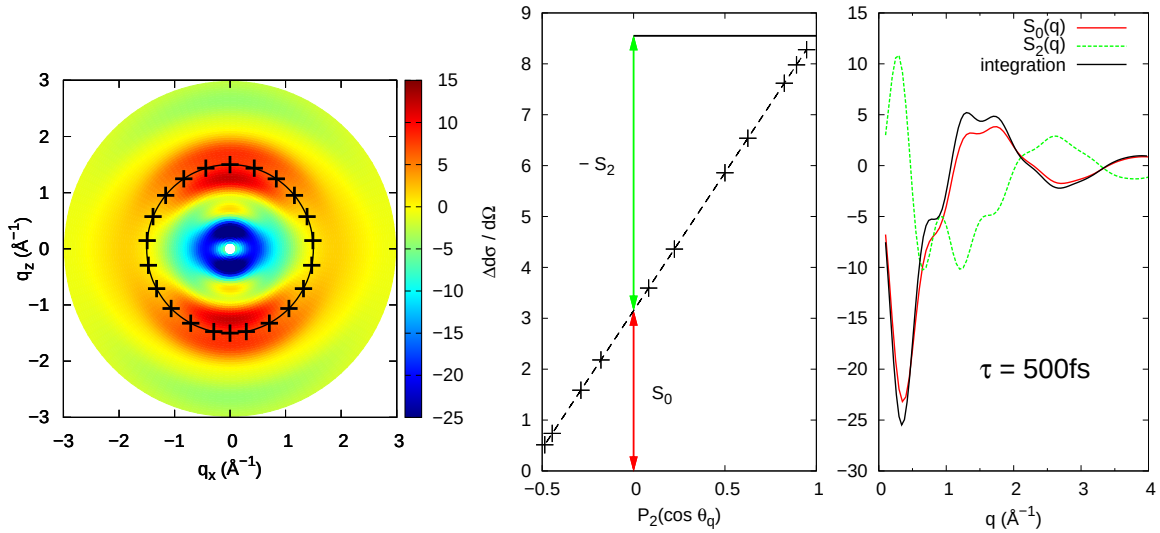

Figure 4. Left: Calculated two-dimensional difference diffraction pattern in arbitrary units for NaI at a pump-probe delay time of 500 fs. The laser polarisation axis and the wave vector of the x-ray beam are perpendicular to each other, and the projection of the polarisation axis is vertical in the image. Middle: Plot of $\Delta \mathrm{d}\sigma/\mathrm{d}\Omega$ as a function of $P_2(\cos\theta_q)$ ($q = 1.5\text{Å}^{-1}$, points correspond to those of the left image). Right: Isotropic and anisotropic curves $S_n(q,\tau)$ encoded in the two-dimensional pattern. Also shown is the result from an azimuthal integration over the detector surface.

That means, $\Delta\varrho_2$ has a contribution of the form $c_2(t)|\psi_{\mathrm{GS}}|^2$, where the prefactor c_2 comes from the cosine in (30), and oscillates slowly. From (9), it is then natural to assign $-|\psi_{\mathrm{GS}}|^2$ to the vibrational difference distribution of the hole species, $c_2(t)$ to the rotational coefficient, and describe the slow oscillation as the rotation of the hole.
We can then wonder what the rotational distribution of the hole at the end of the laser pulse is. Obviously, from (30), this is determined by the value of $\varphi_0^{l=2}$, which in turn depends on the molecule and the laser parameters. That is, while the hole species rotates with an overall period of 45 ps, the initial orientation is determined by the details of the excitation process. For our calculation, we found a phase shift of slightly less than $-\pi/2$, so the hole starts out weakly aligned with the polarisation axis, and the sign of the interference term changes the first time after only 1.5 ps.

4.2. X-ray diffraction from laser-excited NaI

For all results, we assumed an x-ray beam with a $\sin^2$-pulse shape, and a half-width of 100 fs, which should roughly correspond to the situation at the Linear Coherent Light Source (LCLS) including timing jitter [10]. Atomic form factors were taken from [41].
A typical diffraction pattern is shown in figure 4. As detailed in section 2, this rather

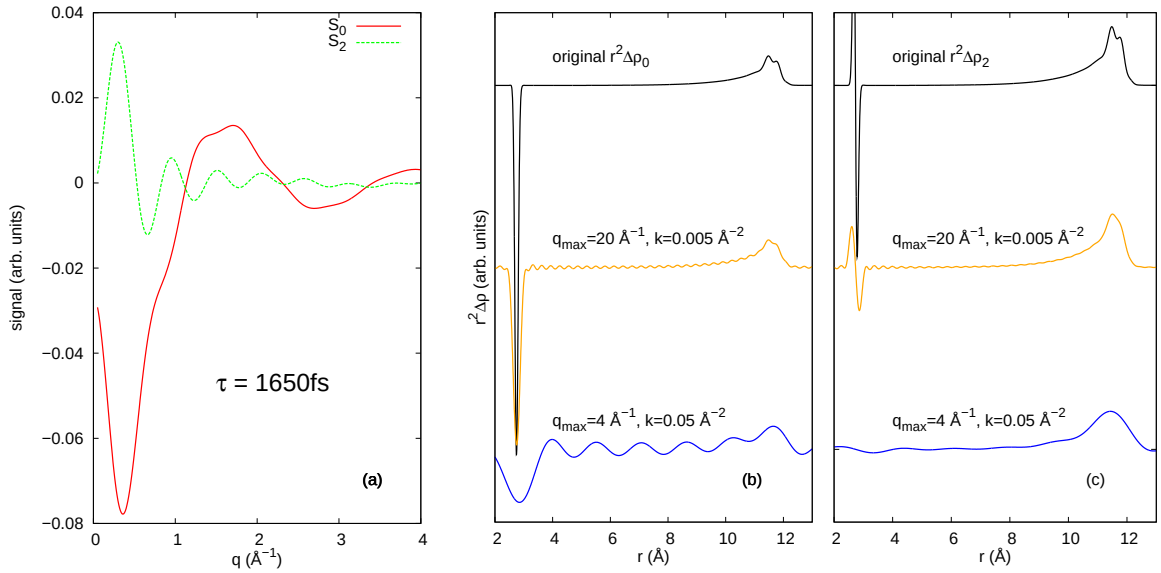

Figure 5. Inversion of the diffraction signal at a pump–probe delay time of 1650 fs. (a): Difference diffraction curves for the isotropic and anisotropic signal; (b): comparison between the original isotropic difference density $r^2\Delta\bar{\varrho}_0$ and the inversion via (19); (c): same for the anisotropic density $r^2\Delta\bar{\varrho}_2$. The upper curve is the original difference density, the other curves are reconstructions with different values of $q_{\max}$ and k.

complex pattern is built up from two diffraction curves (here calculated from (17)), which encode the internal dynamics of the two species, and their rotational coefficients. From section 2, equation (6), we know that for one-photon excitation, the difference signal is up to constant factors given by $\Delta\mathrm{d}\sigma/\mathrm{d}\Omega = S_0(q) - P_2(\cos\theta_q)S_2(q)$. Consequently, if we keep q fixed, and look at different pixels corresponding to different θ_q (crosses for $q = 1.5\text{Å}^{-1}$), we can plot the cross section as a function of $P_2(\cos\theta_q)$, and obtain $S_0(q)$ and $S_2(q)$ from the offset and negative slope, respectively.

Using this procedure for all q gives the two scattering curves. In the case of noisy experimental data, a least squares fit should also yield some measure for the error of the diffraction curves. The isotropic curve can be compared with various approximations, such as an azimuthal integration over the detector plane, which gives surprisingly good results (see [28] for a discussion of this and other approximation schemes). However, we want to point out that the correct decomposition itself is simple enough, so one can easily avoid the loss of accuracy inherent in the approximate scheme.

Formally, we can assign each detector pixel a value of q and θ_q, where the latter depends on the angle between the wave vector of the incoming x-ray beam and the laser polarisation axis. Consequently, we get different diffraction patterns if we vary this angle. However, this only affects how well we can decompose the pattern into the single curves S_n, the curves themselves are independent of the experimental setup. For the figures presented here, we assumed a perpendicular setup where the anisotropy is

most pronounced.

In figure 5, we compared the real difference densities to an inversion from the diffraction data using (19). We used a pump–probe delay time of 1650 fs because the vibrational interference pattern is most pronounced in the anisotropic difference density at this time. We assumed LCLS beam parameters of 8 keV photon energy; with a maximum scattering angle of 60 degrees, only scattering vectors up to $q \approx 4\text{Å}^{-1}$ are collected. We find that this range of scattering vectors is too small to resolve, in particular, the vibrational interference terms, whereas perfect agreement with the original density distribution is obtained with a larger range of scattering vectors as indicated in the figure.

Up to now, we have only studied NaI in the rotational ground state. In practice, one usually starts with a Boltzmann distribution of initial rotational states. However, our basic findings still hold in this case. The orientation of the hole is still determined by an interference term between the unexcited molecular wave function, and a second-order wave function, and the phase between them (i.e., orientation of the hole) depends on the detailed dynamics of the latter. We also find two additional effects that do not occur in the ground-state calculation.

First, we point out that if the molecule absorbs a photon in the rotational ground state, the resulting excited state wave function ψ_{exc} consist of a single rotational quantum state with $l = 1$; the density $|\psi_{\text{exc}}|^2$ is *always* preferentially oriented towards the laser polarisation axis. This is a special case; for a nonzero initial rotational quantum number l_0, ψ_{exc} is composed of contributions with $l_0 + 1$ and $l_0 - 1$. As a consequence, its contribution to the difference density also includes rotational interference terms, and the anisotropic density can show amplitude or sign changes that we can interpret as rotation of the excited molecule.

A second effect that we expect to occur is rotational dephasing [27,31,34]. The rotational interference terms for ensemble members with different initial angular momentum oscillate with different time scales. When performing the ensemble average some time after the excitation, the different anisotropic contributions typically cancel. In effect, the diffraction pattern becomes almost isotropic on a timescale of few picoseconds with alignment revivals at certain times.

5. Conclusions

Whenever we excite molecules with a linearly polarized laser, we prepare anisotropic ensembles. When we probe the subsequent sub-picosecond dynamics with TRXD, the resulting difference diffraction patterns also show a pronounced anisotropy. It has been demonstrated that such signals can be decomposed into an isotropic and one or more anisotropic diffraction curves. For alignment through one-photon absorption, the decomposition turns into a linear fitting procedure, and gives an isotropic and an anisotropic curve. These curves can be processed independently of each other, and they encode the same basic information about the non-equilibrium molecular structure.

The isotropic curve is described by the usual Debye formula [30], and gives the same

signal as we would obtain from an isotropic ensemble. The anisotropic curve contains additional coefficients that describe the rotational distribution of the molecule, which makes data extraction more difficult. On the other hand, it is related to an angle-resolved pair distribution, that is, it also includes explicit information about the orientation of the single bonds with respect to the transition dipole moment, which might be used to supplement the information extracted from the isotropic curve.

We have calculated the diffraction patterns and difference densities for the diatomic NaI molecule excited from the rotational, vibrational, and electronic ground state. We have demonstrated both numerically and analytically that the density distribution can be extracted through an exact inversion procedure.

By interpreting the dynamics with a simple analytic model, we could explicitly demonstrate that the orientation of the hole species is strongly dependent on the details of the excitation process. This should serve as a warning that the orientation of the single species cannot be guessed from simple models that omit quantum-mechanical interference terms (for example, equation (32) in [28] assumes that, when molecules are preferentially excited along the laser polarisation axis, the hole is also oriented in this direction).

Apart from applying the formalism presented here to larger systems, one possible route for expansion is molecular imaging. It has been proposed to align molecules in their stable ground state in the gas phase by a non-resonant laser to extract their structure [20, 42, 43]. In principle, this can be included in the treatment of anisotropic diffraction patterns presented here. However, the problem remains if and how one can create a convergent algorithm to extract the structure of the molecule.

Acknowledgments

This work was supported by the Danish National Research Foundation's Center for Molecular Movies. The authors thank Prof. Martin Centurion for comments on the manuscript.

Appendix A. Density distribution of symmetric tops

In the following, we demonstrate that, for general excitation with a linearly polarized laser, and assuming a symmetric top initial state, the difference density can be expressed as a polynomial of $\cos\theta$ for all delay times.

If we excite the system from a thermal ensemble, the density at an arbitrary time can be written as

$$\varrho(\alpha,\beta,\gamma,t) = \sum_{JMN} w_N^J |\Psi_{MN}^J(\alpha,\beta,\gamma,t)|^2 \ . \tag{A.1}$$

The Euler angles α and γ correspond to a rotation around the laboratory-fixed z-axis, and the body-fixed symmetry axis, respectively. β is the inclination angle of these two axes. If we define the laboratory z-axis to be the laser polarisation axis, and assuming

the transition dipole moment to be along the symmetry axis, the inclination angle is identical to θ defined in figure 1. There is some liberty in defining the signs of α, γ, and we use the convention of [44]. The ensemble average is done with Boltzmann factors w_N^J, and $\Psi_{MN}^J(t)$ is the ensemble member that starts as an eigenstate of the free Hamiltonian with total angular momentum J, and projections M on the laser polarisation axis, and N on the body-fixed symmetry axis. Note that N is only a good quantum number if the molecule in question is a symmetric top.

To show that (A.1) is a polynomial of $\cos\theta$, we consider only a single summand. Within the electric dipole approximation, the Hamiltonian of the system has the form of (22). It consists of a field-free molecular Hamiltonian that preserves all rotational quantum numbers , and the dipole interaction operator $\sim \cos\theta$ that preserves the quantum numbers M, N. During the time evolution, these quantum numbers thus do not change, and the time-dependent wave function can be expanded as

$$\Psi_{MN}^J(\alpha,\theta,\gamma,t) = \sum_{J'} c_{J,J'}(t) D_{MN}^{J'}(\alpha,\theta,\gamma) \tag{A.2}$$

where a complete basis set for rotational wave functions is formed by the eigenstates of a symmetric top Hamiltonian

$$D_{MN}^J(\alpha,\theta,\gamma) = \mathrm{e}^{-\mathrm{i}(\alpha M+\gamma N)} d_{MN}^J(\theta) \tag{A.3}$$

with quantum numbers J, M, N defined previously. For the density, we obtain

$$|\Psi_{MN}^J(\alpha,\theta,\gamma,t)|^2 = \sum_{J_1,J_2} c_{J_1}^*(t) c_{J_2}(t) d_{MN}^{J_1}(\theta) d_{MN}^{J_2}(\theta) \ . \tag{A.4}$$

The d matrices can be expressed as [44]

$$d_{MN}^J(\theta) = \sum_t{}' x_t (\cos\frac{\theta}{2})^{2J+M-N-2t} \ (\sin\frac{\theta}{2})^{2t+N-M} \tag{A.5}$$

where the sum is restricted, and allows only non-negative powers. It can be seen that every product of d matrices in (A.4) reduces to a sum of even powers of $\cos(\theta/2)$ and $\sin(\theta/2)$. Together with standard addition formulas for trigonometric functions, this translates into powers of $\cos\theta$.

References

[1] W. Friedrich, P. Knipping, and M. Laue. Interferenzerscheinungen bei Röntgenstrahlen. *Ann. d. Phys.*, 346:971, 1913.

[2] Haldrup K., M. Christensen, M. Cammarata, Q. Kong, M. Wulff, S. O. Mariager, K. Bechgaard, R. Feidenhans'l, N. Harrit, and M. M. Nielsen. Structural Tracking of a Bimolecular Reaction in Solution by Time-Resolved X-Ray Scattering. *Angewandte Chemie International Edition*, 48:4180–4184, 2009.

[3] T. K. Kim, J. H. Lee, M. Wulff, Q. Kong, and H. Ihee. Spatiotemporal Kinetics in Solution Studied by Time-Resolved X-Ray Liquidography (Solution Scattering). *ChemPhysChem*, 10:1958–1980, 2009.

[4] P. Coppens, J. Benedict, M. Messerschmidt, I. Novozhilova, T. Graber, Y.-S. Chen, I. Vorontsov, S. Scheins, and S.-L. Zheng. Time-resolved synchrotron diffraction and theoretical studies of very short-lived photo-induced molecular species. *Acta Crystallographica Section A*, 66(2):179–188, Mar 2010.

[5] R. W. Schoenlein, S. Chattopadhyay, H. H. W. Chong, T. E. Glover, P. A. Heimann, W. P. Leemans, and C. V. Shank. Generation of femtosecond x-ray pulses via laserelectron beam interaction. *Appl. Phys. B*, 71:1, 2000.

[6] P. Beaud, S. L. Johnson, A. Streun, R. Abela, D. Abramsohn, D. Grolimund, F. Krasniqi, T. Schmidt, V. Schlott, and G. Ingold. Spatiotemporal Stability of a Femtosecond Hard-X-Ray Undulator Source Studied by Control of Coherent Optical Phonons. *Phys. Rev. Lett*, 99:174801, 2007.

[7] M. M. Murnane, H. C. Kapteyn, M. D. Rosen, and R. W. Falcone. Ultrafast x-ray pulses from laser-produced plasmas. *Science*, 251:531, 1991.

[8] N. Zhavoronkov, Gritsai Y., M. Bargheer, M. Woerner, T. Elsaesser, F. Zamponi, I. Uschmann, and E. Förster. Microfocus Cu K_α source for femtosecond x-ray science. *Opt. Lett.*, 30:1737–1739, 2005.

[9] J. et al. Arthur. Linac coherent light source (lcls) conceptual design report. Technical report, Stanford Linear Accelerator Center, 2002.

[10] L. F. DiMauro, J. Arthur, N. Berrah, J. Bozek, J. N. Galayda, and J. Hastings. Progress report on the lcls xfel at slac. *J. Phys.: Conf. Ser.*, 88:012058, 2007.

[11] T. Tanaka and T. (eds) Shintake. Scss x-fel conceptual design report. Technical report, Riken, 2005.

[12] M. Altarelli et al. The European X-Ray Free-Electron Laser - Technical design report. Technical report, DESY, 2007.

[13] C.H. Chao, S.H. Lin, W.K. Liu, and P. Rentzepis. Theory of time-resolved X-ray and electron diffraction. In J.R. Helliwell and P.M. Rentzepis, editors, *Time-Resolved Diffraction*, page 260. Oxford University Press, 1997.

[14] M. Ben-Nun, J. Cao, and K.R. Wilson. Ultrafast X-ray and Electron Diffraction: Theoretical Considerations. *J.Phys.Chem. A*, 101:8743, 1997.

[15] J. Cao and K.R. Wilson. Ultrafast X-ray Diffraction Theory. *J. Phys. Chem. A*, 102:9523, 1998.

[16] S. Tanaka, V. Chernyak, and S Mukamel. Time-resolved spectroscopy: Nonlinear response functions and Liouville-space pathways. *Phys. Rev. A*, 63:063405, 2001.

[17] S. Bratos, F. Mirloup, and R. Vuilleumier. Time-resolved x-ray diffraction: Statistical theory and its application to the photo-physics of molecular iodine. *J. Chem. Phys*, 116:10615, 2002.

[18] T. Rozgonyi, R. Sauerbrey, and T. Feurer. Time-resolved x-ray diffraction in a molecular crystal. *J. Appl. Phys*, 97:013537, 2005.

[19] N.E. Henriksen and K.B. Møller. On the Theory of Time-Resolved X-ray Diffraction. *J. Phys. Chem. B*, 112:558, 2008.

[20] J.H. Phay and R. Santra. Theory of x-ray diffraction from laser-aligned symmetric top molecules. *Phys.Rev. A*, 78:053409, 2008.

[21] U. Lorenz, K. B. Møller, and N. E. Henriksen. Theory of time-resolved inelastic x-ray diffraction. *Phys. Rev. A*, 81(2):023422, Feb 2010.

[22] S. E. Choi and J. C. Light. Use of the discrete variable representation in the quantum dynamics by a wave packet propagation: Predissociation of NaI($^1\Sigma_0^+$)→NaI(0^+)→Na(^2S)+I(^2P). *J. Chem. Phys.*, 90:2593, 1988.

[23] V. Engel and H. Metiu. A quantum-mechanical study of predissociation dynamics of NaI excited by a femtosecond laser pulse. *J. Chem. Phys.*, 90:6116, 1989.

[24] M. Grønager and N.E. Henriksen. Real-time control of electronic motion: Application to NaI. *J. Chem. Phys.*, 109:4335, 1998.

[25] D.A. Kohl and E.J. Shipsey. Elastic electron scattering from state-selected molecules I. Intensities. *Z. Phys. D*, 24:33, 1992.

[26] J.C. Williamson and A.H. Zewail. Ultrafast Electron Diffraction. 4. Molecular Structures and Coherent Dynamics. *J. Phys. Chem.*, 98:2766, 1994.

[27] J.S. Baskin and A.H. Zewail. Ultrafast Electron Diffraction: Oriented Molecular Structures in Space and Time. *ChemPhysChem*, 6:2261, 2005.

[28] J.S. Baskin and A.H. Zewail. Oriented Ensembles in Ultrafast Electron Diffraction. *ChemPhysChem*, 7:1562, 2006.

[29] E.H. van Kleef and I. Powis. Anisotropy in the preparation of symmetric top excited states. I. One-photon electric dipole excitation. *Molecular Physics*, 96:757, 1999.

[30] P. Debye. Zerstreuung von Röntgenstrahlen. *Annalen der Physik*, 351:809, 1915.

[31] Henrik Stapelfeldt and Tamar Seideman. Colloquium: Aligning molecules with strong laser pulses. *Rev. Mod. Phys.*, 75(2):543–557, Apr 2003.

[32] Bretislav Friedrich and Dudley Herschbach. Alignment and trapping of molecules in intense laser fields. *Phys. Rev. Lett.*, 74(23):4623–4626, Jun 1995.

[33] G.A. Korn and T.M. Korn. *Mathematical Handbook for Scientists and Engineers.* McGraw-Hill, 1968.

[34] P. Reckenthaeler, M. Centurion, W. Fuß, S. A. Trushin, F. Krausz, and E. E. Fill. Time-resolved electron diffraction from selectively aligned molecules. *Phys. Rev. Lett*, 102:213001, 2009.

[35] T. S. Rose, M. J. Rosker, and A. H. Zewail. Femtosecond real-time observation of wave packet oscillations (resonance) in dissociation reactions. *J. Chem. Phys.*, 88:6672, 1988.

[36] G.H. Peslherbe, R. Bianco, J.T. Hynes, and B.M. Ladanyi. On the photodissociation of alkali-metal halides in solution. *J. Chem. Soc. Faraday Trans.*, 93:977, 1997.

[37] K. B. Møller, N. E. Henriksen, and A. H. Zewail. On the role of coherence in the transition from kinetics to dynamics: Theory and application to femtosecond unimolecular reactions. *J. Chem. Phys.*, 113:10477, 2000.

[38] U. Lorenz and B. Schmidt. Wavepacket 4.7.2: A program package for quantum-mechanical wavepacket propagation and time-dependent spectroscopy. available via http://wavepacket.sourceforge.net, 2010.

[39] R. Kosloff and H. Tal-Ezer. A direct relaxation method for calculating eigenfunctions and eigenvalues of the schrödinger equation on a grid. *Chem. Phys. Lett.*, 127:223, 1986.

[40] M.R. Hermann and J.A. Fleck Jr. Split-operator spectral method for solving the time-dependent Schrödinger equation in spherical coordinates. *Phys. Rev. A*, 38:6000, 1988.

[41] J.A. Ibers and W.C. Hamilton, editors. *International Tables for X-ray Crystallography.* The Kynoch Press, 1974.

[42] P. J. Ho, D. Starodub, D. K. Saldin, V. L. Shneerson, A. Ourmazd, and R. Santra. Molecular structure determination from x-ray scattering patterns of laser-aligned symmetric-top molecules. *The Journal of Chemical Physics*, 131(13):131101, 2009.

[43] D. K. Saldin, V. L. Shneerson, D. Starodub, and J. C. H. Spence. Reconstruction from a single diffraction pattern of azimuthally projected electron density of molecules aligned parallel to a single axis. *Acta Crystallographica Section A*, 66(1):32–37, Jan 2010.

[44] D.M. Brink and G.R. Satchler. *Angular Momentum.* Clarendon Press, 1968.